Quantum Simulation of the First-Quantized Pauli-Fierz Hamiltonian

Priyanka Mukhopadhyay,[1,*] Torin F. Stetina,[2,3,†] and Nathan Wiebe[4,5,6,‡]

[1] *Department of Physical & Environmental Sciences, University of Toronto, Ontario M1C 1A4, Canada*
[2] *Simons Institute for the Theory of Computing, Berkeley, California 94720, USA*
[3] *Berkeley Quantum Information and Computation Center, University of California, Berkeley, California 94720-1460, USA*
[4] *Department of Computer Science, University of Toronto, Ontario M5S 2E4, Canada*
[5] *Pacific Northwest National Laboratory, Richland, Washington 99354, USA*
[6] *Canadian Institute for Advanced Research, Toronto, Ontario M5G 1M1, Canada*

(Received 27 August 2023; accepted 21 February 2024; published 15 March 2024)

We provide an explicit recursive divide-and-conquer approach for simulating quantum dynamics and derive a discrete first-quantized nonrelativistic QED Hamiltonian based on the many-particle Pauli-Fierz Hamiltonian. We apply this recursive divide-and-conquer algorithm to this Hamiltonian and compare it to a concrete simulation algorithm that uses qubitization. Our divide-and-conquer algorithm, using lowest-order Trotterization, scales for fixed grid spacing as $\widetilde{O}(\Lambda N^2\eta^2 t^2/\epsilon)$ for grid size N, η particles, simulation time t, field cutoff Λ, and error ϵ. Our qubitization algorithm scales as $\widetilde{O}(N(\eta+N)(\eta+\Lambda^2)t\log(1/\epsilon))$. This shows that even a naive partitioning and low-order splitting formula can yield, through our divide-and-conquer formalism, superior scaling to qubitization for large Λ. We compare the relative costs of these two algorithms on systems that are relevant for applications such as the spontaneous emission of photons and the photoionization of electrons. We observe that for different parameter regimes, one method can be favored over the other. Finally, we give new algorithmic and circuit-level techniques for gate optimization, including a new way of implementing a group of multicontrolled-X gates that can be used for better analysis of circuit cost.

DOI: 10.1103/PRXQuantum.5.010345

I. INTRODUCTION

The prospect of simulating quantum systems is a highly anticipated application for fault-tolerant quantum computers of the future. The inception of this application of quantum computation is typically attributed to Richard Feynman in the 1980s [1]. Since then, there has been a flurry of both theoretical and experimental research on Hamiltonian-simulation algorithms [2–11] and specific applications ranging from condensed-matter physics [12–15], through chemistry [16–20], high-energy particle physics [21–26], quantum gravity [27–31], and much more [32–38]. Research in these applications of simulating physics has shown a variety of challenges specific to each regime of interest, and the subtleties of the benefits and limitations of the select Hamiltonian-simulation algorithms have become more apparent as progress has been moving forward.

In this work, we focus on the nonrelativistic regime of chemistry and on condensed matter, which is a very active field in the development of quantum algorithms. Specifically, we use a first-quantized approach to simulating the many electron degrees of freedom, due to their favorable sublinear asymptotic scaling in the number of orbitals or grid points, which is usually much larger than the number of electrons [20,39]. Typically, quantum simulations of chemistry primarily focus on the Coulomb Hamiltonian for electrons, which includes one- and two-body interactions and classical clamped nuclei using the Born-Oppenheimer approximation. While this work is important for understanding many chemical properties including chemical-reaction rates, with both qualitative and quantitative success, there are many basic and applied problems where the fundamental nature of the quantum electromagnetic (EM) field is important. Thus, we would like to treat electrons and the EM field on an even footing,

[*] mukhopadhyay.priyanka@gmail.com, priyanka.mukhopadhyay@utoronto.ca
[†] torin.stetina@gmail.com, torins@berkeley.edu
[‡] nawiebe@cs.toronto.edu

where both have quantum degrees of freedom. One example where this is important is in cavity QED [40–43]. Here, atomic or molecular systems are placed in a mirrored cavity, increasingly coupling the matter system to the fundamental EM mode defined by the cavity size, to the point at which electronic and photonic states combine into so called “polaritonic” states. Obviously, the properties of this system, which require explicit quantum degrees of freedom for the EM field, cannot be modeled properly with electron-only Hamiltonians. Another active area of work is in attosecond science, where experiment and theory are actively investigating the short-time dynamics of electron motion after photoexcitation [44–54]. Here, there are still many unanswered questions about how the electrons move in the short time after interacting with light but the complicated light-matter correlations make this difficult to model theoretically.

Overall, the dynamical properties of quantum EM fields interacting with many-electron systems are still poorly understood but there is significant basic and applied scientific motivation to push our understanding further in this field. One of the main goals of understanding this complex interplay of QED will be to “actively control and manipulate electrons on the attosecond time and angstrom length scale” [55]. In order to attempt to simulate this on a fault-tolerant quantum computer, we must add the proper degrees of freedom to account for the quantum EM field. To simulate nonrelativistic QED, we utilize the multielectron Pauli-Fierz Hamiltonian [sometimes referred to as the nonrelativistic quantum electrodynamical (NRQED) Hamiltonian], which is described in detail in Sec. II A. In short, the physics of the Pauli-Fierz Hamiltonian modifies the electron-only one-body momentum term from the Coulomb Hamiltonian to include a minimal-coupling description of the light-matter interaction and retains the standard two-body Coulomb electronic interaction, with a free EM dynamical field term as well.

A. Our results and contributions

In this paper, we describe a couple of approaches for the Hamiltonian simulation of a first-quantized full NRQED simulation of light-matter interactions using the first-quantized Pauli-Fierz Hamiltonian discretized on a lattice.

(I) In Sec. II A, we describe the derivation of the first-quantized general spin-$1/2$ Pauli-Fierz Hamiltonian for η particles given in Ref. [56]. The real space is discretized onto a lattice, with a truncation of the electric field Hilbert space. According to our knowledge, this is the first derivation of the many-body Pauli-Fierz Hamiltonian in first quantization described in the literature. We consider two approaches to simulate this Hamiltonian, $\hat{H}_{\mathrm{PF}}$.

(II) First, we consider simulation using a recursive divide-and-conquer approach [Algorithm I (see Sec. II C)], improving on the technique introduced in Ref. [6]. Here, we divide the given Hamiltonian into several fragments using Trotter-Suzuki formulas [57,58], simulate each of them separately, possibly using different algorithms, and then combine the results. In Ref. [6], the authors have used Trotterization for each fragment. In this paper, we have combined Trotterization with qubitization. Such approaches can be very useful if we want to exploit the best of many worlds. For some Hamiltonians, especially those with commuting terms, Trotterization gives less gate complexity but it has a superpolynomial scaling of error tolerance. On the other hand, qubitization has a logarithmic dependence on the inverse of tolerable error but the gate complexity depends on the ℓ_1 norm of the coefficients when the Hamiltonian is expressed as a sum of unitaries. For many complicated Hamiltonians, it may be difficult to simulate using one particular existing technique. In such scenarios, the divide-and-conquer approach can be very helpful. Such divide-and-conquer types of approaches have shown their value in Refs. [59,60], where the focus has been on simulation of specific local Hamiltonians. Our approach is more general and can be applied to a broader spectrum of Hamiltonians, in order to achieve better complexity of simulation.
In Sec. II C, we describe the divide-and-conquer algorithm and derive a bound on the gate complexity (Theorem 3). Later, in Appendixes G 1–G 4, we describe in detail the simulation of each of the partitions of $\hat{H}_{\mathrm{PF}}$.

(III) The second algorithm (Algorithm II) that we consider is to use qubitization [5,7,8]. For this, we block encode the entire Hamiltonian $\hat{H}_{\mathrm{PF}}$. In Sec. II B, we describe a divide-and-conquer approach to constructing the block encoding of the sum and product of different Hamiltonians. We show that for many situations, it is advantageous in terms of number of gates when we split the Hamiltonian into separate parts, block encode each of them, and then combine these parts. For both our algorithms, such recursive block encoding has been useful. We describe Algorithm II in Sec. II D and provide a bound on the gate complexity (Theorem 4).

(IV) Both these algorithms have their own pros and cons and depending on the Hamiltonian under consideration, one can be favored over the other for different parameter regimes. To illustrate more on this, in Sec. III, we have compared the relative costs of these two algorithms with those of some model systems of interest. For example, we consider a regime of a small number of electrons in a single-atom system, which is relevant for applications such as spontaneous emission of photons into the field, photoionization of electrons, and the photoelectric effect. Roughly, comparing Theorems 3 and 4, we find that both of these algorithms have a quadratic dependence on the lattice size N. While qubitization has a quadratic dependence on the electric cutoff Λ, divide and conquer shows a subquadratic dependence. The complexity of the latter depends on the partitioning and in this paper we have tried to prioritize Λ. This is reflected when we compare the cost in Figs. 3 and 4. We observe that qubitization scales better with respect to N, while divide and conquer performs better with respect to Λ. Another interesting phenomenon that we have observed is the fact that as we increase the order of the Trotter splitting in divide and conquer, the scaling becomes closer to that of qubitization.

We have also discussed a few possible applications for simulating the Hamiltonian that we consider, e.g., the determination of photoionization time scales in atomic, molecular, and extended systems. Further, we have discussed how the electric cutoff, one of the parameters of interest, scales for certain regimes of applied problems.

(V) On the circuit synthesis and optimization side, we have developed a split-and-merge technique (Theorem 2) to implement a group of multicontrolled-X gates in Sec. II B (see also Appendix D). Such groups of gates occur in many places, e.g., Hamiltonian-simulation algorithms working with a linear combination of unitaries [2–5,7], the synthesis of efficient circuits for exponentiated Paulis [61], the quantum approximate optimization algorithm (QAOA) [62], quantum state preparation [63], quantum machine learning [64], and the construction of quantum read-only memory (QROM) [19] and quantum random access memory (QRAM) [65]. The main intuition is to split and group the control qubits, use extra ancillas to store intermediate information, and then implement the requisite logical function using these ancillas. We show that this can lead to an asymptotic improvement in the gate complexity of SELECT operations, by the shaving of logarithmic factors. Such a circuit-optimization technique may be of independent interest and may be useful for other applications.

(VI) Among other technical contributions, we give improved decompositions of certain matrices as linear combinations of unitaries. Specifically, we give general procedures to decompose diagonal integer matrices as a sum of exponentially fewer numbers of unitaries. This also contributes to the asymptotic improvement in gate complexity. In Appendix F, we describe these decompositions and the computation of the ℓ_1 norm of the Hamiltonian. It has been shown in Ref. [58] that the Trotter error depends on nested commutators. In Lemma 7, we show that these nested commutators depend on pairwise commutators and on the sum of the ℓ_1 norm. The derivations of these terms have also been given in Appendix H. We hope that these technical contributions will be useful in future works for better analyzing the complexity of simulating Hamiltonians.

II. RESULTS

Here, we review the main results of our paper and provide an extended introduction to the physics of the Pauli-Fierz Hamiltonian. The Pauli-Fierz Hamiltonian gives a proper nonrelativistic treatment of single-particle QED. This is frequently augmented to the multiparticle case by including artificial Coulomb interactions between the particles, resulting in a Hamiltonian that is more general than the standard Hamiltonians studied in quantum chemistry simulation. While the Pauli-Fierz Hamiltonian is a well-studied model, it is typically presented in a second-quantized form. We will first review the derivation of its first-quantized form, which we will need in order to have a simulation algorithm the scaling of which is comparable to the best-known simulation results for chemistry *in absentia* of electrodynamical effects.

A. Pauli-Fierz Hamiltonian

In order to simulate the Pauli-Fierz Hamiltonian, we must first discretize the real space onto a lattice and provide a truncation for the electric field Hilbert space. We will denote this cutoff as Λ and discretize the space as a cubic lattice with side length L. N is the total number of grid points and so in each Cartesian direction there are $N^{1/3}$ grid points. A single grid point, $\mathbf{q}$, can then be described as $\mathbf{q} = (q_x, q_y, q_z) \in [0, N^{1/3} - 1]^3 \subset \mathbb{Z}_+^3$. We write that $\mathbf{q}$ varies from 1 to N for brevity, instead of saying that q_x, q_y, and q_z vary from 0 to $N^{1/3} - 1$. $\mathbf{q} + 1_\mu$ refers to the adjacent point of $\mathbf{q}$ in the μth direction, i.e., it is obtained by adding the lattice spacing to q_μ. We often write $\mathbf{q} + \mathbf{1}$ to refer to an adjacent point, when the direction is clear from the context or when we want to refer to all the three neighboring points of $\mathbf{q}$.

In first-quantized representation, the particle number is fixed and each particle has its own "copy" of the grid where it lives. Subsequently, each first-quantized particle interacts with the background field separately. The discretized Hilbert space for the Pauli-Fierz Hamiltonian is then

TABLE I. A list of the important variable definitions used throughout this paper.

Term	Definition
η	Number of particles in the simulation
e	Bare electric charge
m_e	Electron mass
N	Number of lattice sites
G	Set of lattice sites labeled q for a three-dimensional (3D) cubic lattice, where $q \in [0, N^{1/3}]^3 \subset \mathbb{Z}_+^3$
L	Length of one side of the simulation box, where $\{L \in \mathbb{R} \,\vert\, L > 0\}$
$\Omega = L^3$	Volume of box size L
$\Delta = \Omega^{1/3}/N^{1/3}$	Lattice-spacing size
Λ	Maximum cutoff for electric link quantum number
μ, ν	Cartesian indices
σ_μ	The μth Pauli matrix
$A_\mu(q)$	μth component of the magnetic vector potential at link site q

$$\mathcal{H}_{\mathrm{PF}} = \mathcal{H}_p \otimes \mathcal{H}_f \tag{1}$$

$$= L^2(\mathbb{C}^{(2N)^\eta (2\Lambda)^{3N}}), \tag{2}$$

where at each electric link between grid point $\mathbf{q}$ and $\mathbf{q}+\mathbf{1}$, there are $2\Lambda + 1$ possible electric link values. Recall that we have three links per grid point in a periodic basis. However, for practical implementation, the link space will be offset by one, so the total dimension of the Hilbert space at each link is even, 2Λ. Collecting the notation into one place for this paper, we will use the definitions as described in Table I.

The general expression for the Hamiltonian on the N-point cubic lattice with η electrons is

$$\hat{H} = H_\pi + H_s + H_{V_{ee}} + H_{V_{ne}} + H_f\,. \tag{3}$$

Throughout this paper, we often refer to a summand Hamiltonian as a “fragment Hamiltonian,” each of which we will now describe. For convenience, we first describe the registers on which the operators act. The state of the qubits in the registers gives the wave function. There are two registers, the particle register and the link register. We store the spin and position of each of the η particles in the particle register. To be precise, for each particle, we allot one qubit to store the spin and $3\log_2 N^{1/3} = \log_2 N$ qubits to store the Cartesian coordinates of its position in the lattice grid. Thus the particle register is of the form $\bigotimes_{j=1}^{\eta} |s, \mathbf{q}\rangle_j$, where $\mathbf{q} = (q_x, q_y, q_z)$, and it has $\eta\left(1 + \log_2 N\right)$ qubits. Again, we assume a maximum cutoff for the electric link eigenstates, Λ. In the link register, we allot $\log_2(2\Lambda)$ qubits for each of the three links per grid point. Thus there are $3N\log_2(2\Lambda)$ qubits in the link space. In later sections, when we describe the simulation algorithms, we will mention that in each register we keep extra qubits for selecting a subspace on which an operator acts but these do not reflect on the state of the wave function.

Now, we describe each term of the fragment Hamiltonian in Eq. (3). For a more detailed background on the derivation of these Hamiltonian terms, see Appendix A. The operators act on three disjoint subspaces corresponding to the particle spin, the particle position, and the gauge link space. First, we describe the fragment Hamiltonians, $H_{V_{ee}}$ and $H_{V_{ne}}$, that involve only the particle degrees of freedom acting on the $\mathcal{H}_p$ Hilbert space:

$$H_{V_{ee}} = \mathbb{I} \otimes \left(\frac{e^2}{4\pi\epsilon_0\Delta} \sum_{i<j}^{\eta} \sum_{\mathbf{q},\mathbf{r}}^{N} \frac{1}{||\mathbf{q}-\mathbf{r}||_2} |\mathbf{q}\rangle\langle\mathbf{q}|_i\, |\mathbf{r}\rangle\langle\mathbf{r}|_j \right) \otimes \mathbb{I}, \tag{4}$$

$$H_{V_{ne}} = \mathbb{I} \otimes \left(-\frac{e^2}{4\pi\epsilon_0\Delta} \sum_{i}^{\eta} \sum_{\kappa}^{K} \sum_{\mathbf{q}}^{N} \frac{Z_\kappa}{||\mathbf{q}-\mathbf{R}_\kappa||_2} |\mathbf{q}\rangle\langle\mathbf{q}|_i \right) \otimes \mathbb{I}. \tag{5}$$

$H_{V_{ee}}$ and $H_{V_{ne}}$ capture the instantaneous Coulomb-interaction terms between two electrons and the attractive term between an electron and a classical fixed point charge representing a nucleus, respectively. $|\mathbf{q}\rangle\langle\mathbf{q}|_i$ is shorthand notation for the operator acting only on particle i over the η-particle Hilbert space, $\left(\bigotimes_{k=1}^{i-1} \mathbb{I}_k\right) \otimes |\mathbf{q}\rangle\langle\mathbf{q}|_i \otimes \left(\bigotimes_{k=i+1}^{\eta} \mathbb{I}_k\right)$. Additionally, κ indexes K classical nuclei at real-space coordinate $\mathbf{R}_\kappa$.

The free electromagnetic field Hamiltonian, H_f, acting on the EM-field Hilbert space $\mathcal{H}_f$ is described as

$$H_f = \mathbb{I} \otimes \mathbb{I} \left(\sum_{q=1}^{N} \sum_{\mu=1}^{3} \frac{e^2}{2} E_{q,\mu}^2 - \sum_{q=1}^{N} \sum_{\mu\neq\nu=1}^{3} \frac{1}{e^2} W_{q,\mu,\nu}^2 \right), \tag{6}$$

where each link q connects points adjacent to point $\mathbf{q}$ in the lattice. If the inner summation index or subscript of an operator is μ, then link q connects point $\mathbf{q}$ to its neighbor in the μth direction of the lattice. We will explain shortly what the double subscripts μ, ν imply in the case of operator $W_{q,\mu,\nu}$.

In the electric link basis, the $E_{q,\mu}$ operators are defined as

$$E_{q,\mu} = \sum_{\epsilon=-\Lambda}^{\Lambda-1} \epsilon|\epsilon\rangle\langle\epsilon|_{q,\mu}, \quad E^2_{q,\mu} = \sum_{\epsilon=-\Lambda}^{\Lambda-1} \epsilon^2|\epsilon\rangle\langle\epsilon|_{q,\mu}, \quad (7)$$

where $|\epsilon\rangle$ and ϵ correspond to eigenvectors and eigenvalues of a particle in a ring, respectively, for each link q. Here, we note that the cutoffs on the field are asymmetric ($\Lambda - 1$ above and $-\Lambda$ below) because, for convenience, we want the dimension of the space to be a power of 2, which facilitates a simpler binary encoding in our quantum simulations. The magnetic field term can be defined in terms of the "plaquette" operator, which is a product of raising and lowering operators on link sites. The latter is denoted by $U_{q,\mu}$. Specifically,

$$U_{q,\mu} = \sum_{\epsilon=-\Lambda}^{\Lambda-1} |\epsilon+1\rangle\langle\epsilon|_{q,\mu} = \exp\left(i\Delta A_{q,\mu}\right) \quad (8)$$

and the plaquette operator is

$$W^2_{q,\mu,\nu} = \sum_{\mu\neq\nu}^{3} U_{q,\mu} U_{q+1_\mu,\nu} U^\dagger_{q+1_\nu,\mu} U^\dagger_{q,\nu} + \text{H.c.} \quad (9)$$

Here, we note that (q,μ) and (q,ν) are the links connecting point $\mathbf{q}$ to its adjacent point in the μth and νth direction, respectively. We denote these adjacent points by $\mathbf{q}+1_\mu$ and $\mathbf{q}+1_\nu$, respectively. $(q+1_\mu,\nu)$ is the link connecting point $\mathbf{q}+1_\mu$ to its adjacent point in the νth direction, while $(q+1_\nu,\mu)$ is the link connecting point $\mathbf{q}+1_\nu$ to its adjacent point in the μth direction. Thus the operators act on a plaquette, i.e., four edges of a square face in the three-dimensional (3D) cube.

Next, H_π is the modified electron kinetic term including the interaction with the magnetic vector potential, in a familiar form,

$$H_\pi = \sum_{j=1}^{\eta}\sum_{q}^{N} \frac{1}{2m_e}\left(\mathbb{I}\otimes\mathbf{p}_j\otimes\mathbb{I} - \mathbb{I}\otimes\mathbb{I}\otimes\frac{e}{c}\mathbf{A}(q)\right)^2, \quad (10)$$

where we use the canonical quantization of the standard particle momentum $\mathbf{p}\rightarrow -i\boldsymbol{\nabla}$:

$$\begin{aligned} H_\pi &= \frac{1}{2m_e}\sum_{j}^{\eta}\sum_{q}^{N}\left(\mathbb{I}\otimes(-i\boldsymbol{\nabla}_j)\otimes\mathbb{I} - \mathbb{I}\otimes\mathbb{I}\otimes\frac{e}{c}\mathbf{A}(q)\right)^2 \\ &= \frac{1}{2m_e}\sum_{j}^{\eta}\sum_{q}^{N}\sum_{\mu=1}^{3}\Big(\mathbb{I}\otimes(-i\nabla_{j,\mu})\otimes\mathbb{I} \\ &\quad - \mathbb{I}\otimes\mathbb{I}\otimes\frac{e}{c}A_{q,\mu}\Big)^2 \\ &= \frac{1}{2m_e}\sum_{j}^{\eta}\sum_{q}^{N}\sum_{\mu=1}^{3}\Big(-\mathbb{I}\otimes\nabla^2_{j,\mu}\otimes\mathbb{I} + \mathbb{I}\otimes(i\frac{2e}{c}\nabla_{j,\mu}) \\ &\quad \otimes A_{q,\mu} + \mathbb{I}\otimes\mathbb{I}\otimes\frac{e^2}{c^2}A^2_{q,\mu}\Big), \end{aligned} \quad (11)$$

where $\boldsymbol{\nabla}_j$ is the position gradient operator over the 3D grid for particle j and $\mathbf{A}(q)$ represents the vector potential operator acting on the links connecting $\mathbf{q}$ to its adjacent point in each of the three Cartesian directions. Thus, here the summation over μ is implicit, which we will expand on later.

At each link (q,μ), $A_{q,\mu}$ can be expanded from the definition of $U_{q,\mu}$, as noted in Eq. (8) and the latter forms the "electric field ladder operators" along with its adjoint form. Using this representation, we can determine the form of $A_{q,\mu}$ as follows:

$$A_{q,\mu} = \frac{1}{i\Delta}\log\left(U_{q,\mu}\right), \quad (12)$$

$$A_{q,\mu} = \frac{1}{i\Delta}\log\left(\sum_{\epsilon=-\Lambda}^{\Lambda-1}|\epsilon+1\rangle\langle\epsilon|_{q,\mu}\right). \quad (13)$$

By construction, the matrix log of the above operator turns out to be diagonal in the Fourier-transformed basis, where $\mathcal{F}$ is the Fourier-transform operator:

$$\mathcal{F}A_{q,\mu}\mathcal{F}^\dagger = \frac{1}{i\Delta}\log(C)_{q,\mu}, \quad (14)$$

in which C is Sylvester's "clock" matrix,

$$C = \begin{pmatrix} 1 & 0 & 0 & \cdots & 0 \\ 0 & \omega & 0 & \cdots & 0 \\ 0 & 0 & \omega^2 & \cdots & 0 \\ \vdots & \vdots & \vdots & \ddots & \vdots \\ 0 & 0 & 0 & \cdots & \omega^{d-1} \end{pmatrix} \quad (15)$$

where $\omega = e^{2\pi i/d}$, d being the dimension of the matrix. Therefore,

$$\log(C) = \begin{pmatrix} 0 & 0 & 0 & \cdots & 0 \\ 0 & \frac{2\pi i}{d} & 0 & \cdots & 0 \\ 0 & 0 & \frac{2\times 2\pi i}{d} & \cdots & 0 \\ \vdots & \vdots & \vdots & \ddots & \vdots \\ 0 & 0 & 0 & \cdots & \frac{(d-1)2\pi i}{d} \end{pmatrix}. \quad (16)$$

Thus, as expected, the $A_{q,\mu}$ operator on an electric field link is diagonal in the Fourier-transformed electric field basis and so

$$A_{q,\mu} = \frac{1}{i\Delta}\mathcal{F}^{\dagger}\log(C)_{q,\mu}\mathcal{F}. \tag{17}$$

Lastly, the magnetic spin interaction matrix is defined as follows:

$$H_s = -\frac{e}{c}\sum_{j=1}^{\eta}\sum_{q}^{N}\boldsymbol{\sigma}_j\cdot\mathbf{B}(q) = -\frac{e}{c}\sum_{j=1}^{\eta}\sum_{q}^{N}\boldsymbol{\sigma}_j\cdot\left(\boldsymbol{\nabla}\times\mathbf{A}(q)\right), \tag{18}$$

where "×" denotes a vector cross product. This term is derived from the initial particle-field interaction term in Eq. (A1), using the Pauli vector identity, as is described in more detail in Appendix B. Expanding into a sum over Cartesian directions and separating the subspaces, the spin Hamiltonian becomes

$$H_s = -\frac{e}{c}\sum_{j}^{\eta}\sum_{q}^{N}\sum_{\mu\neq\nu\neq\xi}^{3}\sigma_{j,\mu}\otimes\mathbb{I}\otimes\left(\nabla_{\nu}A_{q,\xi}-\nabla_{\xi}A_{q,\nu}\right). \tag{19}$$

Throughout this work, we will assume atomic units, $\hbar = e = m_e = 4\pi\epsilon_0 = 1$, where ϵ_0 is the vacuum permittivity constant, unless otherwise noted. Therefore, the final form of the first-quantized Pauli-Fierz Hamiltonian in atomic units is

$$\begin{aligned}\hat{H}_{\text{PF}} = &\left(\frac{1}{\Delta}\sum_{k<j}^{\eta}\sum_{\mathbf{q},\mathbf{r}=1}^{N}\left(\mathbb{I}\otimes\frac{1}{||\mathbf{q}-\mathbf{r}||_2}\left|\mathbf{q}\right\rangle\left\langle\mathbf{q}\right|_k\left|\mathbf{r}\right\rangle\left\langle\mathbf{r}\right|_j\otimes\mathbb{I}\right)\right.\\
&\left.-\frac{1}{\Delta}\sum_{j=1}^{\eta}\sum_{\kappa=1}^{K}\sum_{\mathbf{q}=1}^{N}\left(\mathbb{I}\otimes\frac{Z_\kappa}{|\mathbf{q}-\mathbf{R}_\kappa\|_2}\left|\mathbf{q}\right\rangle\left\langle\mathbf{q}\right|_j\otimes\mathbb{I}\right)\right)\\
&+\left(\frac{1}{2}\sum_{j=1}^{\eta}\sum_{q=1}^{N}\sum_{\mu=1}^{3}\left(-\mathbb{I}\otimes(i\nabla_{j,\mu}\otimes\mathbb{I}\right.\right.\\
&\left.\left.-\,\mathbb{I}\otimes\mathbb{I}\otimes\frac{1}{c}A_{q,\mu}\right)^2\right)\\
&+\left(\sum_{q=1}^{N}\sum_{\mu=1}^{3}\mathbb{I}\otimes\mathbb{I}\otimes\frac{1}{2}E_{q,\mu}^2-\sum_{q=1}^{N}\sum_{\mu\neq\nu=1}^{3}W_{q,\mu,\nu}^2\right)\\
&-\left(\frac{1}{c}\sum_{j=1}^{\eta}\sum_{q=1}^{N}\sum_{\mu\neq\nu\neq\xi=1}^{3}\sigma_{j,\mu}\otimes\mathbb{I}\right.\\
&\left.\otimes\left(\nabla_\nu A_{q,\xi}-\nabla_\xi A_{q,\nu}\right)\right)\\
:=\;& H_V + H_\pi + H_f + H_s.\end{aligned} \tag{20}$$

For convenience of representation in later parts of this paper, we define the following:

$$H_\pi = H_{1\pi} + H_{2\pi} + H_{3\pi}, \tag{21}$$

where

$$\begin{aligned}H_{1\pi} &= \frac{1}{2}\sum_{j=1}^{\eta}\sum_{q=1}^{N}\sum_{\mu=1}^{3}-\mathbb{I}\otimes\nabla_{j,\mu}^2\otimes\mathbb{I},\\
H_{2\pi} &= \frac{1}{c}\sum_{j=1}^{\eta}\sum_{q=1}^{N}\sum_{\mu=1}^{3}\mathbb{I}\otimes(i\nabla_{j,\mu})\otimes A_{q,\mu},\\
H_{3\pi} &= \frac{1}{2c^2}\sum_{j=1}^{\eta}\sum_{q=1}^{N}\sum_{\mu=1}^{3}\mathbb{I}\otimes\mathbb{I}\otimes A_{q,\mu}^2;\\
H_f &= H_{f1} + H_{f2},\end{aligned} \tag{22}$$

where

$$\begin{aligned}H_{f1} &= \sum_{q=1}^{N}\sum_{\mu=1}^{3}\mathbb{I}\otimes\mathbb{I}\otimes\frac{1}{2}E_{q,\mu}^2,\\
H_{f2} &= -\sum_{q=1}^{N}\sum_{\mu\neq\nu=1}^{3}\mathbb{I}\otimes\mathbb{I}\otimes W_{q,\mu,\nu}^2;\end{aligned}$$

and

$$H_V = H_{V_{ee}} + H_{V_{ne}}, \tag{23}$$

where

$$\begin{aligned}H_{V_{ee}} &= \frac{1}{\Delta}\sum_{k<j}^{\eta}\sum_{\mathbf{q},\mathbf{r}=1}^{N}\left(\mathbb{I}\otimes\frac{1}{||\mathbf{q}-\mathbf{r}||_2}\left|\mathbf{q}\right\rangle\left\langle\mathbf{q}\right|_k\left|\mathbf{r}\right\rangle\left\langle\mathbf{r}\right|_j\otimes\mathbb{I}\right),\\
H_{V_{ne}} &= -\frac{1}{\Delta}\sum_{j=1}^{\eta}\sum_{\kappa=1}^{K}\sum_{\mathbf{q}=1}^{N}\left(\mathbb{I}\otimes\frac{Z_\kappa}{|\mathbf{q}-\mathbf{R}_\kappa\|_2}\left|\mathbf{q}\right\rangle\left\langle\mathbf{q}\right|_j\otimes\mathbb{I}\right).\end{aligned}$$

Our aim in the remainder of the work is to provide methods to block encode each of these pieces so that we can simulate them using qubitization as well as a divide-and-conquer scheme.

B. Recursive block encoding

In simulation algorithms such as qubitization [5,7] and quantum singular-value transformation (QSVT) [8], we need to block encode a matrix into a unitary in a higher-dimensional Hilbert space. In this section, we briefly describe this approach and discuss how block encodings can be recursed through an approach reminiscent of classical divide-and-conquer algorithms [66].

Definition 1 (Block encoding [8]). Suppose that A is an n-qubit operator, $\mu, \epsilon \in \mathbb{R}_+$, and $m \in \mathbb{N}$. We then say that the $(m+n)$-qubit unitary U_A is a (λ, m, ϵ) block encoding of A if

$$\|A - \lambda\left(\langle S| \otimes \mathbb{I}_n\right) U_A \left(|S\rangle \otimes \mathbb{I}_n\right)\|_\infty \leq \epsilon, \tag{24}$$

where $|S\rangle$ is an m-qubit state, also referred to as the "signal state."

We will often drop the second argument and write "$(\lambda, -, \epsilon)$ block encoding of A," because we focus on the gate complexity and the second argument only captures the extra ancilla needed in the block encoding. Often, for even more brevity, if $\epsilon = 0$, then we write "block encoding of A/λ."

Suppose, without loss of generality, that we have a Hamiltonian H_i expressed as a linear combination of unitaries (LCU), i.e., $H_i = \sum_{j=1}^{M_i} h_{ij} U_{ij}$, such that $\lambda_i = \sum_j |h_{ij}|$. In this case, we can have a $(\lambda_i, \log M_i, 0)$ block encoding of H_i using an ancilla-preparation subroutine and a unitary-selection subroutine, which we denote by PREP_i and SELECT_i, respectively:

$$\text{PREP}_i\, |0\rangle^{\log M_i} = \sum_{j=1}^{M_i} \sqrt{\frac{h_{ij}}{\lambda_i}}\, |j\rangle \tag{25}$$

$$\text{SELECT}_i = \sum_{j=1}^{M_i} |j\rangle\langle j| \otimes U_{ij} \tag{26}$$

It can be shown that [3]

$$\langle 0|\, \text{PREP}_i^\dagger \cdot \text{SELECT}_i \cdot \text{PREP}_i\, |0\rangle = \frac{H_i}{\lambda_i}. \tag{27}$$

Suppose that we have M Hamiltonians, $H_1, \ldots, H_M$, each of which has an LCU decomposition and for each one of them we define the subroutines as in Eqs. (25) and (26). Now, we use these subroutines to define the following:

$$\text{PREP}\, |0\rangle^{\log M + \sum_i \log M_i} = \left(\sum_{i=1}^{M} \sqrt{\frac{w_i \lambda_i}{\mathcal{A}}}\, |i\rangle\right) \otimes \bigotimes_{i=1}^{M} \text{PREP}_i \tag{28}$$

$$\text{SELECT} = \sum_{i=1}^{M} \left(|i\rangle\langle i| \otimes \bigotimes_{k=1}^{i-1} \mathbb{I} \otimes \text{SELECT}_i \otimes \bigotimes_{k=i+1}^{M} \mathbb{I} \right), \tag{29}$$

where $w_i > 0$ and $\mathcal{A} = \sum_{i=1}^{M} w_i \lambda_i$. We can use the above two subroutines to block encode a linear combination of Hamiltonians, i.e., we can show that

$$(\langle 0| \otimes 1)\text{PREP}^\dagger \cdot \text{SELECT} \cdot \text{PREP}(|0\rangle \otimes 1) = \frac{1}{\mathcal{A}} \sum_{i=1}^{M} w_i H_i.$$

Similar approaches have been used in previous works such as Refs. [8,18,20] but we provide a general and rigorous statement of this recursive-block-encoding result in the following theorem, where we provide a formal statement.

Theorem 1. Let $H = \sum_{i=1}^{M} w_i H_i$ be the sum of M Hamiltonians and let each of them be expressed as a sum of unitaries, as $H_i = \sum_{j=1}^{M_i} h_{ij} U_{ij}$, such that $\lambda_i = \sum_j |h_{ij}|$, $w_i > 0$. Each of the summand Hamiltonians is block encoded using the subroutines defined in Eqs. (25) and (26). Then, we can have an $(\mathcal{A}, \lceil \log_2(M) \rceil, 0)$ block encoding of H, where $\mathcal{A} = \sum_{i=1}^{M} w_i \lambda_i$, using the ancilla-preparation subroutine (PREP) defined in Eq. (28) and the unitary-selection subroutine (SELECT) defined in Eq. (29):

(1) The PREP subroutine has an implementation cost of $\mathcal{C}_{\text{PREP}} = \sum_{i=1}^{M} \mathcal{C}_{\text{PREP}_i} + \mathcal{C}_w$, where $\mathcal{C}_{\text{PREP}_i}$ is the number of gates to implement PREP_i and $\mathcal{C}_w$ is the cost of preparing the state $\sum_{i=1}^{M} \sqrt{w_i \lambda_i / \mathcal{A}}\, |i\rangle$.

(2) The SELECT subroutine can be implemented with a set of multicontrolled-X gates, $\{M_i$ pairs of $C^{\log_2 M_i + 1} X$ gates : $i = 1, \ldots, M\}$, M pairs of $C^{\log M} X$ gates, and $\sum_{i=1}^{M} M_i$ single-controlled unitaries, $\{cU_{ij} : j = 1, \ldots, M_i; i = 1, \ldots, M\}$.

The proof is given in Appendix C, where we argue that we require fewer gates if we divide and block encode, instead of block encoding H as a sum of $M' = \sum_{i=1}^{M} M_i$ unitaries. As an example, let us compare the number of controlled-NOT (CNOT) and T gates required to implement the SELECT subroutine as follows:

$$\begin{aligned}\text{SELECT} : &|i\rangle\, |0, k_1\rangle_1 \ldots |1, j\rangle_i \ldots |0, k_M\rangle_M\, |\psi\rangle \\ &\mapsto |i\rangle\, |0, k_1\rangle_1 \ldots |1, j\rangle_i \ldots |0, k_M\rangle_M\, U_{ij}\, |\psi\rangle\,.\end{aligned}$$

In the above, we have represented each set of ancilla qubits in the $M+1$ subspaces of PREP as a separate register. We allot one ancilla qubit, initialized to 0, for each PREP_i register. If the state of the first register containing $\log M$ qubits is $|i\rangle$, then the ith register corresponding to PREP_i is selected by flipping this ancilla to 1. We require M (compute-uncompute) pairs of $C^{\log_2 M} X$ gates and M ancillas to make this selection. Now, if the state of the PREP_i register is $|j\rangle$, then we select the jth unitary in the LCU decomposition of H_i, i.e., U_{ij}. To select unitaries of the ith Hamiltonian H_i, we require M_i pairs of $C^{\log_2 M_i + 1} X$. Decomposing these multicontrolled-NOT gates [67,68], we require $\sum_i M_i (4 \log(M_i + 1) - 4) + M(4 \log M - 4)$ T gates and $\sum_i M_i (4 \log(M_i + 1) - 3) + M(4 \log M - 3)$ CNOT gates. The use of logical AND gadgets reduces the gate complexity in the uncomputation part.

Now suppose that we block encode H as a sum of $M' = \sum_{i=1}^{M} M_i$ unitaries. In the SELECT$'$ subroutine, we have M' unitaries, each controlled on $\log_2 M'$ qubits. Each of them, in turn, can be implemented with a (compute-uncompute) pair of $C^{\log_2 M'}X$ and one controlled unitary. Decomposing the multicontrolled-NOT in terms of Clifford+T gates [67, 68], we see that we require at most $M'(4\log_2 M' - 4)$ T gates and $M'(4\log_2 M' - 3)$ CNOT gates.

Thus the difference in the T-gate-count estimate is

$$\sum_i M_i(4\log(M_i+1)-4) + M(4\log M - 4) - \left(4\log\left(\sum_i M_i\right) - 4\right)\left(\sum_i M_i\right) = 4\sum_i M_i \log\left(\frac{M_i+1}{\sum_j M_j}\right) + 4M\log M - 4M,$$

which is less than 0 in most cases. Similarly, we can show that the difference in the CNOT count estimate is

$$4\sum_i M_i \log\left(\frac{M_i+1}{\sum_j M_j}\right) + 4M\log M - 3M,$$

which is again less than 0 in most cases. We use the same number of controlled unitaries in both approaches. Thus, using the divide-and-conquer technique (Theorem 1), it is possible to reduce the implementation cost in terms of the gate count, especially with regard to T gates and CNOT gates.

More details can be found in Appendix C, where we have also explained that we can follow such an approach to block encode the product of Hamiltonians using fewer gates.

Remark 1 (Sum of same Hamiltonians but acting on disjoint subspaces). Suppose, in Theorem 1, that all the H_i are the same but that they act on disjoint subspaces. In this case, each PREP$_i$ is the same and so it is sufficient to keep only one copy of PREP$_i$ in the PREP subroutine of Eq. (28). We can absorb w_i in the weights of the unitaries obtained in the LCU decomposition of H_i. Thus, in this case, we have

$$\text{PREP}\,|0\rangle^{\log M + \log M_i} = \left(\sqrt{\frac{1}{M}}\sum_{i=1}^{M}|i\rangle\right) \otimes \text{PREP}_i. \tag{30}$$

We require only $\lceil \log M \rceil$ Hadamard (H) gates to prepare the superposition in the first register by padding out the number of such subspaces to be a power of 2. This step can be avoided, although standard approaches require amplitude amplification [20]. With this modification in mind, we also need to make slight modifications in the SELECT procedure. This time, we keep an extra ancilla qubit, initialized to 0, in each subspace. Given a particular state of the first register, we select a subspace by flipping the qubit in the corresponding subspace. The unitaries in each subspace are now additionally controlled on this qubit (of its own subspace). In Appendix C, we discuss the more general situation when each PREP$_i$ is the same but the Hamiltonians H_i are different.

We can further optimize the number of gates by implementing the group of multicontrolled unitaries in the SELECT subroutines, using the following theorem. Here, we partition the control qubits into different groups, store intermediate information in some ancillas, and then implement the required logic using these intermediate results.

Theorem 2. Consider the unitary $U = \sum_{j=0}^{M-1} |j\rangle\langle j| \otimes U_j$ for unitary operators U_j that can be implemented controllably. Let us assume that M is a power of 2 for simplicity. Suppose that we have $\log_2 M$ qubits and M (compute-uncompute) pairs of $C^{\log_2 M}X$ gates for selecting the M basis states. Let $r_1, \ldots, r_n \geq 1$ be positive fractions such that $\sum_{i=1}^{n} 1/r_i = 1$ and $\log_2 M/r_i$ are integers. Then, U can be implemented using a circuit with

$$\sum_{i=1}^{n} M^{\frac{1}{r_i}} C^{\frac{\log_2 M}{r_i}} X + MC^n X$$

(compute-uncompute) pairs of gates, M applications of controlled U_j, and at most $\sum_{i=1}^{n} M^{1/r_i}$ ancillas.

The proof is provided in Appendix D. Following the construction in Refs. [67,68], the number of T gates required to implement such multiply controlled gates is

$$\mathcal{T}_n = \sum_{i=1}^{n} M^{\frac{1}{r_i}} \left(\frac{4\log_2 M}{r_i} - 4\right) + M(4n-4) \tag{31}$$

and the difference between the T-count estimates with and without splitting is

$$\mathcal{T}_1 - \mathcal{T}_n = M(4\log_2 M - 4) - \sum_{i=1}^{n} M^{\frac{1}{r_i}}\left(\frac{4\log_2 M}{r_i} - 4\right) - M(4n-4) = 4M(\log_2 M - n) - 4\sum_{i=1}^{n} M^{\frac{1}{r_i}}\left(\frac{\log_2 M}{r_i} - 1\right), \tag{32}$$

which can be positive for many values of $n, r_1, r_2, \ldots, r_n$. For example, if each $1/r_i = 1/n$, i.e., we divide the control qubits into equal-sized groups, then

$$(\mathcal{T}_1 - \mathcal{T}_n)' = 4M(\log_2 M - n) - 4nM^{\frac{1}{n}}\left(\frac{\log_2 M}{n} - 1\right) = 4\left(M - M^{\frac{1}{n}}\right)\left(\log_2 M - n\right), \tag{33}$$

which is 0 if $n = 1$ and $n = \log_2 M$ and is greater than 0 for every $1 < n < \log_2 M$. More illustrations are given in

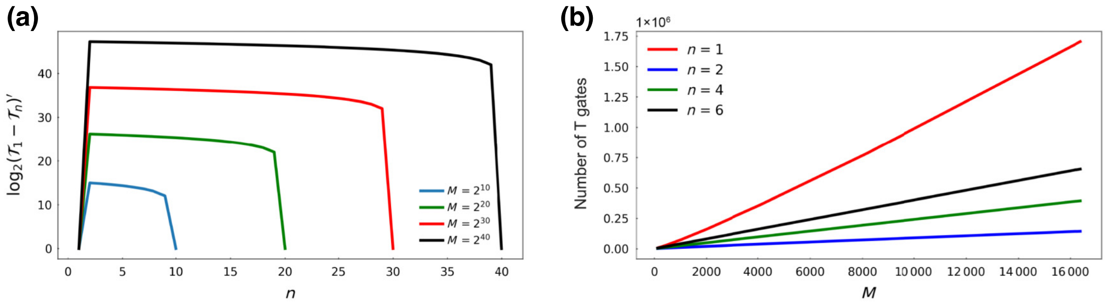

FIG. 1. (a) The logarithm of the difference in the T-gate-count estimates for a SELECT operation with M controlled unitaries, denoted by $(\mathcal{T}_1-\mathcal{T}_n)'$, for various numbers of partitions n, for the case when each partition has an equal number of control qubits, i.e., $\log_2 M/n$. In these cases, we see that the optimal division occurs when $n=2$, which corresponds to the set being split in half. (b) The number of pairs of T gates for different values of M and numbers of partitions n, when we make equal partitioning. In these cases, we observe that the case in which the controls of the SELECT circuit are split into two groups outperforms the other splittings considered.

Fig. 1(a), where we show the variation of this difference [Eq. (33)] for different values of n and M and we find that the maximum difference occurs when we divide into two equal parts. It can be shown that when $0<1/r_i\leq\frac{1}{2}$, then $M^{1/r_i}(\log_2 M/r_i)\leq K'M$, for a large enough constant K'. So, we can say that the number of T gates and CNOT gates is in $O(M)$, saving logarithmic factors in the asymptotic complexity. This bound also holds for many $1/r_i>\frac{1}{2}$ but breaks down at $r_i=1$. In Fig. 1(b), we compare the number of T gates for different values of n when the size of each partition is the same [Eq. (31)]. The linear growth is evident from the curves. Similarly, we can show that we can have a reduction in the number of CNOT gates. With the help of logical AND gadgets, we do not need to use any T gate for the uncomputation part.

C. Algorithm I: Divide and conquer—recursive Trotter splitting

The notion of the divide-and-conquer approach to simulation is simple. The core idea behind it is that a Trotter splitting can be used as a means of dividing the simulation into smaller parts, each of which can be directly simulated or further subdivided into smaller parts. The recursive division of the Hamiltonian naturally forms a tree, as depicted in Fig. 2. The partitions of the Hamiltonian are found according to a heuristic based on various criteria, such as the norm, commutativity, etc., and then simulation of each fragment is performed using different simulation algorithms with sufficient accuracy. We can repeatedly divide each fragment and use the Trotter-Suzuki formula [57,58] to bound the error in the exponentials. The resulting number of operations is bounded by the result of the following theorem.

Theorem 3. Let $p_1\geq 1$ be a constant. Assuming that $\eta,K\leq N$, $1/c\Delta^2\in o(1)$ and $K,Z_{\rm sum}\in O(\eta)$, it is possible to simulate $e^{-i\hat{H}_{\rm PF}t}$ with error ϵ, using a divide-and-conquer algorithm, with gate complexity in

$$\widetilde{O}\left(N^2 t\log^2\Lambda\left(\frac{\eta}{\Delta^2}+\Lambda^2\right)\left(\frac{t\eta}{\epsilon\Delta^2\Lambda}\right)^{\frac{1}{p_1}}\right).$$

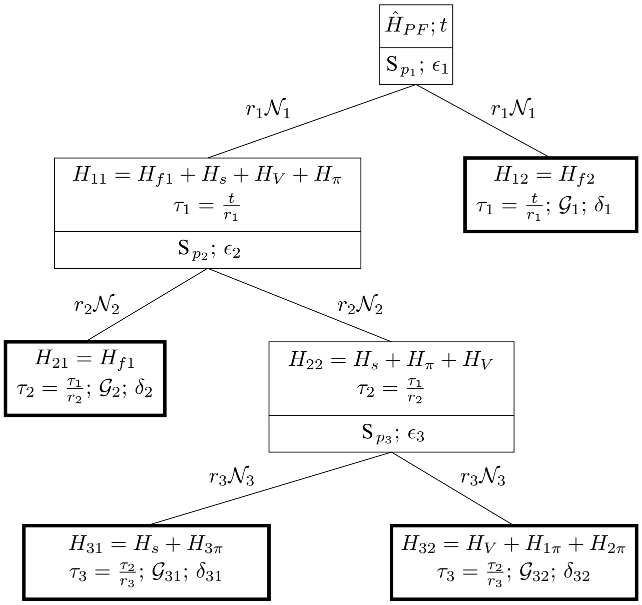
$\hat{H}_{PF};t$
$\mathrm{S}_{p_1};\,\epsilon_1$
$r_1\mathcal{N}_1$
$r_1\mathcal{N}_1$
$H_{11}=H_{f1}+H_s+H_V+H_\pi$
$\tau_1=\frac{t}{r_1}$
$\mathrm{S}_{p_2};\,\epsilon_2$
$H_{12}=H_{f2}$
$\tau_1=\frac{t}{r_1};\,\mathcal{G}_1;\,\delta_1$
$r_2\mathcal{N}_2$
$r_2\mathcal{N}_2$
$H_{21}=H_{f1}$
$\tau_2=\frac{\tau_1}{r_2};\,\mathcal{G}_2;\,\delta_2$
$H_{22}=H_s+H_\pi+H_V$
$\tau_2=\frac{\tau_1}{r_2}$
$\mathrm{S}_{p_3};\,\epsilon_3$
$r_3\mathcal{N}_3$
$r_3\mathcal{N}_3$
$H_{31}=H_s+H_{3\pi}$
$\tau_3=\frac{\tau_2}{r_3};\,\mathcal{G}_{31};\,\delta_{31}$
$H_{32}=H_V+H_{1\pi}+H_{2\pi}$
$\tau_3=\frac{\tau_2}{r_3};\,\mathcal{G}_{32};\,\delta_{32}$

FIG. 2. A tree depicting the partition of the Hamiltonian at different stages. In each rectangular node, we mention the Hamiltonian and the time interval. If the Hamiltonian is partitioned, i.e., it is a parent node, then we divide the rectangle and in the lower half we mention the order of the Trotter-Suzuki formula and the error incurred due to splitting. The leaf nodes (thick rectangles) store the Hamiltonians that are simulated. They store information about the time, gate, and simulation error. The edges are labeled by the number of segments of the time interval of the parent and the number of exponentials (copies of each child node) obtained after applying the Trotter-Suzuki formula.

We take two factors into account for grouping the Hamiltonian terms. First, we consider the pairwise commutators. This is because the error introduced due to splitting is determined by the expansion of the Trotter-Suzuki formula, given in Ref. [58], and depends on the norm of the nested commutators [58]. From Lemma 7 (stated later), we find that the pairwise commutators play a significant role in bounding the nested commutators, especially for lower-order formulas. We must keep in mind that as we increase the order, the number of exponentials and hence the complexity increases. Our algorithm mitigates these errors by grouping together terms with larger commutator bounds, so that this does not reflect on the overall error. The second factor that we consider is the ℓ_1 norm of the fragment Hamiltonians. Specifically, we consider the ℓ_1 norm of the coefficients in an LCU decomposition of the Hamiltonian and this also serves as an upper bound on the spectral norm of the Hamiltonian. In simulation algorithms such as those in Refs. [4,5,7,8] the block encoding of the Hamiltonian is repeated a number of times, proportional to its ℓ_1 norm. So, if we block encode terms with small norm together with terms with larger norm, then we end up repeating the smaller norm terms more frequently than is necessary. Instead, we group these terms separately and adjust the error accordingly. We summarize the different ℓ_1-norm and pairwise commutators in Tables II and III and in Appendices F and H we give a more detailed description of our calculations.

Let $U = e^{-i\hat{H}_{\text{PF}}t}$, where t is the total evolution time and $\widetilde{U}$ is the final unitary that we implement. In the first level of splitting, we divide $\hat{H}_{\text{PF}}$ into two parts, i.e., $\hat{H}_{\text{PF}} = H_{11} + H_{12}$, where $H_{11} = H_{f1} + H_s + H_V + H_\pi$ and $H_{12} = H_{f2}$. This is because the innermost commutators between H_s, H_V, and H_π are significantly higher (Table III) and we have tried to avoid terms with Λ. By grouping them together, we have tried to keep the error small and independent of Λ. We divide t into r_1 intervals, each of length $\tau_1 = t/r_1$, such that we can approximate the Trotter-Suzuki formula of order p_1 well within each time segment. If $\widehat{U}$ is the unitary that we obtain by approximating U, then invoking [69,

TABLE II. A summary of the number of unitaries in the decomposition of different Hamiltonians and operators and an upper bound on the ℓ_1 norm of the coefficients in an LCU decomposition of the Hamiltonian. The latter is also an upper bound on the spectral norm of the Hamiltonian. In the last column, we have mentioned the unitaries occurring in the decompositions of the operators. For A^2 and E^2, we have given the unitaries for the decomposition provided in this paper, which yields the number of unitaries shown in brackets. Here, $2a+1$ is the number of points used in the finite-difference approximation and h is the spatial scaling of the grid used in the finite-difference formula.

Hamiltonian or operator	Number of unitaries	ℓ_1 norm	Types of unitaries
A	$\lceil \log_2 d \rceil + 1$	$\frac{2\pi}{\Delta}$	Z (Corollary 1)
A^2	$2\lceil \log_2 d \rceil \left(\text{or } \frac{\log_2^2 d + \log_2 d}{2}\right)$	$\frac{4\pi^2}{\Delta^2}$	Z (Corollary 2)
∇	$2a$	$\frac{\ln(2a^2)}{h}$	Adder (Lemma 18)
∇^2	$2a+1$	$\frac{4\pi^2}{3h^2}$	Adder (Lemma 16)
E^2	$2\log_2 \Lambda \left(\text{or } \frac{\log_2^2 \Lambda + \log_2 \Lambda + 2}{2}\right)$	Λ^2	Z [Eq. (F6)]
U	1	1	Rotation, QFT (Corollary 3)
$H_{1\pi}$	$6a\eta N$	$\frac{8\pi^2\eta N}{h^2}$	·
$H_{2\pi}$	$6a\eta N \log_2 d$	$\frac{12\pi\eta N \ln 2a^2}{ch\Delta}$	·
$H_{3\pi}$	$6\eta N \log_2 d$	$\frac{12\pi^2\eta N}{c^2\Delta^2}$	·
$H_{V_{ee}}$	$\frac{\eta(\eta-1)N}{2}$	$\frac{\eta(\eta-1)}{2\Delta^2}$	·
$H_{V_{ne}}$	$\eta L N$	$\frac{\eta}{\Delta^2}\left(\sum_{\kappa=1}^{K} \lvert Z_\kappa \rvert\right) := \frac{\eta Z_{\text{sum}}}{\Delta^2}$	·
H_{f1}	$6N \log_2 \Lambda$	$\frac{3N\Lambda^2}{2}$	·
H_{f2}	$6N$	$6N$	·
H_s	$12\eta N a \log_2 d$	$\frac{12\pi\eta N \ln 2a^2}{ch\Delta}$	·

TABLE III. A summary of the bounds on the norm of the pairwise commutators between types of terms that appear in the Pauli-Fierz Hamiltonian. Components that can be computed using the antisymmetry of the commutator have been dropped from the table for clarity.

	H_π	$H_{V_{ee}}$	$H_{V_{ne}}$	$H_{f\,1}$	$H_{f\,2}$	H_s
H_π	0	$\cdots$	$\cdots$	$\cdot$	$\cdot$	$\cdot$
$H_{V_{ee}}$	$\frac{4\pi\eta(\eta-1)N^{8/3}}{h^2\Delta^2}\left(\pi+\frac{6h\ln(2a^2)}{c\Delta}\right)$	0	-	$\cdot$	$\cdot$	$\cdot$
$H_{V_{ne}}$	$\frac{4\pi\eta N^{5/3}KZ_{\max}}{h^2\Delta^2}\left(\pi+\frac{6h\ln(2a^2)}{h\Delta}\right)$	-	0	$\cdot$	$\cdot$	$\cdot$
$H_{f\,1}$	$\frac{6\pi\eta N\Lambda^2}{c\Delta}\left(\frac{\ln(2a^2)}{h}+\frac{2\pi}{c\Delta}\right)$	0	0	0	$\cdot$	$\cdot$
$H_{f\,2}$	$\frac{198\pi\eta N}{c\Delta}\left(\frac{\ln(2a^2)}{h}+\frac{\pi}{c\Delta}\right)$	0	0	$12N\Lambda$	0	$\cdot$
H_s	$\frac{96\pi^2\eta^2N\ln(2a^2)}{hc^2\Delta^2}\left(\frac{\ln(2a^2)}{h}+\frac{\pi}{c\Delta}\right)$	0	0	$\frac{24\pi\eta N\Lambda^2\ln(2a^2)}{ch\Delta}$	$\frac{288\pi\eta N\ln(2a^2)}{ch\Delta}$	0

Box 4.1],

$$\begin{aligned}\|U-\widehat{U}\| &= \|\left(e^{-i\hat{H}_{\mathrm{PF}}t/r_1}\right)^{r_1}-\left(\mathscr{S}_{p_1}(H_{11},H_{12};t/r_1)\right)^{r_1}\|\\ &\le r_1\|e^{-i\hat{H}_{\mathrm{PF}}\tau_1}-\mathscr{S}_{p_1}(H_{11},H_{12},\tau_1)\| := r_1\epsilon_1.\end{aligned}\tag{34}$$

Suppose, after approximating $e^{-i\hat{H}_{\mathrm{PF}}\tau_1}$ using the Trotter-Suzuki formula, that we obtain at most $\mathcal{N}_1$ terms of the form $e^{-iH_{11}\tau_1}=U^{(1)}_{1\tau_1}$ and $e^{-iH_{12}\tau_1}=U^{(1)}_{2\tau_1}$. We denote the unitary implementation of $U_{1\tau}$ and $U_{2\tau}$ by $\widetilde{U}^{(1)}_{1\tau_1}$ and $\widetilde{U}^{(1)}_{2\tau_1}$, respectively. Thus,

$$\begin{aligned}\|\widehat{U}-\widetilde{U}\| &\le r_1\mathcal{N}_1\|U^{(1)}_{1\tau_1}-\widetilde{U}^{(1)}_{1\tau_1}\|+r_1\mathcal{N}_1\|U^{(1)}_{2\tau_1}-\widetilde{U}^{(1)}_{2\tau_1}\|\\ &:= r_1\mathcal{N}_1\|U^{(1)}_{1\tau_1}-\widetilde{U}^{(1)}_{1\tau_1}\|+r_1\mathcal{N}_1\delta_1.\end{aligned}\tag{35}$$

Thus, after the first level of splitting in the figure, using Eqs. (34) and (35), we have

$$\begin{aligned}\|U-\widetilde{U}\| &\le \|U-\widehat{U}\|+\|\widehat{U}-\widetilde{U}\|\\ &\le r_1\epsilon_1+r_1\mathcal{N}_1\delta_1+r_1\mathcal{N}_1\|U^{(1)}_{1\tau_1}-\widetilde{U}^{(1)}_{1\tau_1}\|.\end{aligned}\tag{36}$$

In the second level of splitting depicted in the figure, we divide H_{11} into two groups, $H_{21}=H_{f\,1}$ and $H_{22}=H_s+H_V+H_\pi$. We further divide τ_1 into r_2 intervals, each of length $\tau_2=\tau_1/r_2$. Let $\widehat{U}^{(1)}_{1\tau_1}$ be the unitary that we obtain by approximating $U^{(1)}_{1\tau_1}$ with a Trotter-Suzuki formula of order p_2. Then,

$$\begin{aligned}&\|U^{(1)}_{1\tau_1}-\widehat{U}^{(1)}_{1\tau_1}\|\\ &\quad=\|\left(e^{-iH_{11}\tau_1/r_2}\right)^{r_2}-\left(\mathscr{S}_{p_2}(H_{21},H_{22};\tau_1/r_2)\right)^{r_2}\|\\ &\quad\le r_2\|e^{-iH_{11}\tau_2}-\mathscr{S}_{p_2}(H_{21},H_{22};\tau_2)\|. := r_2\epsilon_2,\end{aligned}\tag{37}$$

After approximating $e^{-iH_{11}\tau_2}$, suppose that we obtain at most $\mathcal{N}_1$ $e^{-iH_{21}\tau_2}=U^{(2)}_{1\tau_2}$ and $e^{-iH_{22}\tau_2}=U^{(2)}_{2\tau_2}$. The unitary implementations of $e^{-iH_{21}\tau_2}$ and $e^{-iH_{22}\tau_2}$ are denoted by $\widetilde{U}^{(2)}_{1\tau_2}$ and $\widetilde{U}^{(2)}_{2\tau_2}$, respectively. Thus,

$$\begin{aligned}&\|\widehat{U}^{(1)}_{1\tau_1}-\widetilde{U}^{(1)}_{1\tau_1}\|\\ &\quad\le r_2\mathcal{N}_2\|U^{(2)}_{1\tau_2}-\widetilde{U}^{(2)}_{1\tau_2}\|+r_2\mathcal{N}_2\|U^{(2)}_{2\tau_2}-\widetilde{U}^{(2)}_{2\tau_2}\|\\ &\quad:= r_2\mathcal{N}_2\delta_2+r_2\mathcal{N}_2\|U^{(2)}_{2\tau_2}-\widetilde{U}^{(2)}_{2\tau_2}\|\end{aligned}\tag{38}$$

and so by plugging Eqs. (37) and (38) into Eq. (36), we obtain the following after the second level of splitting:

$$\begin{aligned}\|U-\widetilde{U}\| &\le r_1\epsilon_1+r_1\mathcal{N}_1\delta_1+r_1\mathcal{N}_1\left(r_2\epsilon_2+r_2\mathcal{N}_2\delta_2\right.\\ &\quad\left.+\,r_2\mathcal{N}_2\|U^{(2)}_{2\tau_2}-\widetilde{U}^{(2)}_{2\tau_2}\|\right).\end{aligned}\tag{39}$$

In the third level of splitting, we divide H_{22} into two groups, $H_{31}=H_s+H_{3\pi}$ and $H_{32}=H_V+H_{1\pi}+H_{2\pi}$. We also divide τ_2 into r_3 intervals, each of length $\tau_3=\tau_2/r_3$. Let $\widehat{U}^{(2)}_{2\tau}$ be the unitary that we obtain by approximating $U^{(2)}_{2\tau_2}$ with a Trotter-Suzuki formula of order p_3. Then,

$$\begin{aligned}&\|U^{(2)}_{2\tau_2}-\widehat{U}^{(2)}_{2\tau_2}\|\\ &\quad=\|\left(e^{-iH_{22}\tau_2/r_3}\right)^{r_3}-\left(\mathscr{S}_{p_3}(H_{31},H_{32};\tau_2/r_3)\right)^{r_3}\|\\ &\quad\le r_3\|e^{-iH_{22}\tau_3}-\mathscr{S}_{p_3}(H_{31},H_{32};\tau_3)\| := r_3\epsilon_3.\end{aligned}\tag{40}$$

After approximation, suppose that we obtain at most $\mathcal{N}_3$ $e^{-iH_{31}\tau_3}:=U^{(3)}_{1\tau_3}$ and $e^{-iH_{32}\tau_3}:=U^{(3)}_{2\tau_3}$. The unitary implementations of $e^{-iH_{31}\tau_3}$ and $e^{-iH_{32}\tau_3}$ are denoted by $\widetilde{U}^{(3)}_{1\tau_3}$ and $\widetilde{U}^{(3)}_{2\tau_3}$, respectively. So,

$$\begin{aligned}\|\widehat{U}^{(2)}_{2\tau_2}-\widetilde{U}^{(2)}_{2\tau_2}\| &\le r_3\mathcal{N}_3\|U^{(3)}_{1\tau_3}-\widetilde{U}^{(3)}_{1\tau_3}\|\\ &\quad+r_3\mathcal{N}_3\|U^{(3)}_{2\tau_3}-\widetilde{U}^{(3)}_{2\tau_3}\|\\ &:= r_3\mathcal{N}_3\delta_{31}+r_3\mathcal{N}_3\delta_{32}\end{aligned}\tag{41}$$

and hence plugging Eqs. (40) and (41) into Eq. (39), we obtain the following bound on the simulation error after the third and final level of splitting:

$$\begin{aligned}\|U-\widetilde{U}\| &\leq r_1\epsilon_1 + r_1\mathcal{N}_1\delta_1 + r_1r_2\mathcal{N}_1\epsilon_2 + r_1r_2\mathcal{N}_1\mathcal{N}_2\delta_2\\ &\quad + r_1r_2\mathcal{N}_1\mathcal{N}_2\left(r_3\epsilon_3 + r_3\mathcal{N}_3\delta_{31} + r_3\mathcal{N}_3\delta_{32}\right)\\ &= r_1\epsilon_1 + r_1\mathcal{N}_1\delta_1 + r_1r_2\mathcal{N}_1\epsilon_2\\ &\quad + r_1r_2\mathcal{N}_1\mathcal{N}_2\delta_2 + r_1r_2r_3\mathcal{N}_1\mathcal{N}_2\epsilon_3\\ &\quad + r_1r_2r_3\mathcal{N}_1\mathcal{N}_2\mathcal{N}_3(\delta_{31}+\delta_{32}). \end{aligned} \tag{42}$$

Let the numbers of gates required to implement the unitaries $U^{(1)}_{2\tau_1}, U^{(2)}_{1\tau_2}, U^{(3)}_{1\tau_3}$, and $U^{(3)}_{2\tau_3}$ be $\mathcal{G}_1$, $\mathcal{G}_2$, $\mathcal{G}_{31}$, and $\mathcal{G}_{32}$, respectively. Thus, the total number of gates for implementing $U = e^{-i\hat{H}_{\rm PF}t}$ is

$$\begin{aligned}\mathcal{G} &\leq r_1\mathcal{N}_1\mathcal{G}_1 + r_1r_2\mathcal{N}_1\mathcal{N}_2\mathcal{G}_2\\ &\quad + r_1r_2r_3\mathcal{N}_1\mathcal{N}_2\mathcal{N}_3\left(\mathcal{G}_{31}+\mathcal{G}_{32}\right). \end{aligned} \tag{43}$$

We summarize the above results in the following lemma. For simplicity, we assume that the time lengths are always exactly divisible by the number of segments. This lemma can be generalized for arbitrary divisions, for which we can draw a tree similar to Fig. 2, which may be useful in deriving bounds on the error and gate complexity.

Lemma 1. Let $\mathcal{N}_1$, $\mathcal{N}_2$, and $\mathcal{N}_3$ be the number of operator exponentials that appear in the divide-and-conquer simulation method given in Fig. 2, where the τ_i refer to the time step, ϵ_i the error tolerance at the level of the division, δ_i is the synthesis error that is tolerable, and $\mathcal{G}_i$ represents the gate count required for implementing the resulting exponentials. If $U = e^{-i\hat{H}_{\rm PF}t}$ and $\widetilde{U}$ is the final unitary implementation of U, then the total simulation error is

$$\begin{aligned}\|U-\widetilde{U}\| &= r_1\left(\epsilon_1 + \mathcal{N}_1\left(\delta_1 + r_2\left(\epsilon_2 + \mathcal{N}_2\left(\delta_2 + r_3\epsilon_3\right.\right.\right.\right.\\ &\quad \left.\left.\left.\left. +\ r_3\mathcal{N}_3(\delta_{31}+\delta_{32})\right)\right)\right)\right)\end{aligned}$$

and the total number of gates required is

$$\mathcal{G} \leq r_1\mathcal{N}_1\left(\mathcal{G}_1 + r_2\mathcal{N}_2\left(\mathcal{G}_2 + r_3\mathcal{N}_3\left(\mathcal{G}_{31}+\mathcal{G}_{32}\right)\right)\right).$$

We describe the algorithms to simulate the exponentials of the four fragments H_{12}, H_{21}, H_{31}, and H_{32} in Appendix G. Above, we state the complexity of the circuits in terms of Clifford+T and (controlled)-rotation gates. Clifford+T is one of the most popular fault-tolerant universal gate sets but not all unitaries can be exactly implementable by it. Therefore, we have used rotation gates, which are the only approximately implementable gates that we use. The T-count of the (controlled-)rotation gate is proportional to the logarithm of the synthesis error [70–73] and thus low T-counts are often observed for reasonable error budgets. In all cases, we have separately reported the complexity of the (controlled-)rotation gates, without further decomposing it with the Clifford+T gate set. This is because in this paper we do not account for the gate-synthesis error.

The decomposition of the operators is described explicitly in Appendix F. We summarize these decompositions in Table II. We give the number of unitaries and the ℓ_1 norm and for the operators in the last column we mention the types of unitaries in these decompositions. For our analysis, we also require bounds on the pairwise commutators of the different Hamiltonian partitions. We summarize these bounds in Table III and we give a detailed derivation in Appendix H.

Here, in the following lemmas, we summarize the bounds on the total number of gates required for simulating each of the fragment Hamiltonians. This information will be useful for deriving the complexity of simulating $e^{-i\hat{H}_{\rm PF}t}$, using both of the algorithms that we consider. The proofs can be found in Appendixes G 1–G 4. Here, we give some brief explanations of mainly the PREP and SELECT subroutines while block encoding.

Lemma 2. Let $H_{12} = -\sum_{q=1}^{N}\sum_{\mu\neq\nu=1}^{3}\mathbb{I}\otimes\mathbb{I}\otimes W^2_{q,\mu,\nu}$, where $W^2_{q,\mu,\nu}$ is the plaquette operator described in Eq. (9). Then, we require

$$\mathcal{G}'_1 \in O\left(N\log d\right)$$

gates to have a $(6N,-,0)$ block encoding of H_{12} and hence the number of gates required for simulating $e^{iH_{12}\tau_1}$ with error $\delta_{12} > 0$, using qubitization, is

$$\mathcal{G}_1 \in O\left(N^2\tau_1\log d + \frac{\log(1/\delta_{12})}{\log\log(1/\delta_{12})}N\log d\right).$$

We know that $H_{12} = H_{f2}$ [Eq. (22)], which corresponds to the plaquette terms in the dynamics of the system. In Corollary 3, we show that the raising operator $U_{q,\mu}$ [defined in Eq. (8)] is as follows:

$$U_{q,\mu} = \mathcal{F}_{q,\mu}\left(\bigotimes_{k=1}^{\log_2 d-1} R_z(\theta_k)\right)_{q,\mu}\mathcal{F}^{\dagger}_{q,\mu},$$

where $\theta_k = \frac{2\pi}{d}2^k$ and $\mathcal{F}$ is the Fourier transform. This shows that an individual $U_{q,\mu}$ can be implemented using $\log_2(d)$ single-qubit rotations. The plaquette operator $W_{q,\mu,\nu}$ can be implemented using four such terms and thus $W^2_{q,\mu,\nu}$ [Eq. (9)] can be implemented by a layer of at most $4\log_2 d$ parallel rotations, conjugated by Fourier transformation. The ancilla-preparation subroutine does the following:

$$\text{PREP}_{f\,2}\,|0\rangle^{*} = \left(\frac{1}{\sqrt{N}}\sum_{q=1}^{N}|q\rangle\right)\otimes\left(\frac{1}{\sqrt{6}}\sum_{\mu\neq\nu=1}^{3}\sum_{k=0}^{1}|\mu\rangle\,|\nu\rangle\,|k\rangle\right).$$

First, we have the $\log_2 N$-qubit electric link index register that stores the N electric link indices in equal superposition. Next, we have the $(4+1)$-qubit spin-index register. The first four qubits store the value of μ, ν. The last qubit indicates whether we apply the H.c. If $\mu = \nu$ or $\mu, \nu > 3$, then we discard. Throughout this paper, by "discarding" we mean unfollowing a computation path. This is indicated by an ancilla qubit, which when set to $|1\rangle$, we only apply $\mathbb{I}$.

The unitary-selection operator can be expressed as

$$\begin{aligned}\text{SELECT}_{f\,2} = &\sum_{q=1}^{N}\sum_{\mu\neq\nu=1}^{3}\sum_{k=0}^{1}|q,\mu,\nu,0\rangle\,\langle q,\mu,\nu,0|\\ &\otimes U_{q,\mu}U_{q+1_{\mu},\nu}U_{q+1_{\nu},\mu}U_{q,\nu}\\ &+\sum_{q=1}^{N}\sum_{\mu\neq\nu=1}^{3}\sum_{k=0}^{1}|q,\mu,\nu,1\rangle\,\langle q,\mu,\nu,1|\\ &\otimes U^{\dagger}_{q,\nu}U^{\dagger}_{q+1_{\nu},\mu}U^{\dagger}_{q+1_{\mu},\nu}U^{\dagger}_{q,\mu},\end{aligned}$$

by which we can conveniently prove that

$$\langle 0|\,\text{PREP}^{\dagger}_{f\,2}\cdot\text{SELECT}_{f\,2}\cdot\text{PREP}_{f\,2}\,|0\rangle = \frac{H_{f\,2}}{6N},$$

providing a $(6N, ., 0)$ block encoding if $H_{f\,2}$. A more detailed analysis of the gate complexity can be found in Appendix G 1.

Lemma 3. Let $H_{21} = \sum_{q=1}^{N}\sum_{\mu=1}^{3}\mathbb{I}\otimes\mathbb{I}\otimes\frac{1}{2}E^2_{q,\mu}$, where $E^2_{q,\mu}$ is the operator described in Eq. (7). Then, with Trotterization, we can implement $e^{-iH_{21}\tau_2}$ exactly using the following number of gates:

$$\mathcal{G}_2 \in O\left(N\log^2\Lambda\right).$$

Alternatively, we can have a $(3N\Lambda^2/2, -, 0)$ block encoding of H_{21} with the following number of gates:

$$\mathcal{G}'_2 \in O\left(N\log^2\Lambda\right).$$

We know that $H_{21} = H_{f\,1}$ [Eq. (22)] and since $[E^2_{\ell,\mu}, E^2_{q,\nu}] = 0$ if $\ell \neq q$, so $e^{-iH_{f\,1}\tau_2} = \prod_{q=1}^{N}\prod_{\mu=1}^{3}\mathbb{I}\otimes\mathbb{I}\otimes e^{-i(1/2)E^2_{q,\mu}\tau_2}$. If $\zeta = 1+\log_2\Lambda$, then E^2 can be written as a sum of Z operators, as shown below, and we simulate $e^{-iH_{f\,1}\tau_2}$ by Trotterization, as done in Ref. [24]:

$$E^2 = \frac{1}{6}\left(2^{2\zeta-1}+1\right)\mathbb{I}+\sum_{j=0}^{\zeta-1}2^{j-1}\mathrm{Z}_j+\sum_{j=0}^{\zeta-2}\sum_{k>j}^{\zeta-1}2^{j+k-1}\mathrm{Z}_j\mathrm{Z}_k. \tag{44}$$

Lemma 4 (Lemma 2 in Ref. [24]). There exists a circuit that implements $e^{-iE^2\tau_2}$ on ζ qubits exactly, up to an (efficiently computable) global phase, using $(\zeta+2)(\zeta-1)/2$ CNOT operations and $\zeta(\zeta+1)/2$ single-qubit rotations. Here, $\zeta = 1+\log_2\Lambda$.

Since E^2 is expressed as a sum of Pauli operators, we can use the algorithm in Ref. [61] to optimize the rotation gates, possibly at the cost of a small increase in the number of Toffoli gates. More details on the gate complexity can be found in Appendix G 2.

Alternatively, we can use qubitization to simulate $e^{-iH_{21}\tau_2}$. Algorithm II, described in Sec. II D, applies qubitization on the entire Hamiltonian $\hat{H}_{\text{PF}}$ and for this we need to block encode H_{21}, which we briefly describe here. The ancilla-preparation subroutine is defined as follows:

$$\begin{aligned}\text{PREP}_{f\,1}\,|0\rangle^{*} = &\left(\frac{1}{\sqrt{N}}\sum_{q=1}^{N}|q\rangle\right)\otimes\left(\frac{1}{\sqrt{3}}\sum_{\mu=1}^{3}|\mu\rangle\right)\\ &\times\otimes\left(\sum_{k=1}^{\frac{\log^2(2\Lambda)+\log(2\Lambda)+2}{2}}\sqrt{\frac{w_k}{\sum_k w_k}}\,|k\rangle\right).\end{aligned}$$

Here, the w_k are the weights of the unitaries in the LCU decomposition of E^2 [Eq. (44)]. In the first $\log_2 N$-qubit electric link index register, we store the N electric link indices in equal superposition. In the next two-qubit spin-index register, we store the values of μ. Since E^2 is a sum of $(\log_2^2(2\Lambda)+\log_2(2\Lambda)+2)/2 = (\log_2^2\Lambda+3\log_2\Lambda+4)/2$ unitaries [Eq. (44)], the last register of $\log_2\left(\log_2^2\Lambda+3\log_2\Lambda+4\right)-1$ qubits stores the indices of the unitaries in a superposition, weighted according to Eq. (44).

The unitary-selection subroutine does the following:

$$\begin{aligned}\text{SELECT}_{f\,1} : |q\rangle\,|\mu\rangle\,|k\rangle\left(\bigotimes_{q=1}^{N}\bigotimes_{\mu'=1}^{3}|f_e=0\rangle_{q,\mu'}\right)|\phi\rangle\\ \mapsto |q\rangle\,|\mu\rangle\,|k\rangle\,(|1\rangle)_{q,\mu}\left(E^2_k\right)_{q,\mu}|\phi\rangle\end{aligned}$$

and it follows in a straightforward manner that

$$\langle 0|\,\text{PREP}^{\dagger}_{f\,1}\cdot\text{SELECT}_{f\,1}\cdot\text{PREP}_{f\,1}\,|0\rangle = \frac{H_{f\,1}}{3N\Lambda^2/2};$$

here too we keep in mind that $\|H_{f\,1}\| \leq 3N\Lambda^2/2$, from Table II. More details on the gate complexity for block encoding can be found in Appendix G 2. We omit discussion of the number of gates required for simulating $e^{-iH_{21}\tau_2}$ using qubitization because it is not needed in this paper and also it is quite straightforward to derive.

Lemma 5. Let

$$H_{31} = -\frac{1}{c}\sum_{j=1}^{\eta}\sum_{q=1}^{N}\sum_{\mu\neq\nu\neq\xi=1}^{3}\left(\sigma_{j,\mu}\otimes\mathbb{I}\right)\otimes\left(\nabla_\nu A_{q,\xi}-\nabla_\xi A_{q,\nu}\right)$$
$$+\frac{1}{2c^2}\sum_{j=1}^{\eta}\sum_{q=1}^{N}\sum_{\mu=1}^{3}\mathbb{I}\otimes\mathbb{I}\otimes A_{q,\mu}^2,$$

where $A_{q,\mu}$ is the operator described in Eq. (17). Then, we can have a $(\mathcal{A}_{31},-,0)$ block encoding H_{31}, where $\mathcal{A}_{31} = 12\pi\eta N\ln 2a^2/ch\Delta + 12\pi^2\eta N/c^2\Delta^2$, with

$$\mathcal{G}'_{31}\in O\left(\eta+N(a+\log d)\log d\right)$$

gates and hence the number of gates required for simulating $e^{iH_{31}\tau_3}$ with error $\delta_{31}>0$, using qubitization, is as follows:

$$\mathcal{G}_{31}\in O\left(\frac{\eta^2N\ln(2a^2)}{\Delta^2}\tau_3+\frac{\eta N^2\ln(2a^2)\log d}{\Delta^2}(a+\log d)\tau_3\right.$$
$$\left.+\frac{\log(1/\delta_{31})}{\log\log(1/\delta_{31})}\left(\eta+N(a+\log d)\log d\right)\right).$$

We block encode $H_{31}=H_s+H_{3\pi}$ in a recursive manner, using Theorem 1 repeatedly. Let

$$H_s^{j,q} = -\sum_{\mu\neq\nu\neq\xi=1}^{3}\left(\sigma_{j,\mu}\otimes\mathbb{I}\right)\otimes\left(\nabla_\nu A_{q,\xi}-\nabla_\xi A_{q,\nu}\right)$$
$$=\sum_{\mu\neq\nu\neq\xi=1}^{3}\left(\sigma_{j,\mu}\otimes\mathbb{I}\right)\otimes\left(\nabla_\xi A_{q,\nu}-\nabla_\nu A_{q,\xi}\right)$$

and

$$H_{3\pi}^{j,q}=\sum_{\mu=1}^{3}\mathbb{I}\otimes\mathbb{I}\otimes A_{q,\mu}^2,$$

such that

$$H_{31}^{j,q}=\frac{1}{c}H_s^{j,q}+\frac{1}{2c^2}H_{3\pi}^{j,q},\qquad H_{31}^{j}=\sum_{q=1}^{N}H_{31}^{j,q},$$
$$H_{31}=\sum_{j=1}^{\eta}H_{31}^{j}.$$

1. Block encoding of $H_s^{j,q}$

The ancilla-preparation subroutine, denoted by $\text{PREP}_s^{j,q}$, does the following:

$$\text{PREP}_s^{j,q}\left|0\right\rangle^{*}=\left(\frac{1}{\sqrt{6}}\sum_{\mu\neq\nu\neq\xi}^{3}\sum_{b=0}^{1}\left|\mu\right\rangle\left|\nu\right\rangle\left|\xi\right\rangle\left|b\right\rangle\right)$$
$$\otimes\left(\sum_{k=-a}^{a}\sqrt{\frac{|d'_{2a+1,k}|}{\sum_k|d'_{2a+1,k}|}}\left|k+a\right\rangle\right)$$
$$\otimes\left(\sum_{k'=1}^{\log_2 d}\sqrt{\frac{w'_{k'}}{\sum_{k'}w'_{k'}}}\left|k'\right\rangle\right).$$

The first $(2\times 3+1)=7$-qubit spin-index register stores directions or spins in equal superposition and the last qubit selects between $\nabla_\nu A_{q,\xi}$ and $\nabla_\xi A_{q,\nu}$. The second and third registers, with $\log_2(2a)$ and $\log_2\log_2 d$ qubits, respectively, indicate which adder to apply or on which qubit Z gate should be applied. These are unitaries obtained in the LCU decomposition of ∇ (Lemma 18) and A (Corollary 1) in Appendix F. We denote the next subroutine by $\text{SELECT}_s^{j,q}$, which is described as follows:

$$\text{SELECT}_s^{j,q}:\left|\mu,\nu,\xi,0\right\rangle\left|k''\right\rangle\left|k'\right\rangle\left|\phi\right\rangle$$
$$\mapsto\ \left|\mu,\nu,\xi,0\right\rangle\left|k''\right\rangle\left|k'\right\rangle\left(\sigma_\mu\otimes\mathbb{I}\right)_j\left(\nabla_{k''}\right)_{q,\nu}\left(A_{k'}\right)_{q,\xi}\left|\phi\right\rangle.$$

Controlled on $|\mu\rangle$, we apply σ_μ on the spin subspace of the jth particle. Controlled on $|\nu,\xi\rangle$ we select spin subspaces of the qth link register. Controlled on $|k''\rangle$ and $|k'\rangle$, we apply the k''th and k'th unitaries in the LCU decompositions of ∇ and A, respectively. If the third qubit in the spin register is $|1\rangle$, then we apply ∇_ξ and A_ν. It follows that

$$\left\langle 0\right|\text{PREP}_s^{j,q\dagger}\cdot\text{SELECT}_s^{j,q}\cdot\text{PREP}_s^{j,q}\left|0\right\rangle=\frac{H_s^{j,q}}{12\pi\ \ln 2a^2/h\Delta}$$

and thus we have a $(12\pi\ \ln 2a^2/h\Delta,.,0)$ block encoding of $H_s^{j,q}$.

2. Block encoding of $H_{3\pi}^{j,q}$

The first ancilla-preparation subroutine is described as follows:

$$\text{PREP}_{3\pi}^{j,q}\left|0\right\rangle^{*}=\left(\frac{1}{\sqrt{3}}\sum_{\mu'=1}^{3}\left|\mu'\right\rangle\right)\otimes\left(\sum_{k=1}^{\frac{\log^2 d+\log d}{2}}\sqrt{\frac{w'_k}{\sum_k w'_k}}\left|k\right\rangle\right).$$

The first two-qubit register is the spin-index register. Since A^2 is a sum of $(\log_2^2 d+\log_2 d)/2$ unitaries (Table II), we prepare a $\log_2\left[(\log_2^2 d+\log_2 d)/2\right]$-qubit register in a superposition weighted according to the LCU decomposition of A^2 (Corollary 2 in Appendix F). The next subroutine is described as follows:

$$\text{SELECT}_{3\pi}^{j,q} : |\mu'\rangle\,|k\rangle\,|\phi\rangle \mapsto |k\rangle \left(A_k^2\right)_{q,\mu'} |\phi\rangle\,.$$

It follows that

$$\langle 0|\,\text{PREP}_{3\pi}^{j,q\dagger} \cdot \text{SELECT}_{3\pi}^{j,q} \cdot \text{PREP}_{3\pi}^{j,q}\,|0\rangle = \frac{H_{3\pi}^{j,q}}{24\pi^2/\Delta^2}$$

and thus we have a $(24\pi^2/\Delta^2, ., 0)$ block encoding of $H_{3\pi}^{j,q}$.

3. Block encoding of H_{31}

We use Theorem 1 repeatedly. First, we block encode $H_{31}^{j,q} = (1/c)H_s^{j,q} + (1/2c^2)H_{3\pi}^{j,q}$ with $O(1)$ extra gate cost. Next, we consider $H_{31}^{j} = \sum_{q=1}^{N} H_{31}^{j,q}$, where each of the summand Hamiltonians acts on separate link registers, and finally we consider $H_{31} = \sum_{j=1}^{\eta} H_{31}^{j}$, where again the summands act on separate subspaces. Thus the overall ancilla-preparation subroutine is

$$\text{PREP}_{31}\,|0\rangle^{*} = \left(\frac{1}{\sqrt{\eta}}\sum_{j=1}^{\eta}|j\rangle\right) \otimes \left(\frac{1}{\sqrt{N}}\sum_{q=1}^{N}|q\rangle\right) \otimes \left(\sqrt{\frac{\lambda_s}{c\mathcal{A}}}\,|0\rangle + \sqrt{\frac{\lambda_{3\pi}}{2c^2\mathcal{A}}}\,|1\rangle\right) \otimes \text{PREP}_s^{j,q} \otimes \text{PREP}_{3\pi}^{j,q},$$

where $\lambda_s = \|H_s^{j,q}\| = 12\pi \ln 2a^2/h\Delta$, $\lambda_{3\pi} = \|H_{3\pi}^{j,q}\| = 24\pi^2/\Delta^2$, and $\mathcal{A} = (\lambda_s/c) + (\lambda_{3\pi}/2c^2)$. The overall unitary-selection subroutine is as follows:

$$\begin{aligned}
\text{SELECT}_{31} &: |j,q,0\rangle\,|\mu,\nu,\xi,b,k'',k'\rangle\,|\mu',k\rangle\,|\phi\rangle \\
&\mapsto |j,q,0\rangle\,|\mu',k\rangle\,\text{SELECT}_s^{j,q}\left(|\mu,\nu,\xi,b,k'',k'\rangle\,|\phi\rangle\right) \\
\text{SELECT}_{31} &: |j,q,1\rangle\,|\mu,\nu,\xi,b,k'',k'\rangle\,|\mu',k\rangle\,|\phi\rangle \\
&\mapsto |j,q,1\rangle\,|\mu,\nu,\xi,b,k'',k'\rangle\,\text{SELECT}_{3\pi}^{j,q}\left(|\mu',k\rangle\,|\phi\rangle\right).
\end{aligned}$$

It is straightforward to check that

$$\langle 0|\,\text{PREP}_{31}^{\dagger} \cdot \text{SELECT}_{31} \cdot \text{PREP}_{31}\,|0\rangle = \frac{H_{31}}{\eta N\mathcal{A}},$$

where $\eta N\mathcal{A} = (12\pi\eta N \ln 2a^2/ch\Delta) + (12\pi^2\eta N/c^2\Delta^2)$, which is also the sum of the norms of the Hamiltonians H_s and $H_{3\pi}$ in Table II. Thus we have a $(\eta N\mathcal{A}, ., 0)$ block encoding of H_{31}. More details about the procedures and gate-complexity analysis can be found in Appendix G 3.

Lemma 6. Let

$$\begin{aligned}
H_{32} = {} & \frac{1}{\Delta}\sum_{k<j}^{\eta}\sum_{\mathbf{q},\mathbf{r}=1}^{N}\left(\mathbb{I}\otimes\frac{1}{||\mathbf{q}-\mathbf{r}||_2}\,|\mathbf{q}\rangle\langle\mathbf{q}|_k\,|\mathbf{r}\rangle\langle\mathbf{r}|_j\otimes\mathbb{I}\right) \\
& -\frac{1}{\Delta}\sum_{j=1}^{\eta}\sum_{\kappa=1}^{K}\sum_{\mathbf{q}=1}^{N}\left(\mathbb{I}\otimes\frac{Z_\kappa}{|\mathbf{q}-\mathbf{R}_\kappa\|_2}|\mathbf{q}\rangle\langle\mathbf{q}|_j\otimes\mathbb{I}\right) \\
& \times\sum_{j=1}^{\eta}\sum_{q=1}^{N}\sum_{\mu=1}^{3}\left(\mathbb{I}\otimes\left(-\frac{1}{2}\nabla_{j,\mu}^2\right)\otimes\mathbb{I}+\frac{1}{c}\mathbb{I}\right. \\
& \left.\otimes\left(\frac{i}{c}\nabla_{j,\mu}\right)\otimes A_{q,\mu}\right),
\end{aligned}$$

where $A_{q,\mu}$ is the operator described in Eq. (17). Then, we can have a $(\mathcal{A}_{32}, -, 0)$ block encoding of H_{32}, where $[\eta(\eta-1)/2\Delta^2] + (\eta Z_{\text{sum}}/\Delta^2) + (8\pi^2\eta N/h^2) + (12\pi\eta N \ln 2a^2/ch\Delta)$, with

$$\mathcal{G}'_{32} \in O\left(\eta a \log_2 N + N\log_2 d + \log_2 N \log_2\frac{N}{\delta'} + K\log_2\frac{1}{\delta''}\right)$$

gates, where $\delta', \delta'' > 0$. Let $R_{32} \in O\left(\eta N/\Delta^2\,[1+(\eta_s/N)]\,\tau_3 + [\log(1/\delta_{32})/\log\log(1/\delta_{32})]\right)$. Then, the number of gates required for simulating $e^{iH_{32}\tau_3}$ with error $\delta_{32} > 0$, using qubitization, is $\mathcal{G}_{32} \in R_{32}\cdot\mathcal{G}'_{32}$.

Again, we use Theorem 1 to block encode $H_{32} = H_V + H_{1\pi} + H_{2\pi}$ in a recursive manner. We define the following:

$$H_{1\pi}^{j,q,\mu} = -\mathbb{I}\otimes\nabla_{j,\mu}^2\otimes\mathbb{I}, \quad H_{2\pi}^{j,q,\mu} = \mathbb{I}\otimes\left(i\nabla_{j,\mu}\right)\otimes A_{q,\mu},$$

$$H_{12\pi}^{j,q,\mu} = \frac{1}{2}H_{1\pi}^{j,q,\mu} + \frac{1}{c}H_{2\pi}^{j,q,\mu}, \quad H_{12\pi} = \sum_{j=1}^{\eta}\sum_{q=1}^{N}\sum_{\mu=1}^{3}H_{12\pi}^{j,q,\mu}.$$

4. Block encoding of $H_{12\pi}$

As in the case of H_{31}, we first block encode $H_{1\pi}^{j,q,\mu}$ and $H_{2\pi}^{j,q,\mu}$ separately, using the ancilla-preparation subroutines $\text{PREP}_{1\pi}^{j,q,\mu}$ and $\text{PREP}_{2\pi}^{j,q,\mu}$, respectively, followed by the unitary-selection subroutines $\text{SELECT}_{1\pi}^{j,q,\mu}$ and $\text{SELECT}_{2\pi}^{j,q,\mu}$, respectively. Then, we block encode $H_{12\pi}^{j,q,\mu}$ and $H_{12\pi}$, as discussed in Theorem 1. Thus our overall ancilla-preparation subroutine is as follows:

$$
\begin{aligned}
\text{PREP}_{12\pi}\,|0\rangle^* = {}& \left(\frac{1}{\sqrt{\eta}}\sum_{j=1}^{\eta}|j\rangle\right)\otimes\left(\frac{1}{\sqrt{N}}\sum_{q=1}^{N}|q\rangle\right)\\
&\otimes\left(\frac{1}{\sqrt{3}}\sum_{\mu=1}^{3}|\mu\rangle\right)\\
&\otimes\left(\sqrt{\frac{\lambda_1}{2\mathcal{A}'}}\,|0\rangle+\sqrt{\frac{\lambda_2}{c\mathcal{A}'}}\,|1\rangle\right)\otimes\text{PREP}_{1\pi}^{j,q,\mu}\\
&\otimes\text{PREP}_{2\pi}^{j,q,\mu},
\end{aligned}
$$

where $\lambda_1 = \|2H_{1\pi}\|, \lambda_2 = \|cH_{2\pi}\|, \mathcal{A}' = (\lambda_1/2) + (\lambda_2/c) = (8\pi^2\eta N/h^2) + (12\pi\eta N\ln 2a^2/ch\Delta)$ and

$$
\text{PREP}_{1\pi}^{j,q,\mu}\,|0\rangle^* = \left(\sum_{k=-a}^{a}\sqrt{\frac{|d_{2a+1,k}|}{\sum_k|d_{2a+1,k}|}}\,|k+a\rangle\right),
$$

$$
\begin{aligned}
\text{PREP}_{2\pi}^{j,q,\mu}\,|0\rangle^* = {}& \left(\sum_{k_1=-a}^{a}\sqrt{\frac{|d''_{2a+1,k_1}|}{\sum_{k_1}|d''_{2a+1,k_1}|}}\,|k_1+a\rangle\right)\\
&\otimes\left(\sum_{k_2=1}^{\log_2 d}\sqrt{\frac{w_{k_2}}{\sum_{k_2}w_{k_2}}}\,|k_2\rangle\right).
\end{aligned}
$$

The overall unitary-selection subroutine is as follows:

$$
\begin{aligned}
&\text{SELECT}_{1\pi}^{j,q,\mu}:|k'\rangle|\phi\rangle\mapsto|k'\rangle\left(\mathbb{I}\otimes\nabla^2_{k'}\right)_{j,\mu}|\phi\rangle,\\
&\text{SELECT}_{2\pi}^{j,q,\mu}:|k'_1\rangle|k'_2\rangle|\phi\rangle\mapsto|k'_1\rangle|k'_2\rangle\left(\nabla_{k'_1}\right)_{j,\mu}\left(A_{k'_2}\right)_{q,\mu}|\phi\rangle,\\
&\text{SELECT}_{12\pi}:|j,q,\mu,0\rangle|k'\rangle|k'_1,k'_2\rangle|\phi\rangle\\
&\quad\mapsto|j,q,\mu,0\rangle|k'_1,k'_2\rangle\,\text{SELECT}_{1\pi}^{j,q,\mu}\left(|k'\rangle|\phi\rangle\right),\\
&\text{SELECT}_{12\pi}:|j,q,\mu,1\rangle|k'\rangle|k'_1,k'_2\rangle|\phi\rangle\\
&\quad\mapsto|j,q,\mu,1\rangle|k'\rangle\,\text{SELECT}_{2\pi}^{j,q,\mu}\left(|k'_1,k'_2\rangle|\phi\rangle\right).
\end{aligned}
$$

It can be verified in a straightforward manner that

$$
\langle 0|\,\text{PREP}_{12\pi}^{\dagger}\cdot\text{SELECT}_{12\pi}\cdot\text{PREP}_{12\pi}\,|0\rangle=\frac{H_{12\pi}}{\mathcal{A}'},
$$

where $\mathcal{A}' = (8\pi^2\eta N/h^2) + (12\pi\eta N\ln 2a^2/ch\Delta)$, which is also the sum of the norms of $H_{1\pi}$ and $H_{2\pi}$ (Table II).

5. Block encoding of H_V

We know that $H_V = H_{V_{ee}} + H_{V_{ne}}$ and we block encode it, following the approach taken in Refs. [18,20], with some modifications and incorporating the optimizations in Theorem 2. The ancilla-preparation subroutine is as follows:

$$
\begin{aligned}
&\text{PREP}_V\,|1\rangle\,|0\rangle^*\\
&\quad\propto|0\rangle\sum_{i<j}^{\eta}\sum_{v_x,v_y,v_z=-N^{1/3}}^{N^{1/3}}\frac{1}{\|\mathbf{v}\|_2}\,|i\rangle\,|j\rangle\,|v_x,v_y,v_z\rangle\\
&\qquad-|1\rangle\sum_{i=1}^{\eta}\sum_{\kappa=1}^{K}\sum_{v_x,v_y,v_z=-N^{1/3}}^{N^{1/3}}\frac{\sqrt{Z_\kappa}}{\|\mathbf{v}\|_2}\,|i\rangle\,|\kappa\rangle\,|v_x,v_y,v_z\rangle\,.
\end{aligned}
$$

The first ancilla is used to select between $H_{V_{ee}}$ and $H_{V_{ne}}$. Next, the $\log_2\eta$-qubit register stores the particle indices in equal superposition. We follow the state-preparation procedure, described in Ref. [18], to prepare $\sum_{v_x,v_y,v_z=-N^{1/3}}^{N^{1/3}} 1/\|v\|_2\,|\mathbf{v}\rangle$. This is described in Appendix I. The unitary-selection subroutine is described as follows:

$$
\begin{aligned}
&\text{SELECT}_V:|0\rangle\,|i\rangle\,|j\rangle\,|\mathbf{v}\rangle\,|\mathbf{q}_1,\ldots\mathbf{q}_i,\ldots\mathbf{q}_j,\ldots\mathbf{q}_\eta\rangle\,|0\rangle\\
&\quad\mapsto|0\rangle\,|i\rangle\,|j\rangle\,|\mathbf{v}\rangle\,|\mathbf{q}_1,\ldots\mathbf{q}_i,\ldots\mathbf{q}_j,\ldots\mathbf{q}_\eta\rangle\,|\mathbf{q}_i-\mathbf{q}_j\rangle\,,\\
&\text{SELECT}_V:|1\rangle\,|i\rangle\,|\kappa\rangle\,|\mathbf{v}\rangle\,|\mathbf{q}_1,\ldots\mathbf{q}_i,\ldots\mathbf{q}_\eta\rangle\,|0\rangle\\
&\quad\mapsto|1\rangle\,|i\rangle\,|\kappa\rangle\,\mathbf{v}\,|\mathbf{q}_1,\ldots\mathbf{q}_i,\ldots\mathbf{q}_\eta\rangle\,|\mathbf{R}_\kappa-\mathbf{q}_i\rangle\,.
\end{aligned}
$$

If the first qubit is $|0\rangle$, we discard if $\mathbf{q}_i - \mathbf{q}_j \neq \mathbf{v}$. Since, for each pair of $\mathbf{q}_i$ and $\mathbf{q}_j$, only one value of $\mathbf{v}$ survives, the probability distribution is unaffected. If the first register is $|1\rangle$, then we use a classical database to access $\mathbf{R}_\kappa$. Controlled on the particle-index register, we take the difference $\mathbf{R}_\kappa - \mathbf{q}_i$ and discard the computational path if it is not equal to $\mathbf{v}$.

6. Block encoding of H_{32}

Since H_V has a probabilistic ancilla-preparation subroutine, we can block encode $H_{32} = H_V + H_{12\pi}$ using the procedure described in Ref. [20], by repeating the PREP$_V$ subroutine a constant number of times. This does not change the asymptotic gate complexity. In Appendix G 4, we give a more detailed description of these block-encoding procedures and the gate complexity.

7. Trotter error

Now, we derive bounds on the Trotter errors ϵ_1, ϵ_2, and ϵ_3, thus bounding the simulation error described in Lemma 1. If a Hamiltonian $H = \sum_{\gamma=1}^{\Gamma} H_\gamma$ is a sum of Γ fragment Hamiltonians, then e^{-itH} can be approximated by a product of exponentials, using the pth-order Trotter-Suzuki formula [57], $\mathscr{S}_p(t) = e^{-itH} + \mathscr{A}(t)$, where $\|\mathscr{A}(t)\| \in O\left(\widetilde{\alpha}_{\text{comm}}t^{p+1}\right)$ if each H_γ is Hermitian [58]. Here, $\widetilde{\alpha}_{\text{comm}} = \sum_{\gamma_1,\gamma_2,\ldots,\gamma_{p+1}=1}^{\Gamma} \|[H_{\gamma_{p+1}},\ldots[H_{\gamma_2},H_{\gamma_1}]]\|$. The following result provides an upper bound on $\widetilde{\alpha}_{\text{comm}}$. The proof is given in Appendix H, where we also explained some variations that can lead to tighter bounds.

Lemma 7. Let $H = \sum_{\gamma=1}^{\Gamma} H_\gamma$ and $\widetilde{\alpha}_{\text{comm}} = \sum_{\gamma_1,\gamma_2,\ldots,\gamma_{p+1}=1}^{\Gamma} \|[H_{\gamma_{p+1}}, \ldots [H_{\gamma_2}, H_{\gamma_1}]]\|$. Then, for any integer $1 \le p' \le p$,

$$\widetilde{\alpha}_{\text{comm}} \le 2^{p-(p'+1)} \sum_{\gamma_{i_1},\gamma_{i_2},\ldots,\gamma_{i_{p'+1}}} \|[H_{\gamma_{p'+1}}, [\ldots [H_{\gamma_3}, [H_{\gamma_2}, H_{\gamma_1}]] \ldots]]\| \left(\sum_{\gamma=1}^{\Gamma} \|H_\gamma\|\right)^{p-p'}.$$

In this paper, we take $p' = 1$; hence the need to compute all the first-order commutators in Table III, as well as the norm in Table II. Now, we have the results needed to prove our main theorem about divide-and-conquer simulations in Theorem 3.

Proof of Theorem 3. It is clear that we can bound the Trotter errors due to repeated splitting of the Hamiltonian $\hat{H}_{\text{PF}}$, using the bounds in Tables II and III. In the rest of the paper, we assume that $h \le K_h \Delta$, for some constant K_h, that a is a constant, and we let

$$\eta_s := \eta + Z_{\text{sum}}, \tag{45}$$

where $Z_{\text{sum}} = \sum_{\kappa=1}^{K} |Z_\kappa|$. In the first level (Fig. 2), we have two partitions, $H_{11} = H_{f\,1} + H_s + H_V + H_\pi$ and $H_{12} = H_{f\,2}$, and the error introduced due to this split [Eq. (34)] is

$$\epsilon_1 \in O\left(\widetilde{\alpha}_{1\text{comm}} (t/r_1)^{p_1+1}\right), \tag{46}$$

where

$$\widetilde{\alpha}_{1\text{comm}} \le 2^{p_1-2} \|[H_{f\,2}, H_{f\,1} + H_s + H_V + H_\pi]\| \cdot \left(\|H_\pi\| + \|H_V\| + \|H_f\| + \|H_s\|\right)^{p_1-1}. \tag{47}$$

Using the bounds in Table II, we obtain

$$\begin{aligned} \|H_\pi\| + \|H_V\| + \|H_f\| + \|H_s\| &\le \frac{12\pi^2\eta N}{c^2\Delta^2} + \frac{8\pi^2\eta N}{h^2} + \frac{24\pi\eta N \ln(2a^2)}{ch\Delta} + \frac{\eta(\eta-1)}{2\Delta^2} + \frac{\eta Z_{\text{sum}}}{\Delta^2} + \frac{3N\Lambda^2}{2} + 6N \\ &= \frac{\eta N}{\Delta^2}\left(8\pi^2\frac{\Delta^2}{h^2} + \frac{12\pi^2}{c^2} + \frac{24\pi\ln(2a^2)}{c}\cdot\frac{\Delta}{h} + \frac{\eta + 2Z_{\text{sum}}}{2N} + \frac{6\Delta^2}{\eta} + \frac{3\Lambda^2\Delta^2}{2\eta}\right) \\ &\lessapprox K_1 \frac{\eta N}{\Delta^2}\left(1 + \frac{\eta_s}{N} + \frac{\Delta^2\Lambda^2}{\eta}\right) \quad \text{[for some constant } K_1\text{]}. \end{aligned} \tag{48}$$

From Table III, we obtain

$$\begin{aligned} \|[H_{f\,2}, H_{f\,1} + H_s + H_\pi + H_V]\| &\le \|[H_{f\,2}, H_{f\,1}]\| + \|[H_{f\,2}, H_s]\| + \|[H_{f\,2}, H_\pi]\| + \|[H_{f\,2}, H_V]\| \\ &\le 12N\Lambda + \frac{288\pi\eta N\ln(2a^2)}{ch\Delta} + \frac{198\pi\eta N}{c\Delta}\left(\frac{\ln(2a^2)}{h} + \frac{\pi}{c\Delta}\right) \\ &= \frac{\eta N}{\Delta^2}\left(12\frac{\Delta^2\Lambda}{\eta} + \frac{486\pi\ln(2a^2)}{c}\cdot\frac{\Delta}{h} + \frac{198\pi^2}{c^2}\right) \\ &\le K_2\frac{\eta N}{\Delta^2}\left(1 + \frac{\Delta^2\Lambda}{\eta}\right) \qquad \text{[for some constant } K_2\text{]} \end{aligned}$$

and so

$$\widetilde{\alpha}_{1\text{comm}} \le 2^{p_1-2} K_1 K_2^{p_1-1} \left(\frac{\eta N}{\Delta^2}\right)^{p_1} \left(1 + \frac{\Delta^2\Lambda}{\eta}\right)\left(1 + \frac{\eta_s}{N} + \frac{\Delta^2\Lambda^2}{\eta}\right)^{p_1-1},$$

and hence

$$\epsilon_1 \in O\left(\left(\frac{\eta N}{\Delta^2}\right)^{p_1}\left(1 + \frac{\Delta^2\Lambda}{\eta}\right)\left(1 + \frac{\eta_s}{N} + \frac{\Delta^2\Lambda^2}{\eta}\right)^{p_1-1}\left(\frac{t}{r_1}\right)^{p_1+1}\right). \tag{49}$$

In the second level (Fig. 2), we have partitioned H_{11} into $H_{21} = H_{f\,1}$ and $H_{22} = H_s + H_V + H_\pi$ and so the error [Eq. (37)] introduced is

$$\epsilon_2 \in O\left(\widetilde{\alpha}_{2\text{comm}}(t/r_1 r_2)^{p_2+1}\right),$$
$$\text{where} \quad \widetilde{\alpha}_{2\text{comm}} \le 2^{p_2-2}\|[H_{f\,1}, H_s + H_V + H_\pi]\| \cdot \left(\|H_{f\,1}\| + \|H_s\| + \|H_V\| + \|H_\pi\|\right)^{p_2-1}.$$

From Table III, we have

$$\|[H_{f\,1}, H_s + H_V + H_\pi]\| \le \frac{6\pi\eta N\Lambda^2}{c\Delta}\left(\frac{\ln(2a^2)}{h} + \frac{2\pi}{c\Delta}\right) + \frac{24\pi\eta N\Lambda^2\ln(2a^2)}{ch\Delta} \le K_3\frac{\eta N\Lambda^2}{\Delta^2},$$

for some constant K_3, and from Table II, somewhat similarly to Eq. (48), we have

$$\|H_{f\,1}\| + \|H_s\| + \|H_V\| + \|H_\pi\| \le K_4\frac{\eta N}{\Delta^2}\left(1 + \frac{\eta_s}{N} + \frac{\Delta^2\Lambda^2}{\eta}\right).$$

So, $\widetilde{\alpha}_{2\text{comm}} \le K_3 K_4^{p_2-1}\Lambda^2 2^{p_2-2}\left(\eta N/\Delta^2\right)^{p_2}\left[1 + (\eta_s/N) + (\Delta^2\Lambda^2/\eta)\right]^{p_2-1}$ and hence

$$\epsilon_2 \in O\left(\Lambda^2\left(\frac{\eta N}{\Delta^2}\right)^{p_2}\left(1 + \frac{\eta_s}{N} + \frac{\Delta^2\Lambda^2}{\eta}\right)^{p_2-1}\left(\frac{t}{r_1 r_2}\right)^{p_2+1}\right). \tag{50}$$

In the third level of the divide-and-conquer algorithm (Fig. 2), H_{22} is divided into $H_{31} = H_s + H_{3\pi}$ and $H_{32} = H_V + H_{1\pi} + H_{2\pi}$ and so the error [Eq. (40)] is

$$\epsilon_3 \in O\left(\widetilde{\alpha}_{3\text{comm}}(t/r_1 r_2 r_3)^{p_3+1}\right),$$
$$\text{where} \quad \widetilde{\alpha}_{3\text{comm}} \le 2^{p_3-2}\|[H_s + H_{3\pi}, H_V + H_{1\pi} + H_{2\pi}]\| \cdot (\|H_s\| + \|H_V\| + \|H_\pi\|)^{p_3-1}.$$

From Table III, we have

$$\begin{aligned}\|[H_{31}, H_{32}]\| &= \|[H_V, H_s] + [H_{1\pi}, H_s] + [H_{2\pi}, H_s] + [H_V, H_{3\pi}] + [H_{1\pi}, H_{3\pi}] + [H_{2\pi}, H_{3\pi}]\|\\ &= \|[H_{2\pi}, H_s]\| \le K_5\frac{\eta^2 N}{\Delta^4} \quad [\text{for some constant } K_5]\end{aligned}$$

and from Table II we have, in the nonrelativistic limit where $\log(a)/c\Delta^2 \in O(1)$ and since $N \ge \eta$,

$$\begin{aligned}\|H_s\| + \|H_V\| + \|H_\pi\| &\le \frac{8\pi^2\eta N}{h^2} + \frac{12\pi^2\eta N}{c^2\Delta^2} + \frac{24\pi\eta N\ln(2a^2)}{ch\Delta} + \frac{\eta(\eta-1)}{2\Delta^2} + \frac{\eta Z_{\text{sum}}}{\Delta^2}\\ &\le K_6\frac{\eta N}{\Delta^2}\left(1 + \frac{\eta_s}{N}\right) \quad [\text{for some constant } K_6].\end{aligned}$$

So, $\widetilde{\alpha}_{3\text{comm}} \le K_5 K_6^{p_3-1}(\eta/\Delta^2)2^{p_3-2}\left(\eta N/\Delta^2\right)^{p_3}[1 + (\eta_s/N)]^{p_3-1}$, and hence

$$\epsilon_3 \in O\left(\frac{\eta}{\Delta^2}\left(\frac{\eta N}{\Delta^2}\right)^{p_3}\left(1 + \frac{\eta_s}{N}\right)^{p_3-1}\left(\frac{t}{r_1 r_2 r_3}\right)^{p_3+1}\right). \tag{51}$$

We can bound the overall simulation error ϵ using Lemma 1, where we take $\mathcal{N}_i \leq 2 \cdot 5^{p_i - 1}$. Using Eqs. (49)–(51), we obtain

$$\begin{aligned}
\epsilon &\leq r_1\epsilon_1 + r_1 r_2 \mathcal{N}_1 \epsilon_2 + r_1 r_2 r_3 \mathcal{N}_1 \mathcal{N}_2 \epsilon_3 + r_1 \mathcal{N}_1 \delta_1 + r_1 r_2 \mathcal{N}_1 \mathcal{N}_2 \delta_2 + r_1 r_2 r_3 \mathcal{N}_1 \mathcal{N}_2 \mathcal{N}_3 (\delta_{31} + \delta_{32}) \\
&\in O\left(t^{p_1+1} \left(\frac{\eta N}{r_1 \Delta^2} \right)^{p_1} \left(1 + \frac{\Delta^2 \Lambda}{\eta} \right) \left(1 + \frac{\eta_s}{N} + \frac{\Delta^2 \Lambda^2}{\eta} \right)^{p_1 - 1} \right. \\
&\quad + 5^{p_1} \Lambda^2 t^{p_2+1} \left(\frac{\eta N}{\Delta^2 r_1 r_2} \right)^{p_2} \left(1 + \frac{\eta_s}{N} + \frac{\Delta^2 \Lambda^2}{\eta} \right)^{p_2 - 1} \\
&\quad + 5^{p_1+p_2} \frac{\eta}{\Delta^2} t^{p_3+1} \left(\frac{\eta N}{\Delta^2 r_1 r_2 r_3} \right)^{p_3} \left(1 + \frac{\eta_s}{N} \right)^{p_3 - 1} + r_1 5^{p_1} \delta_1 + r_1 r_2 5^{p_1+p_2} \delta_2 \\
&\quad \left. + r_1 r_2 r_3 5^{p_1+p_2+p_3} (\delta_{31} + \delta_{32}) \right).
\end{aligned} \tag{52}$$

Also, from Lemma 1 we have the following bound on the total gate complexity:

$$\mathcal{G} \in O\left(5^{p_1} r_1 \mathcal{G}_1 + 5^{p_1+p_2} r_1 r_2 \mathcal{G}_2 + 5^{p_1+p_2+p_3} r_1 r_2 r_3 (\mathcal{G}_{31} + \mathcal{G}_{32}) \right), \tag{53}$$

where $\mathcal{G}_1$, $\mathcal{G}_2$, $\mathcal{G}_{31}$, and $\mathcal{G}_{32}$ are the gate complexities given in Lemmas 2–6. We make the additional assumption that $\delta' = \delta''$ and observe that because of our choice of asymmetric cutoffs on the field, $2\Lambda = d$, which follows from the dimension of operator A that acts on the link space. Then, substituting these values, we find that

$$\begin{aligned}
\mathcal{G}_1 &\in O\left(N^2 \frac{t}{r_1} \log \Lambda + \frac{\log(1/\delta_1)}{\log\log(1/\delta_1)} N \log \Lambda \right), \\
\mathcal{G}_2 &\in O\left(N \log^2 \Lambda \right), \\
\mathcal{G}_{31} &\in O\left(\frac{\eta^2 N}{\Delta^2} \frac{t}{r_1 r_2 r_3} + \frac{\eta N^2 \log^2 \Lambda}{\Delta^2} \frac{t}{r_1 r_2 r_3} + \frac{\log(1/\delta_{31})}{\log\log(1/\delta_{31})} (\eta + N \log^2 \Lambda) \right), \\
\mathcal{G}_{32} &\in R_{32} \cdot \mathcal{G}'_{32}, \\
R_{32} &\in O\left(\frac{\eta N}{\Delta^2} \left(1 + \frac{\eta_s}{N} \right) \frac{t}{r_1 r_2 r_3} + \frac{\log(1/\delta_{32})}{\log\log(1/\delta_{32})} \right), \\
\mathcal{G}'_{32} &\in O\left(\eta \log N + N \log \Lambda + \log N \log \frac{N}{\delta'} + K \log \frac{1}{\delta'} \right).
\end{aligned}$$

In principle, the least upper bound on the cost of the simulation can be found by optimizing over r_1, r_2, r_3, p_1, p_2, p_3, δ_1, δ_2, δ_{31}, and δ_{32}, while ensuring the constraint on the overall error in Eq. (52). However, this is a difficult nonlinear optimization problem and the true optima are difficult to find. Nonetheless, any choice of values will yield an upper bound on the complexity and, for simplicity, we take the simplest choice that satisfies the bound on the error in Eq. (52). We take the orders of the splitting formulas $p_1 = p_2 = p_3$ to be the same:

$$\begin{aligned}
&r_1 \in O\left(\left(\frac{t}{\epsilon} \right)^{\frac{1}{p_1}} \frac{t\eta N}{\Delta^2} \left(1 + \frac{\eta_s}{N} + \frac{\Delta^2 \Lambda^2}{\eta} \right)^{1 - \frac{1}{p_1}} \left(1 + \frac{\Delta^2 \Lambda}{\eta} \right)^{\frac{1}{p_1}} \right), \quad r_2 \in O\left(\Lambda^{\frac{2}{p_1}} \left(1 + \frac{\Delta^2 \Lambda}{\eta} \right)^{-\frac{1}{p_1}} \right), \\
&r_3 \in O\left(\left(\frac{\eta}{\Delta^2 \Lambda^2} \right)^{\frac{1}{p_1}} \right).
\end{aligned}$$

We take

$$\begin{aligned}
&\delta_1 \in O\left(\frac{\epsilon}{r_1} \right) \in O\left(\left(\frac{\epsilon}{t} \right)^{1 + \frac{1}{p_1}} \left(\frac{\eta N}{\Delta^2} \right)^{-1} \left(1 + \frac{\eta_s}{N} + \frac{\Delta^2 \Lambda^2}{\eta} \right)^{\frac{1}{p_1} - 1} \right), \\
&\delta_2 \in O\left(\frac{\epsilon}{r_1 r_2} \right), \quad \delta_{31}, \delta_{32} \in O\left(\frac{\epsilon}{r_1 r_2 r_3} \right).
\end{aligned}$$

Since $r_2, r_3 \geq 1$, for simplicity we choose $\delta_2, \delta_{31}, \delta_{32} \in O(\delta_1)$. δ' is included in the error of block encoding H_{32}, so we can assume that $\delta' \in O(\delta_1)$.

For brevity, let

$$L_1 := 1 + \frac{\eta_s}{N} + \frac{\Delta^2 \Lambda^2}{\eta}. \tag{54}$$

Then, we have

$$\begin{aligned} & r_1 \mathcal{G}_1 + r_1 r_2 \mathcal{G}_2 \\ & \in O\left(N^2 t \log \Lambda + \frac{\log(1/\delta_1)}{\log\log(1/\delta_1)} \left(\frac{t}{\epsilon}\left(1 + \frac{\Delta^2 \Lambda}{\eta}\right)\right)^{\frac{1}{p_1}} L_1^{1-\frac{1}{p_1}} \frac{t\eta N^2 \log \Lambda}{\Delta^2} + \left(\frac{t}{\epsilon}\right)^{\frac{1}{p_1}} L_1^{1-\frac{1}{p_1}} \frac{t\eta N^2 \log^2 \Lambda}{\Delta^2} \Lambda^{\frac{2}{p_1}} \right) \\ & \in O\left(\frac{\log(1/\delta_1)}{\log\log(1/\delta_1)} \left(\frac{t}{\epsilon}\left(1 + \frac{\Delta^2 \Lambda}{\eta}\right)\right)^{\frac{1}{p_1}} L_1^{1-\frac{1}{p_1}} \frac{t\eta N^2 \log \Lambda}{\Delta^2} + \left(\frac{t}{\epsilon}\right)^{\frac{1}{p_1}} L_1^{1-\frac{1}{p_1}} \frac{t\eta N^2 \log^2 \Lambda}{\Delta^2} \Lambda^{\frac{2}{p_1}} \right) \end{aligned} \tag{55}$$

and

$$\begin{aligned} r_1 r_2 r_3 \mathcal{G}_{31} & \in O\left(\frac{\eta^2 N t}{\Delta^2} + \frac{\eta N^2 t \log^2 \Lambda}{\Delta^2} + \frac{\log(1/\delta_1)}{\log\log(1/\delta_1)} \left(\frac{t}{\epsilon}\right)^{\frac{1}{p_1}} L_1^{1-\frac{1}{p_1}} \left(\frac{\eta^2 N t}{\Delta^2} + \frac{t\eta N^2 \log^2 \Lambda}{\Delta^2} \right) \left(\frac{\eta}{\Delta^2}\right)^{\frac{1}{p_1}} \right) \\ & \in O\left(\frac{\log(1/\delta_1)}{\log\log(1/\delta_1)} \left(\frac{t\eta}{\epsilon \Delta^2}\right)^{\frac{1}{p_1}} L_1^{1-\frac{1}{p_1}} \left(\frac{\eta^2 N t}{\Delta^2} + \frac{t\eta N^2 \log^2 \Lambda}{\Delta^2} \right) \right). \end{aligned} \tag{56}$$

Now, let $\eta_s + N := N_s$. Then,

$$\begin{aligned} r_1 r_2 r_3 \mathcal{G}_{32} & \in O\left(\frac{\eta N_s t}{\Delta^2} \mathcal{G}'_{32} + \frac{\log(1/\delta_1)}{\log\log(1/\delta_1)} \left(\frac{t}{\epsilon}\right)^{\frac{1}{p_1}} \frac{\eta N t}{\Delta^2} L_1^{1-\frac{1}{p_1}} \mathcal{G}'_{32} \left(\frac{\eta}{\Delta^2}\right)^{\frac{1}{p_1}} \right) \\ & \in O\left(\frac{\eta N'_s t}{\Delta^2} \mathcal{G}'_{32} \right) \left[N_s + N \frac{\log(1/\delta_1)}{\log\log(1/\delta_1)} \left(\frac{t\eta}{\epsilon \Delta^2}\right)^{\frac{1}{p_1}} L_1^{1-\frac{1}{p_1}} := N'_s \right] \\ & \in O\left(\frac{\eta^2 N'_s t \log N}{\Delta^2} + \frac{\eta N N'_s t \log \Lambda}{\Delta^2} + \frac{\eta N'_s t}{\Delta^2} \log N \log \frac{N}{\delta'} + \frac{\eta N'_s K t}{\Delta^2} \log \frac{1}{\delta'} \right) \end{aligned} \tag{57}$$

and so

$$\begin{aligned} \mathcal{G} & \in r_1 \mathcal{G}_1 + r_1 r_2 \mathcal{G}_2 + r_1 r_2 r_3 \left(\mathcal{G}_{31} + \mathcal{G}_{32}\right) \\ & \in O\left(\frac{\eta^2 N'_s t \log N}{\Delta^2} + \frac{\eta N N'_s t \log^2 \Lambda}{\Delta^2} \left(1 + \frac{\Delta^2 \Lambda}{\eta}\right)^{\frac{1}{p_1}} + \frac{\eta N'_s t}{\Delta^2} \log N \log \frac{N}{\delta'} + \frac{\eta N'_s K t}{\Delta^2} \log \frac{1}{\delta'} \right), \end{aligned} \tag{58}$$

where $N_s = \eta + Z_{\mathrm{sum}} + N$, $N'_s = N_s + N[\log(1/\delta_1)/\log\log(1/\delta_1)] \left(t\eta/\epsilon \Delta^2\right)^{1/p_1} L_1^{1-(1/p_1)}$, and $L_1 = 1 + [(\eta + Z_{\mathrm{sum}}))/N] + (\Delta^2 \Lambda^2/\eta)$. Also, $\delta' \in O\left((\epsilon/t)^{1+(1/p_1)} \left(\eta N/\Delta^2\right)^{-1} L_1^{(1/p_1)-1} \right)$. The result of Theorem 3 then follows by making these substitutions and using $\widetilde{O}$ notation to drop subdominant logarithmic factors from the asymptotic bound on the gate complexity in Eq. (58). ■

D. Algorithm II: Qubitization without divide and conquer

In this section, we describe another algorithm for simulating $e^{-i\hat{H}_{\mathrm{PF}}t}$, where we apply qubitization on the entire exponential, i.e., we do not divide the Hamiltonian and apply different algorithms to simulate each fragment. So now, we block encode the entire $\hat{H}_{\mathrm{PF}}$.

From Lemmas 2–6, we know the gate complexities $\mathcal{G}_1'$, $\mathcal{G}_2'$, $\mathcal{G}_{31}'$, and $\mathcal{G}_{32}'$ for block encoding H_{12}/λ_{12}, H_{21}/λ_{21}, H_{31}/λ_{31}, and H_{32}/λ_{32}, where $\lambda_{12}=\|H_{12}\|$, $\lambda_{21}=\|H_{21}\|$, $\lambda_{31}=\|H_{31}\|$, and $\lambda_{32}=\|H_{32}\|$, respectively. We remind the readers that in this paper $\|H_i\|$ for any Hamiltonian H_i is equal to the sum of the coefficients in an LCU decomposition of H_i, which can also be used as a bound on the ℓ_1 norm of H_i. Since $\hat{H}_{\mathrm{PF}}=H_{12}+H_{21}+H_{31}+H_{32}$, using Theorem 1 we can say that the cost of having a $(\lambda_{12}+\lambda_{21}+\lambda_{31}+\lambda 32,-,0)$ block encoding of $\hat{H}_{\mathrm{PF}}$ is

$$\mathcal{G}'\in O\left(\mathcal{G}_2'+\mathcal{G}_1'+\mathcal{G}_{31}'+\mathcal{G}_{32}'\right), \tag{59}$$

where $\mathcal{G}_1'$, $\mathcal{G}_2'$, $\mathcal{G}_{31}'$, and $\mathcal{G}_{32}'$ are the gate complexities described in Lemmas 2–6. With the assumptions made in the previous section, we have

$$\begin{aligned}
\mathcal{G}_1' &\in O\left(N\log\Lambda\right),\\
\mathcal{G}_2' &\in O\left(N\log^2\Lambda\right),\\
\mathcal{G}_{31}' &\in O\left(\eta+N\log^2\Lambda\right),\\
\mathcal{G}_{32}' &\in O\left(\eta\log N+N\log\Lambda+\log N\log\frac{N}{\delta'}+K\log\frac{1}{\delta'}\right)
\end{aligned}$$

and so

$$\begin{aligned}
\mathcal{G}' &\in O\left(\eta\log N+N\log^2\Lambda+\log N\log\frac{N}{\delta'}+K\log\frac{1}{\delta'}\right)\\
&\in O\left((\eta+\log N)\log N+(K+\log N)\log\frac{1}{\delta'}\right.\\
&\qquad\left.+N\log^2\Lambda\right).
\end{aligned}$$

Also, from Eq. (48),

$$\begin{aligned}
\|\hat{H}_{\mathrm{PF}}\| &\le \|H_\pi\|+\|H_V\|+\|H_s\|+\|H_f\|\\
&\in O\left(\frac{\eta N}{\Delta^2}L_1\right),
\end{aligned}$$

where

$$L_1=1+\frac{\eta+Z_{\mathrm{sum}}}{N}+\frac{\Delta^2\Lambda^2}{\eta},$$

and so we require $O\left\{(\eta Nt/\Delta^2)L_1+[\log(1/\epsilon)/\log\log(1/\epsilon)]\right\}$ calls to the block encoding of $\hat{H}_{\mathrm{PF}}$ in order to implement an ϵ-precise block encoding of $e^{-i\hat{H}_{\mathrm{PF}}t}$ [8]. We can assume that $\delta'\in O\left[(\epsilon\Delta^2/\eta NtL_1)\right]$. Thus the number of gates required is as follows:

$$\begin{aligned}
\mathcal{G}''\in O\Bigg(\left(\frac{\eta Nt}{\Delta^2}L_1+\frac{\log(1/\epsilon)}{\log\log(1/\epsilon)}\right)&((\eta+\log N)\log N\\
&+(K+\log N)\log\frac{1}{\delta'}+N\log^2\Lambda)\Bigg).
\end{aligned} \tag{60}$$

Hence we obtain the following theorem.

Theorem 4. Assuming that $\eta,K\le N$, a is constant, $1/\Delta^2c\in O(1)$, and $K,Z_{\mathrm{sum}}\in O(\eta)$, then there exists an algorithm that simulates $e^{-i\hat{H}_{\mathrm{PF}}t}$ with error ϵ, using qubitization, with gate complexity in

$$\widetilde{O}\left(Nt\left(\frac{\eta}{\Delta^2}+\Lambda^2\right)\left(\eta\log\frac{1}{\epsilon}+N\log^2\Lambda\right)\right).$$

This shows that we can achieve similar scaling to that attainable with Trotter-Suzuki simulations. One important difference, however, is that the scaling with the cutoff is superior for the divide-and-conquer approach for the case in which $p_1=1$. The scaling with respect to ϵ and t is, however, superior for qubitization. This shows that we expect both simulation algorithms to offer advantages in appropriate regimes. We observe this for chemical applications in the following section.

III. APPLICATIONS

As we saw in Sec. II, there are different asymptotic advantages and disadvantages to simulating the Pauli-Fierz Hamiltonian using either qubitization or the divide-and-conquer algorithm. One advantage of divide and conquer is the fact that we do not have to repeat the simulations of all the fragments, H_{12}, H_{21}, H_{31}, and H_{32}, the number of times proportional to the ℓ_1 norm of the complete $\hat{H}_{\mathrm{PF}}$. Rather, each fragment is repeated a number of times proportional to a smaller Hamiltonian with a lower ℓ_1 norm (refer to Fig. 2 for convenience)—see Eqs. (55)–(57). Due to Trotter splitting, we do have to repeat the number of times more than the ℓ_1 norm but by a clever choice of grouping such that the commutators are less and by an appropriate selection of the order of splitting, it is possible to reduce the gate complexities. Further, since we have the liberty to apply different simulation algorithms, it has been possible to simulate part of the Hamiltonian (i.e., H_{21}) by Trotterization, which has a much lower gate complexity.

However, a direct comparison of these costs is obfuscated by the high number of different variables and terms. In this section, we will compare the relative costs of these algorithms compared to some model system of interest, while scaling a single important system variable, in order to gain an intuition for which algorithm one would choose depending on the explicit physical regimes of the selected systems of interest. The main two regimes that we want to explore here are small atomic systems, with many degrees of freedom on the electromagnetic links, and large extended material systems in the thermodynamic limit with many electrons. Since we only have expressions for the asymptotic costs of these algorithms, we will fix a starting instance of the problem with set values and then take the ratio of the algorithm with itself, as a single variable is changed. In this way, the missing constant factors become irrelevant and we can fairly compare the two algorithms on the same footing, at the expense of the fact that the "cost ratio" is dependent on the initial problem instance and has no clear meaning in terms of actual gate complexity.

A. Atomic and/or molecular regime

First, we will compare costs for the regime of a small number of electrons in a single-atom system, to investigate regimes of application such as spontaneous emission of photons into the field, as well as photoionization of electrons, also known as the photoelectric effect. For example, in the latter case, state-of-the-art attosecond-laser-pulse experiments have attempted to probe electronic dynamics after photoexcitation [44]. In many theoretical models and given previous experimental limitations, this excitation is typically treated as instantaneous but on the attosecond time scale, complicated electron-photon dynamics occur that are still poorly understood. Here, the theoretical predictions do not match the experimental values. Specifically, in the neon atom, an experiment has concluded that there is a (21 ± 5)-as delay between photoemission of the $2p$ orbital with respect to the $2s$ orbital from the same approximately 100-eV photon source [45]. The origin of this effect is still not fully understood and various different explanations have been explored by theoretical investigations [46–54]. In the bigger picture, we can see a possible benefit of full quantum simulation on fault-tolerant quantum computers to settle these mysteries in ways that cannot be done without computing correlated electrons and quantum EM fields, especially for even more complicated molecular and material systems.

Using the neon attosecond-photoemission experiment as an example reference system, we can compare the gate-complexity cost ratio of the different Hamiltonian-simulation algorithms with respect to one variable at a time. This allows us to compare the asymptotic gate complexity of the algorithms indirectly on the same footing, without having to worry about the constant factors that have been dropped for ease of analysis. The asymptotic gate complexity for the divide-and-conquer algorithm (DC) and the qubitization algorithm have previously been reported in Eqs. (58) and (60), respectively. To create a reference instance inspired by the above attosecond experiment on neon, we refer to the following unless otherwise noted: $\eta = Z_{\text{sum}} = 10$, the simulation box size is $\Omega^{1/3} = 30$ (Bohr), which is roughly 10 times the atomic radius of neon, $N = 10^6$ lattice sites, $\Lambda = 100$, and the simulation time is $t = 83$, where $83 \approx 2000$ as. Additionally, the error $\epsilon = 10^{-3}$ in all cases.

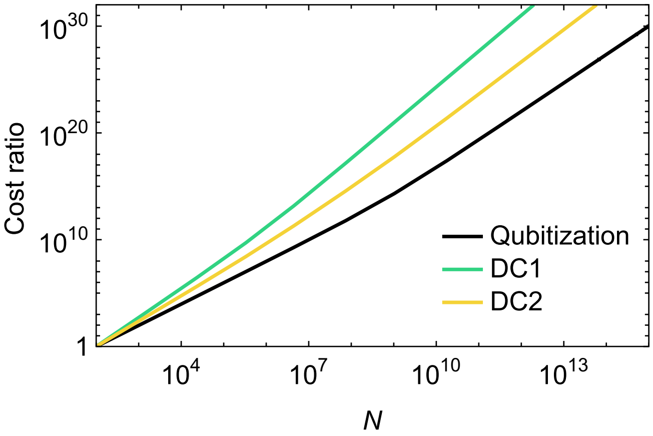

FIG. 3. The cost ratio of both the qubitization simulation algorithm and the divide-and-conquer algorithm when the order of the outermost Trotter splitting, i.e., $p_1 = 1$ (DC1) and $p_1 = 2$ (DC2), with respect to the reference single-neon-atom system as a function of N grid points. For the reference, we have $N = 100$.

First, we examine the cost ratio, as a function of N, of the simulation algorithms with respect to the reference neon calculation at $N = 10^2$. This is shown in Fig. 3. We have also varied the order of the outermost Trotter splitting (Fig. 2), i.e., variable p_1 in Eq. (58), and plotted the cost ratio as a function of N. We see qubitization scales better for all N up to 10^{15}. However, by choosing a higher value of p_1, we begin to approach the qubitization cost-ratio scaling, emphasizing that the divide-and-conquer technique can be "tuned" to the problem instance at hand, depending on the most important variable(s) of interest. Again, note that the meaning of the "cost ratio" on the y axis is ambiguous for actual gate costs but is a useful tool for comparing which algorithms scale better when choosing a variable and picking a specific problem instance.

Another variable of interest is Λ, the cutoff on the value for the electric field link space. To compare the scalings in terms of Λ, we maintain the same neon-atom reference calculation but set the minimum cutoff to $\Lambda = 2$ and compare up to $\Lambda = 10^{10}$. The cost ratio compared to the $\Lambda = 2$ instance is shown in Fig. 4. In Fig. 4(a), we can see a sizable difference in the cost ratios on the log-log scale, where the DC algorithm outperforms qubitization. Again, selecting a higher-order value for the outermost Trotter splitting, i.e., variable p_1 in Eq. (58) in the DC algorithm, changes the cost ratio to approach the qubitization result. In Fig. 4(b), we look at small values of Λ (on a standard linear plot) and see that even for small values of Λ, the cost ratio can be dramatically different between the two algorithms.

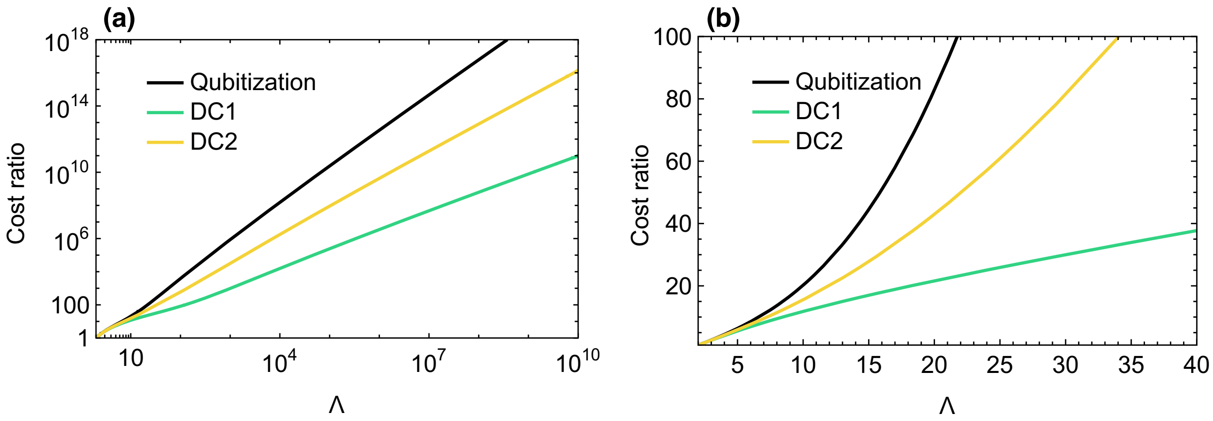

FIG. 4. The cost ratio of both the qubitization simulation algorithm and the divide-and-conquer algorithm when the order of the outermost Trotter split, i.e., $p_1 = 1$ (DC1) and $p_1 = 2$ (DC2), with respect to the reference single-neon-atom system as a function of Λ. For the reference, we have $\Lambda = 2$. (a) A log-log plot in which we compare up to higher values of Λ. (b) The same data in a standard linear plot, where we focus on a smaller range for the value of Λ.

Intuitively, this is expected because we have partitioned in such a way that the gate complexity has less dependence on Λ. For example, as mentioned before, we have grouped H_s, H_V, and H_π together within H_{11} and ensured that the commutator error between H_{11} and H_{12} (Fig. 2) is independent of Λ. Again, we emphasize that different partitionings of $\hat{H}_{\mathrm{PF}}$ and tuning of parameters such as the order of splitting in the divide-and-conquer algorithm can yield different results.

B. Bounds on Λ

While we have discussed the cost of simulation with respect to the chosen cutoff, Λ, with respect to each electric field link, we now want to discuss how Λ scales for certain regimes of applied problems. In order to quantify this, we need a more formal method to discuss the quality of a given choice of Λ. A succinct way to quantify this has been presented in Ref. [26], with a quantity denoted as "leakage." Specifically, leakage quantifies the probability that for some initial state λ on the links between the bounds $\pm\Lambda_0$, the state grows beyond Λ at time t, defined as

$$\left\| \left(1 - \Pi_{[-\Lambda,\Lambda]}\right) e^{-itH} \Pi_{[-\Lambda_0,\Lambda_0]} \right\|, \tag{61}$$

where H is the Hamiltonian and the projectors Π are defined as

$$\Pi_{[-\Lambda,\Lambda]} = \sum_{|\lambda|\le\Lambda} \Pi_\lambda \tag{62}$$

and

$$\Pi_\lambda = |\lambda\rangle\langle\lambda| \tag{63}$$

for a single link site. Using this definition, the long-time leakage bound has been defined in Ref. [26, Theorem 3] and is a quantity that quantifies a bound on Λ given a specific time t, using the $t = 0$ starting bounds, Λ_0. The long-time leakage bound can be computed as

$$\Lambda(t) = \Lambda_0 + \left\lceil \frac{1}{\delta - 1} \left(\left(\Lambda_0^{1-r} + 2\chi|t|(1-r)(\delta-1)\right)^{\frac{1}{1-r}} - \Lambda_0 \right) \right\rceil (\delta - 1), \tag{64}$$

where $r = 0$ for lattice gauge theories, δ is an integer, where $\delta > 0$, and χ is a constant dependent on the definition of the Hamiltonian. Specifically, we can choose χ to upper bound the spectral norm of the Hamiltonian terms that modify the value on the electric link spaces. Using similar notation in Ref. [26], we denote this Hamiltonian as H_W^ℓ, acting on a single choice of link ℓ:

$$H_W^\ell = \sum_j^\eta \left(\frac{2i}{c} \nabla_j \otimes A_\ell + \frac{1}{c^2} \mathbb{I} \otimes A_\ell^2 \right) + \sum_{\mu\neq\nu=1}^{3} \left(U_{\ell,\mu} U_{\ell+1,\nu}, U_{\ell+1,\mu}^\dagger U_{\ell,\nu}^\dagger + \text{H.c.} \right). \tag{65}$$

Therefore, the upper bound of the spectral norm of H_W^ℓ is

$$||H_W^\ell|| \le \frac{4\pi\eta\ln(2)}{\Delta^2 c} + \frac{4\pi^2}{\Delta^2 c} + 6, \tag{66}$$

using (Table II). By setting χ equal to this value, this implies that

$$\chi = ||H_W^\ell|| \in O\left(\frac{\eta N^{2/3}}{\Omega^{2/3}} \right). \tag{67}$$

Therefore,

$$\Lambda(t) \in O\left(\frac{\eta N^{2/3} t}{\Omega^{2/3}}\right). \tag{68}$$

Note that this bound increases linearly with time. This is potentially problematic for long-time evolutions as, in effect, it causes the time dependence of the simulation to scale polynomially with t.

C. Heuristic Λ estimate for typical light-matter interaction energies

While the leakage bound provides a formal guarantee on the Λ bounds in the worst-case scenario, we do not expect it to be tight in most physically reasonable situations. In particular, a major assumption made by the above analysis is that the input state has maximally bad scaling and in turn leads to linear scaling of the error bound with time. In practice, however, if we are interested in low-energy physics of a system, then these worst-case scenarios are unlikely to occur. Here, we provide a proposed way to address this by giving physically informed estimates to heuristically bound Λ for the systems of interest in nonrelativistic light-matter interactions. First, we can assume that for a single-particle-like excitation between an incoming photon, will be upper bounded by the deepest potential well on the heaviest atom. Specifically, for a hydrogenic atom, the single-electron energy levels in units of hartrees are

$$E_n = -\frac{Z^2}{2n^2}, \tag{69}$$

where n is the principle quantum number and the zero-point energy is set at $n = \infty$, or when the electron is unbound, and Z is the charge of the nucleus modeled as a point charge. Therefore, the highest bound-state energy needed naturally corresponds to the deepest ($1s$) orbital, where $n = 1$. Therefore, we will fix $n = 1$ and take the absolute value of the energy expression with the maximum Z value in the system to correspond to the highest effective Λ as

$$\tilde{\Lambda}^{1e} = \frac{Z_{\max}^2}{2}. \tag{70}$$

for a single-electron excitation. Now, for a system containing η electrons, we can assume that they are all noninteracting and occupy the lowest-energy state of the $Z_{\max}$ hydrogenic ion and the effective cutoff is then upper bounded as

$$\tilde{\Lambda} \leq \frac{\eta Z_{\max}^2}{2}. \tag{71}$$

This upper bound roughly corresponds to assuming that all η electrons are occupying the $1s$ orbital of the deepest potential well and that η individual photons interact and excite the system into the continuum.

IV. CONCLUSIONS

We have derived the first-quantized representation of the many-body Pauli-Fierz Hamiltonian (also referred to as the nonrelativistic QED Hamiltonian) and subsequently designed two algorithms to simulate its dynamics. First, we have developed a divide-and-conquer algorithm that partitions the Hamiltonian terms and simulates each one using different simulation algorithms, such as Trotterization and qubitization. Next, we have derived the complexity of simulating this Hamiltonian using complete qubitization. Additionally, we have discussed some potential applications, such as simulating the attosecond dynamics of photoionization in atoms and molecules. We have also discussed the relative merits of using these two algorithms for different parameter regimes. We have observed that, depending on the partitioning scheme, the divide-and-conquer approach has the potential to yield smaller gate costs. For example, one particular parameter of interest is the electric cutoff Λ. Roughly, the complexity of qubitization varies quadratically with Λ, while divide and conquer shows a subquadratic dependence. While both of these algorithms scale quadratically with the lattice size N, it appears that the cost of qubitization scales more favorably with this parameter overall. Another interesting observation is the fact that as we increase the order of the Trotter splitting in the divide-and-conquer method, the scaling approaches that of qubitization. Finally, we have also developed efficient techniques to implement a group of multicontrolled-X gates, which shaves off log factors in the asymptotic complexity and thus can yield a significant improvement in the cost of implementing the SELECT operations.

Overall, we have found that the quantum simulation of the first-quantized many-body Pauli-Fierz Hamiltonian is efficient but there are many avenues for future work. First, we expect that there are many opportunities for optimizing this simulation in general and especially when tailored to specific applications of interest. Second, since the Pauli-Fierz Hamiltonian captures so much of the phenomena in the low-energy regime of molecules and condensed matter interacting with light, we expect that many new applications of this model can be employed that have not not discussed here. In fact, the identification of key applications of this model and the computation of exact gate counts for said applications is an exciting avenue to probe for evidence of practical advantages of this simulation routine on future fault-tolerant quantum computers.

Looking ahead, there are a number of ways in which this work can be built on. An open question involves whether these ideas can be generalized to a broader class of field theories, including non-Abelian gauge theories. Further, while the Pauli-Fierz model is appropriate for a strong electromagnetic field coupled with the system, it is not capable of capturing all of the QED because of its inability to generate electromagnetic fields directly through particle motion; instead, it relies on the *ad hoc* introduction of the Coulomb potential. Providing ways to go beyond the limitations of this model would be an important step toward completing our understanding of how to simulate QED on a quantum computer.

ACKNOWLEDGMENTS

T.F.S. is a Quantum Postdoctoral Fellow at the Simons Institute for the Theory of Computing, supported by the U.S. Department of Energy, Office of Science, National Quantum Information Science Research Centers, Quantum Systems Accelerator. N.W. and P.M. acknowledge funding from the "Embedding QC into Many-Body Frameworks for Strongly Correlated Molecular and Materials Systems" project, which is funded by the U.S. Department of Energy, Office of Science, Office of Basic Energy Sciences, the Division of Chemical Sciences, Geosciences, and Biosciences. The Pacific Northwest National Laboratory is operated by Battelle for the U.S. Department of Energy under Contract DE-AC05-76RL01830. P.M. and N.W. further acknowledge support from Google Inc. The authors thank the anonymous reviewers for helpful comments, that have helped improve the manuscript.

APPENDIX A: DERIVATION OF THE FIRST-QUANTIZED PAULI-FIERZ HAMILTONIAN

In this appendix, we derive the first-quantized Pauli-Fierz Hamiltonian. The full (rigged) Hilbert space of the Pauli-Fierz model, $\mathscr{H}_{\mathrm{PF}}$, in Euclidean 3D space, describing spin-1/2 electrons as fermions and the bosonic gauge field, has the form

$$\mathscr{H}_{\mathrm{PF}} = \mathscr{H}_p \otimes \mathscr{H}_f,$$

where $\mathcal{H}_p$ is the Hilbert space of the particles and $\mathcal{H}_f$ is the Hilbert space of the electromagnetic (EM) field. The Hilbert space that describes the particles is

$$\mathscr{H}_p = P_a \left(\bigotimes^{\eta} L^2(\mathbb{R}^3, \mathbb{C}^2) \right),$$

where P_a is the projection onto the antisymmetric subspace of the η-particle system. The Hilbert space for the EM field $\mathscr{H}_f$ is then

$$\mathscr{H}_f = L^2(\mathbb{R}^3 \times \{-\infty, \infty\}),$$

where the spectrum of the field is unbounded. Naturally, for a finite simulation, the maximum allowed values on the EM field need to be related to a cutoff Λ. This needs to be quantitatively estimated for the energy scales in the problem of interest and is discussed in Sec. III. The general spin-1/2 Pauli-Fierz Hamiltonian for η particles is the following:

$$\hat{H} = \sum_j^{\eta} \left[\boldsymbol{\sigma}_j \cdot \left(\mathbf{p}_j - \frac{e}{c}\mathbf{A}(\mathbf{x}) \right) \right]^2 + \hat{H}_f + \hat{H}_V. \tag{A1}$$

This follows the form of Ref. [56, Equation 20.2], where the bold notation corresponds to vectors. $\boldsymbol{\sigma}_j$ is the vector of Pauli matrices $\{\sigma_1, \sigma_2, \sigma_3\}$ acting on the spin-1/2 degree of freedom for particle j, $\mathbf{p}_j$ is the 3-vector of momentum $\{p_x, p_y, p_z\}$ for the jth particle in 3D space, e is the electric charge constant, c is the speed of light, and $\mathbf{A}(\mathbf{x})$ is the magnetic vector potential $\{A_x(\mathbf{x}), A_y(\mathbf{x}), A_z(\mathbf{x})\}$, where $\mathbf{x} \in \mathbb{R}^3$ is the position space coordinate. This Hamiltonian is represented in the Coulomb gauge, $\nabla \cdot \mathbf{A} = 0$, meaning that the divergence of the magnetic vector potential is chosen to be 0.

The $\hat{H}_f$ term in Eq. (A1) is the free-photon-space Hamiltonian, defined as the following:

$$\hat{H}_f = \frac{1}{2} \int d^3x \mathbf{E}(\mathbf{x})^2 + \mathbf{B}(\mathbf{x})^2, \tag{A2}$$

where $\mathbf{E}(\mathbf{x})$ is the electric field component and $\mathbf{B}(\mathbf{x})$ is the magnetic field component, defined as the following in terms of $\mathbf{A}(\mathbf{x})$:

$$\mathbf{E}(\mathbf{x}) = -\frac{1}{c}\frac{\partial}{\partial t}\mathbf{A}(\mathbf{x}), \tag{A3}$$

$$\mathbf{B}(\mathbf{x}) = \nabla \times \mathbf{A}(\mathbf{x}). \tag{A4}$$

The $\hat{H}_V$ term in Eq. (A1) is the instantaneous two-particle Coulomb-repulsion interaction, defined as

$$\hat{H}_V = \sum_{i \neq j}^{\eta} \frac{e_i e_j}{2||\mathbf{r}_i - \mathbf{r}_j||_2}, \tag{A5}$$

where $\mathbf{r}_j$ is the position vector of particle j. This gives a continuous Hamiltonian that describes the dynamics of a fermionic system that is coupled to an external electromagnetic field. In order for the relativistic limit to hold, we need to assume that $1/c \ll 1$. This limit also removes any need to incorporate Ampere's law in the calculation, because such corrections only contribute at higher order in $1/c$. However, it is worth noting that if the magnetic fields generated by the fermions are substantial, then models such as these may not be applicable.

APPENDIX B: NONRELATIVISTIC SPIN TERM IN THE STANDARD PAULI-FIERZ HAMILTONIAN

Following the derivation from Ref. [56], the general spin-1/2 Pauli-Fierz Hamiltonian for η particles is the following:

$$\hat{H} = \sum_{j}^{\eta} \left[\boldsymbol{\sigma}_j \cdot \left(\mathbf{p}_j - \frac{e}{c}\mathbf{A}(x)\right)\right]^2 + \hat{H}_f + \hat{H}_V, \tag{B1}$$

where we are only focused on the first term, which includes the spin-1/2 particles coupled to the field. With this definition, we can then expand the first term in Eq. (A1) to isolate the spin-dependent terms.

The first term in Eq. (A1) can be expanded as follows for a single particle j using the Pauli vector identity $(\boldsymbol{\sigma} \cdot \mathbf{a})(\boldsymbol{\sigma} \cdot \mathbf{b}) = \mathbf{a} \cdot \mathbf{b} + i\boldsymbol{\sigma} \cdot (\mathbf{a} \times \mathbf{b})$:

$$\begin{aligned}
&\left[\boldsymbol{\sigma}_j \cdot \left(\mathbf{p}_j - \frac{e}{c}\mathbf{A}(x)\right)\right]^2 \\
&\quad = \left[\boldsymbol{\sigma}_j \cdot \left(\mathbf{p}_j - \frac{e}{c}\mathbf{A}(x)\right)\right]\left[\boldsymbol{\sigma}_j \cdot \left(\mathbf{p}_j - \frac{e}{c}\mathbf{A}(x)\right)\right] && \text{(B2)} \\
&\quad = \left(\mathbf{p}_j - \frac{e}{c}\mathbf{A}(x)\right) \cdot \left(\mathbf{p}_j - \frac{e}{c}\mathbf{A}(x)\right) \\
&\qquad + i\boldsymbol{\sigma} \cdot \left(\left(\mathbf{p}_j - \frac{e}{c}\mathbf{A}(x)\right) \times \left(\mathbf{p}_j - \frac{e}{c}\mathbf{A}(x)\right)\right). && \text{(B3)}
\end{aligned}$$

The first term just reduces back to the original kinetic momentum term without spin. Therefore, using the fact that the cross products $\mathbf{p} \times \mathbf{p}$ and $\mathbf{A} \times \mathbf{A}$ vanish,

$$\begin{aligned}
&\left[\boldsymbol{\sigma}_j \cdot \left(\mathbf{p}_j - \frac{e}{c}\mathbf{A}(x)\right)\right]^2 \\
&\quad = \left(\mathbf{p}_j - \frac{e}{c}\mathbf{A}(x)\right)^2 + i\boldsymbol{\sigma} \\
&\qquad \cdot \left(\left(\mathbf{p}_j - \frac{e}{c}\mathbf{A}(x)\right) \times \left(\mathbf{p}_j - \frac{e}{c}\mathbf{A}(x)\right)\right) && \text{(B4)} \\
&\quad = \left(\mathbf{p}_j - \frac{e}{c}\mathbf{A}(x)\right)^2 + i\boldsymbol{\sigma} \cdot \left(\mathbf{p} \times \mathbf{p} - \frac{e}{c}\mathbf{p}\right. \\
&\qquad \left. \times \mathbf{A}(x) - \frac{e}{c}\mathbf{A}(x) \times \mathbf{p} + \frac{e^2}{c^2}\mathbf{A}(x) \times \mathbf{A}(x)\right) && \text{(B5)} \\
&\quad = \left(\mathbf{p}_j - \frac{e}{c}\mathbf{A}(x)\right)^2 + i\boldsymbol{\sigma} \cdot \left(-\frac{e}{c}\mathbf{p} \times \mathbf{A}(x) - \frac{e}{c}\mathbf{A}(x) \times \mathbf{p}\right) && \text{(B6)} \\
&\quad = \left(\mathbf{p}_j - \frac{e}{c}\mathbf{A}(x)\right)^2 - i\frac{e}{c}\boldsymbol{\sigma} \cdot (\mathbf{p} \times \mathbf{A}(x) + \mathbf{A}(x) \times \mathbf{p}). && \text{(B7)}
\end{aligned}$$

Now, by substituting in $\mathbf{p} \rightarrow -i\nabla$, assuming that this operates on a scalar function ψ, and subsequently using the vector identity $\nabla \times (\psi\mathbf{A}) = \psi(\nabla \times \mathbf{A}) - (\mathbf{A} \times \nabla)\psi$, we obtain

$$\begin{aligned}
&\left[\boldsymbol{\sigma}_j \cdot \left(\mathbf{p}_j - \frac{e}{c}\mathbf{A}(x)\right)\right]^2 \psi \\
&\quad = \left(\nabla_j - \frac{e}{c}\mathbf{A}(x)\right)^2 \psi - \frac{e}{c}\boldsymbol{\sigma}\psi \\
&\qquad \cdot \left(\nabla_j \times \mathbf{A}(x) + \mathbf{A}(x) \times \nabla_j\right)\psi && \text{(B8)} \\
&\quad = \left(\nabla_j - \frac{e}{c}\mathbf{A}(x)\right)^2 \psi - \frac{e}{c}\boldsymbol{\sigma} \\
&\qquad \cdot \left(\nabla_j \times (\mathbf{A}(x)\psi) + \mathbf{A}(x) \times (\nabla_j\psi)\right) && \text{(B9)} \\
&\quad = \left(\nabla_j - \frac{e}{c}\mathbf{A}(x)\right)^2 \psi - \frac{e}{c}\boldsymbol{\sigma} \cdot \left(\psi(\nabla_j \times (\mathbf{A}(x))\right. \\
&\quad \left. -(\mathbf{A}(x) \times \nabla_j)\psi + \mathbf{A}(x) \times (\nabla_j\psi)\right) && \text{(B10)} \\
&\quad = \left(\nabla_j - \frac{e}{c}\mathbf{A}(x)\right)^2 \psi - \frac{e}{c}\boldsymbol{\sigma} \cdot \left(\nabla_j \times \mathbf{A}(x)\psi\right) && \text{(B11)} \\
&\quad = \left(\nabla_j - \frac{e}{c}\mathbf{A}(x)\right)^2 \psi - \frac{e}{c}\boldsymbol{\sigma} \cdot \mathbf{B}(x)\psi. && \text{(B12)}
\end{aligned}$$

Therefore, the Pauli-Fierz Hamiltonian including spin simplifies to

$$\hat{H} = \sum_{j}^{\eta} \left[\left(\mathbf{p}_j - \frac{e}{c}\mathbf{A}(x)\right)^2 - \frac{e}{c}\boldsymbol{\sigma}_j \cdot \mathbf{B}(x)\right] + \hat{H}_f + \hat{V}_{\text{coul}}, \tag{B13}$$

where the only spin-dependent term at the one-body-interaction level is the $\boldsymbol{\sigma}_j \cdot \mathbf{B}(x)$ term.

APPENDIX C: DIVIDE AND CONQUER FOR BLOCK ENCODING

In this appendix, we describe a divide-and-conquer approach for block encoding of weighted linear combination or the product of Hamiltonians. Suppose that we have M Hamiltonians, $H_1, \ldots, H_M$, such that each has an LCU decomposition as $H_i = \sum_{j=1}^{M_i} h_{ij} U_{ij}$ and $\lambda_i = |h_{ij}|$. We can have a $(\lambda_i, \log M_i, 0)$ block encoding of H_i using an ancilla-preparation subroutine and a unitary-selection subroutine, which we denote by PREP$_i$ and SELECT$_i$, respectively:

$$\text{PREP}_i \, |0\rangle^{\log M_i} = \sum_{j=1}^{M_i} \sqrt{\frac{h_{ij}}{\lambda_i}} \, |j\rangle, \tag{C1}$$

$$\text{SELECT}_i = \sum_{j=1}^{M_i} |j\rangle\langle j| \otimes U_{ij}, \tag{C2}$$

$$\langle 0| \, \text{PREP}_i^{\dagger} \cdot \text{SELECT}_i \cdot \text{PREP}_i \, |0\rangle = \frac{H_i}{\lambda_i}. \tag{C3}$$

Now, we use these subroutines to define the following:

$$\text{PREP}\,|0\rangle^{\log M+\sum_i \log M_i} = \left(\sum_{i=1}^{M}\sqrt{\frac{w_i\lambda_i}{\mathcal{A}}}\,|i\rangle\right)\otimes\bigotimes_{i=1}^{M}\text{PREP}_i, \tag{C4}$$

$$\text{SELECT} = \sum_{i=1}^{M}\left(|i\rangle\langle i|\otimes\bigotimes_{k=1}^{i-1}\mathbb{I}\otimes\text{SELECT}_i \otimes\bigotimes_{k=i+1}^{M}\mathbb{I}\right), \tag{C5}$$

where $w_i > 0$ and $\mathcal{A} = \sum_{i=1}^{M} w_i\lambda_i$. In the following theorem, we show that we can block encode a linear combination of these Hamiltonians using the above subroutines.

Theorem 5. Let $H = \sum_{i=1}^{M} w_i H_i$ be the sum of M Hamiltonians and let each of them be expressed as a sum of unitaries, as $H_i = \sum_{j=1}^{M_i} h_{ij}U_{ij}$, such that $\lambda_i = \sum_j |h_{ij}|$, $w_i > 0$. Each of the summand Hamiltonians is block encoded using the subroutines defined in Eqs. C1 and C2. Then, we can have a $(\mathcal{A}, \lceil\log_2(M)\rceil, 0)$ block encoding of $H/\mathcal{A}$, where $\mathcal{A} = \sum_{i=1}^{M} w_i\lambda_i$, using the ancilla-preparation subroutine (PREP) defined in Eq. (C4) and the unitary-selection subroutine (SELECT) defined in Eq. (C5):

(1) The PREP subroutine has an implementation cost of $\mathcal{C}_{\text{PREP}} = \sum_{i=1}^{M}\mathcal{C}_{\text{PREP}_i} + \mathcal{C}_w$, where $\mathcal{C}_{\text{PREP}_i}$ is the number of gates to implement PREP_i and $\mathcal{C}_w$ is the cost of preparing the state $\sum_{i=1}^{M}\sqrt{w_i\lambda_i/\mathcal{A}}\,|i\rangle$.

(2) The SELECT subroutine can be implemented with a set of multicontrolled-X gates, $\{M_i$ pairs of $C^{\log_2 M_i+1}X$ gates $: i = 1,\ldots,M\}$, M pairs of $C^{\log M}X$ gates, and $\sum_{i=1}^{M} M_i$ single-controlled unitaries - $\{cU_{ij} : j = 1,\ldots,M_i; i = 1,\ldots,M\}$.

Proof. The ancilla-preparation and unitary-selection subroutines for the block encoding of $H/\mathcal{A}$ have been defined in Eqs. C4 and C5:

$$\text{PREP}\,|0\rangle^{\log M+\sum_i \log M_i} = \left(\sum_{i=1}^{M}\sqrt{\frac{w_i\lambda_i}{\mathcal{A}}}\,|i\rangle\right)\otimes\bigotimes_{i=1}^{M}\text{PREP}_i = \left(\sum_{i=1}^{M}\sqrt{\frac{w_i\lambda_i}{\mathcal{A}}}\,|i\rangle\right)\otimes\bigotimes_{i=1}^{M}\left(\sum_{j=1}^{M_i}\sqrt{\frac{h_{ij}}{\lambda_i}}\,|j\rangle\right),$$

$$\begin{aligned}\text{SELECT} &= \sum_{i=1}^{M}\left(|i\rangle\langle i|\otimes\bigotimes_{k=1}^{i-1}\mathbb{I}\otimes\text{SELECT}_i\otimes\bigotimes_{k=i+1}^{M}\mathbb{I}\right)\\ &= \sum_{i=1}^{M}\left(|i\rangle\langle i|\otimes\bigotimes_{k=1}^{i-1}\mathbb{I}\otimes\left(\sum_{j=1}^{M_i}|j\rangle\langle j|\otimes U_{ij}\right)\otimes\bigotimes_{k=i+1}^{M}\mathbb{I}\right).\end{aligned}$$

Thus,

$$\text{SELECT}\cdot\text{PREP}\,|0\rangle\,|\psi\rangle = \sum_{i=1}^{M}\sum_{j_i=1}^{M_i}\left(\sqrt{\frac{w_i\lambda_i}{\mathcal{A}}}\,|i\rangle\otimes\bigotimes_{k=1}^{i-1}\left(\sum_{j_k=1}^{M_k}\sqrt{\frac{h_{kj}}{\lambda_k}}\,|j_k\rangle\right)\otimes\sqrt{\frac{h_{ij_i}}{\lambda_i}}\,|j_i\rangle\otimes\bigotimes_{k=i+1}^{M}\left(\sum_{j_k=1}^{M_k}\sqrt{\frac{h_{kj}}{\lambda_k}}\,|j_k\rangle\right)\right)U_{ij_i}\,|\psi\rangle$$

and

$$\langle 0|\,\text{PREP}^{\dagger} = (\text{PREP}\,|0\rangle)^{\dagger} = \left(\sum_{i=1}^{M}\sqrt{\frac{w_i\lambda_i}{\mathcal{A}}}\,\langle i|\right)\otimes\bigotimes_{i=1}^{M}\left(\sum_{j=1}^{M_i}\sqrt{\frac{h_{ij}}{\lambda_i}}\,\langle j|\right)$$

and hence

$$\langle 0|\,\text{PREP}^{\dagger}\cdot\text{SELECT}\cdot\text{PREP}\,|0\rangle\,|\psi\rangle = \sum_{i=1}^{M}\sum_{j_i=1}^{M_i}\frac{w_i\lambda_i}{\mathcal{A}}\frac{h_{ij_i}}{\lambda_i}U_{ij_i}\,|\psi\rangle + |\Psi^{\perp}\rangle = \left(\frac{1}{\mathcal{A}}\sum_{i=1}^{M}w_iH_i\right)|\psi\rangle + |\Psi^{\perp}\rangle\,.$$

Thus we have a block encoding of $H/\mathcal{A}$.

It is quite clear that the cost of implementing PREP is as given in the statement of the lemma. So now we describe the implementation of SELECT, which can be written as follows:

$$\begin{aligned}\textsc{select}: &\left|i\right\rangle\left|0,k_1\right\rangle_1\ldots\left|1,j\right\rangle_i\ldots\left|0,k_M\right\rangle_M\left|\psi\right\rangle\\ &\mapsto\left|i\right\rangle\left|0,k_1\right\rangle_1\ldots\left|1,j\right\rangle_i\ldots\left|0,k_M\right\rangle_M U_{ij}\left|\psi\right\rangle.\end{aligned}$$

In the above, we have represented each set of ancilla qubits in the $M+1$ subspaces of PREP as a separate register. We allot one ancilla qubit, initialized to 0, for each $\textsc{prep}_i$ register. If state of the first register containing $\log M$ qubits is $|i\rangle$, then the ith register corresponding to $\textsc{prep}_i$ is selected by flipping this ancilla to 1. We require M (compute-uncompute) pairs of $C^{\log_2 M}X$ gates and M ancillas to make this selection. Now, if the state of the $\textsc{prep}_i$ register is $|j\rangle$, then we select the jth unitary in the LCU decomposition of H_i, i.e., U_{ij}. To select unitaries of the ith Hamiltonian H_i, we require M_i pairs of $C^{\log_2 M_i+1}X$. Each of these flip another ancilla corresponding to each unitary in the LCU decomposition. The unitaries are implemented controlled on this ancilla. This explains the implementation cost of the SELECT subroutine. ■

1. Advantages

Now, we explain that we can have a decrease in gate complexity if we follow this divide-and-conquer approach, instead of block encoding H as a sum of $M'=\sum_{i=1}^{M}M_i$ unitaries:

$$H=\sum_{i=1}^{M}w_iH_i=\sum_{i=1}^{M}\sum_{j=1}^{M_i}w_ih_{ij}U_{ij}.$$

We have a PREP′ subroutine, acting on $\log_2 M'$ ancilla qubits, the states of which select a particular unitary in the decomposition. A superposition of these basis states with weights w_ih_{ij} can be obtained by using approximately $\log_2 M'=\log_2(\sum_i M_i)$ H gates, $2M'+3\log_2 M'-7=2\sum_i M_i+3\log_2(\sum_i M_i)-7$ CNOT gates, and $2M'-2=2\sum_i M_i-2$ rotation gates [74–76]. In the SELECT′ subroutine, we have M' unitaries, each controlled on $\log_2 M'$ qubits. Each of them, in turn, can be implemented with a (compute-uncompute) pair of $C^{\log_2 M'}X$ and one controlled unitary. Decomposing the multicontrolled-NOT in terms of Clifford+T [67,68], we see that we require at most $M'(4\log_2 M'-4)$ T, $M'(4\log_2 M'-3)$ CNOT. The use of logical AND gadgets reduces the gate complexity in the uncomputation part.

Now, let us use the divide-and-conquer method described in Theorem 5. For the PREP subroutine, we require $\log_2 M+\sum_i\log_2 M_i=\log(M\prod_i M_i)$ H gates, $2(M+\sum_i M_i)+3(\log_2 M+\sum_i\log_2 M_i)-7(M+1)=2(M+\sum_i M_i)+3\log(M\prod_i M_i)-7(M+1)$ CNOT gates, and $2(M+\sum_i M_i)-2(M+1)=2\sum_i M_i-2$ rotation gates. Comparing with the above estimate, we see that we require the same number of rotation gates and more H gates, and the difference in the CNOT count is

$$\begin{aligned}&2(M+\sum_i M_i)+3\log(M\prod_i M_i)-7(M+1)\\&\quad-2\sum_i M_i-3\log(\sum_i M_i)+7\\&=2M+3\log\left(\frac{M\prod_i M_i}{\sum_i M_i}\right)-7M\\&=3\log\left(\frac{M\prod_i M_i}{\sum_i M_i}\right)-5M,\end{aligned}\tag{C6}$$

which can be less than 0 for certain values of M and M_i. For the SELECT subroutine, we require, for each i, M_i pairs of $C^{\log_2 M_i+1}X$ and M pairs of $C^{\log_2 M}X$. Decomposing these [67,68], we require $\sum_i M_i(4\log(M_i+1)-4)+M(4\log M-4)$ T gates and $\sum_i M_i(4\log(M_i+1)-3)+M(4\log M-3)$ CNOT gates. Thus the difference in the T-gate-count estimate is

$$\begin{aligned}&\sum_i M_i(4\log(M_i+1)-4)+M(4\log M-4)\\&\quad-(4\log(\sum_i M_i)-4)(\sum_i M_i)\\&=4\sum_i M_i\log\left(\frac{M_i+1}{\sum_j M_j}\right)+4M\log M-4M,\end{aligned}$$

which is less than 0 in most cases. Similarly, we can show that the difference in the CNOT count estimate is

$$4\sum_i M_i\log\left(\frac{M_i+1}{\sum_j M_j}\right)+4M\log M-3M,$$

which is again less than 0 in most cases. We use the same number of controlled unitaries in both approaches. Thus, using the divide-and-conquer technique (Theorem 5), it is possible to reduce the implementation cost in terms of the gate count, especially with regard to the T gate and the CNOT gate.

2. Block encoding of Hamiltonians with same ancilla-preparation subroutine

Suppose, in Theorem 5, that each $\textsc{prep}_i$ is the same, which can occur if the LCU decomposition of each H_i has the same weights. We note that the unitaries in the decomposition can be different. Then, in the PREP subroutine of

Eq. (C4), it is sufficient to keep only one copy of $\textsc{prep}_i$:

$$\textsc{prep}\,|0\rangle^{\log M+\log M_i}=\left(\sum_{i=1}^{M}\sqrt{\frac{w_i\lambda_i}{\mathcal{A}}}\,|i\rangle\right)\otimes\textsc{prep}_i. \tag{C7}$$

In the special case when all H_i are the same but are acting on disjoint subspaces, then the first $\log M$ qubits need to be in equal superposition. This has been explained in Sec. II B, as it is more pertinent for our paper.

3. Block encoding of product of Hamiltonians

Suppose that we have $H_p=\prod_{i=1}^{M}H_i$, where each H_i can be block encoded with subroutines described in Eqs. (C1)–(C3). Let $\mathcal{A}'=\prod_{i=1}^{M}\lambda_i$. Then, we can block encode $H_p/\mathcal{A}'$ using the following subroutines:

$$\textsc{prep}_p\,|0\rangle^{\sum_i\log_2 M_i}=\bigotimes_{i=1}^{M}\left(\sum_{j_i=1}^{M_i}\sqrt{\frac{h_{ij_i}}{\lambda_i}}\,|j_i\rangle\right)=\sum_{j_1=1}^{M_1}\sum_{j_2=1}^{M_2}\cdots\sum_{j_M=1}^{M_M}\left(\sqrt{\frac{\prod_{k=1}^{M}h_{kj_k}}{\mathcal{A}'}}\bigotimes_{k=1}^{M}|j_k\rangle\right), \tag{C8}$$

$$\textsc{select}_p=\sum_{j_1=1}^{M_1}\sum_{j_2=1}^{M_2}\cdots\sum_{j_M=1}^{M_M}\left(\bigotimes_{k=1}^{M}|j_k\rangle\langle j_k|\otimes\prod_{k=1}^{M}U_{kj_k}\right). \tag{C9}$$

It follows that

$$\begin{aligned}&\langle 0|\,\textsc{prep}_p^{\dagger}\cdot\textsc{select}_p\cdot\textsc{prep}_p\,|0\rangle\,|\psi\rangle\\&=\frac{1}{\mathcal{A}'}\sum_{j_1=1}^{M_1}\sum_{j_2=1}^{M_2}\cdots\sum_{j_M=1}^{M_M}\prod_{k=1}^{M}h_{kj_k}U_{kj_k}\,|\psi\rangle+|\Psi^{\perp}\rangle\\&=\left(\frac{1}{\mathcal{A}}\prod_{i=1}^{M}H_i\,|\psi\rangle\right)+|\Psi^{\perp}\rangle\end{aligned} \tag{C10}$$

and it is also easy to see that the total implementation cost is the sum of the cost of implementing the block encoding of each H_i. Hence we have the following theorem.

Theorem 6. If $H_p=\prod_{i=1}^{M}H_i$ is a product of M Hamiltonians, such that H_i can be block encoded with the subroutine defined in Eqs. (C1)–(C2), then we can block encode $H_p/\mathcal{A}'$ with the $\textsc{prep}_p$ and $\textsc{select}_p$ subroutines defined in Eqs. (C8)–(C9):

(1) The $\textsc{prep}_p$ subroutine has an implementation cost of $\sum_{i=1}^{M}\mathcal{C}_{\textsc{prep}_i}$, where $\mathcal{C}_{\textsc{prep}_i}$ is the implementation cost of $\textsc{prep}_i$.

(2) The $\textsc{select}_p$ subroutine has an implementation cost of $\sum_{i=1}^{M}\mathcal{C}_{\textsc{select}_i}$, where $\mathcal{C}_{\textsc{select}_i}$ is the implementation cost of $\textsc{select}_i$.

4. Advantages

Now, let us compare with the procedure in which we block encode H_p by expressing it as a sum of $M''=\prod_{i=1}^{M}M_i$ unitaries. We can have an ancilla-preparation subroutine with $\log_2 M''$ ancillas and for arbitrary weights we require $\log_2 M''$ H gates, $2M''+3\log_2 M''-7$ CNOT gates, and $2M''-2$ rotation gates for preparing the weighted superposition. Using Theorem 6, we require the same number of H gates but the number of CNOT gates required is at most $2\sum_i M_i+3\sum_i\log_2 M_i-\sum_i 7$ and the number of rotation gates required is at most $2\sum_i M_i-\sum_i 2$, which is much less. The difference in the number of CNOT gates is

$$\begin{aligned}&2\sum_i M_i+3\sum_i\log M_i-7M-2\prod_i M_i\\&\quad-3\log(\prod_i M_i)+7\\&\quad=2\left(\sum_i M_i-\prod_i M_i\right)-7(M-1)<0,\end{aligned}$$

while the difference in the number of rotation gates is

$$\begin{aligned}&2\sum_i M_i-2M-2\prod_i M_i+2\\&\quad=2\left(\sum_i M_i-\prod_i M_i\right)-2(M-1)<0.\end{aligned}$$

Without using Theorem 6, for the unitary-selection subroutine we require M'' unitaries, each of which is controlled on $\log_2 M''$ ancillas. So we require M'' pairs of $C^{\log_2 M''}X$ gates and M'' controlled unitaries. Decomposing the multicontrolled-X gates, we require $M''(4\log_2 M''-4)$ T gates and $M''(4\log_2 M''-3)$ CNOT gates. Using Theorem 6 we require, for each i, M_i pairs of $C^{\log_2 M_i}X$ gates and M_i controlled unitaries. Thus, in total, we require

$\sum_i M_i(4\log_2 M_i - 4)$ T gates and $\sum_i M_i(4\log_2 M_i - 3)$ CNOT gates. The difference in the T-gate-count estimate is

$$\begin{aligned}
&4\sum_i M_i \log M_i - 4\left(\prod_i M_i\right)\log\left(\prod_i M_i\right)\\
&\qquad - 4\sum_i M_i + 4\prod_i M_i\\
&\quad = 4\sum_i M_i \log M_i - 4\left(\prod_i M_i\right)\sum_i \log M_i\\
&\qquad - 4\left(\sum_i M_i - \prod_i M_i\right)\\
&\quad \le 4\sum_i\left(M_i - \prod_j M_j\right)\log M_i - 4\sum_i\left(M_i - \prod_j M_j\right)\\
&\quad = 4\sum_i\left(M_i - \prod_j M_j\right)\log_2\frac{M_i}{2} \qquad \text{(C11)}
\end{aligned}$$

and the difference in the CNOT-gate-count estimate is

$$4\sum_i\left(M_i - \prod_i M_i\right)\log M_i - 3\left(\sum_i M_i - \prod_i M_i\right),$$

both of which are less than 0 in most cases. Clearly, we get much lower gate counts using the divide-and-conquer approach (Theorem 6).

APPENDIX D: SYNTHESIZING A GROUP OF MULTICONTROLLED-X GATES : SPLIT AND MERGE

Situations often arise in which we need to select and implement something. For example, in many simulation algorithms [2–5,7,8], we need to selectively implement all the unitaries appearing in a LCU decomposition of a Hamiltonian. Let M be the number of unitaries and, for simplicity, let us assume that M is a power of 2. Usually, we allot $\log_2 M$ ancillas, the state of which selects an unitary. Thus we require M unitaries, each controlled on $\log_2 M$ qubits. Each of these multicontrolled unitaries can be implemented with a (compute-uncompute) pair of $C^{\log_2 M}X$ gates and a single-controlled unitary. Such sets can also appear in other applications, as in Refs. [19,61–65], and so the technique that we develop here can also be useful in those cases. In our case, the size of this set is M and the number of T gates required, following the construction in Ref. [67,68], is $\mathcal{T}_1 = M(4\log_2 M - 4)$, while the number of CNOT gates required is $M(4\log_2 M - 3)$. The use of logical AND gadgets eliminates the need to use any T gate for the uncomputation part.

We can reduce the number of gates by "splitting" the control and "merging" the resulting logic. The basic intuition is as follows. Each unitary is associated with a $\log_2 M$-bit binary string, corresponding to a basis state of the $\log_2 M$ control qubits. Suppose that we split the control qubits into two sets, each of length $\log_2 M/2$, and associate each unitary with a pair of binary strings of length $\log_2 M/2$. For each set, we use $M^{1/2}$ $C^{\log_2 M/2}X$ gates to select $M^{1/2}$ basis states by flipping $M^{1/2}$ ancillas. Then, we use $M^{1/2}\cdot M^{1/2}$ C^2X gates to select a basis state from each set and associate it with a unitary. Thus we require $M^{1/2}C^{\log_2 M/2}X + MC^2X$ pairs of gates (compute and uncompute) and hence the number of T gates required is at most $\sqrt{M}\left[(4\log_2 M/2) - 4\right] + M \times 4$ [67]. This constitutes a saving of a log factor in the complexity. The difference in the cost compared with the case without splitting is

$$\begin{aligned}
&M(4\log_2 M - 8) - \sqrt{M}(4\log_2 M - 8) - 4M\\
&\quad = 4\sqrt{M}\left(\sqrt{M} - 1\right)(\log_2 M - 2) > 0
\end{aligned}$$

when $M \ge 4$. Similarly, we can show that we require fewer CNOT gates at the price of extra ancillas. The number of extra ancillas required is at most $\sqrt{M} + \sqrt{M} = 2\sqrt{M}$. This technique can be generalized to the case in which the controls are split into multiple sets, as stated in the following theorem.

Theorem 7. Consider the unitary $U = \sum_{j=0}^{M-1} |j\rangle\langle j| \otimes U_j$ for unitary operators U_j that can be implemented controllably. Let us assume that M is a power of 2, for simplicity. Suppose that we have $\log_2 M$ qubits and M (compute-uncompute) pairs of $C^{\log_2 M}X$ gates for selecting the M basis states. Let $r_1, \ldots, r_n \ge 1$ be positive fractions such that $\sum_{i=1}^n 1/r_i = 1$ and $\log_2 M/r_i$ are integers. Then, U can be implemented with a circuit with

$$\sum_{i=1}^{n} M^{\frac{1}{r_i}} C^{\frac{\log_2 M}{r_i}} X + MC^n X$$

(compute-uncompute) pairs of gates, M applications of controlled U_j, and at most $\sum_{i=1}^n M^{1/r_i}$ ancillas.

Proof. We split the $\log_2 M$ qubits into n sets, such that the ith set has $\log_2 M/r_i$ qubits. Using M^{1/r_i} $C^{\log M/r_i}X$ gates, we select from a set of $2^{\log_2 M/r_i} = M^{1/r_i}$ extra ancilla qubits, each corresponding to a basis state of the qubits in this set. That is, each multicontrolled-X gate has a target on one of these extra ancilla qubits, which gets selected (i.e., state flips) if the control qubits are in a certain basis state. We can use $\left(\prod_{i=1}^n M^{1/r_i}\right) = M$ C^nX gates, such that each has one control in an ancilla qubit of each of the n sets, in order to select the basis states of the $\log_2 M$ qubits. ■

A very simple illustration is given in Fig. 5, where $M = 8$.

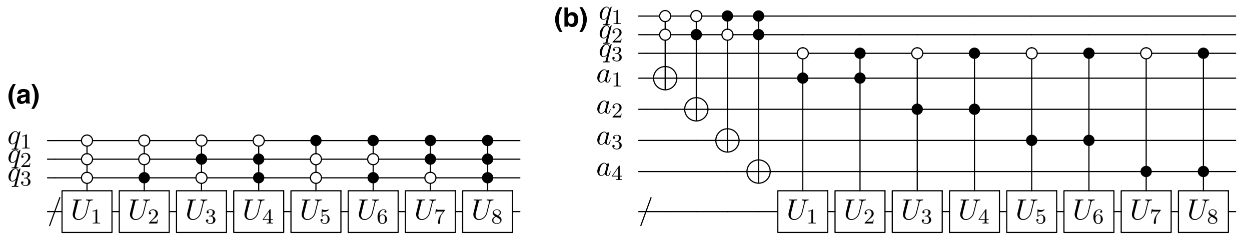

FIG. 5. (a) A SELECT circuit, consisting of eight unitaries and three qubits. (b) An implementation of the same circuit using the split-and-merge technique (Theorem 7).

APPENDIX E: REQUIRED RESULTS ON NORM AND COMMUTATOR OF MATRICES

In this appendix, we give some results on the norm and commutator of matrices, which we use repeatedly throughout our paper. The spectral norm of a matrix A, denoted by $\|A\|$, is its largest singular value.

Theorem 8 ([77]). Let $A \in \mathbb{R}^{m\times n}$ have a singular-value decomposition $U_A\Sigma_A V_A^T$ and let $B \in \mathbb{R}^{p\times q}$ have a singular-value decomposition $U_B\Sigma_B V_B^T$. Then,

$$(U_A \otimes U_B)(\Sigma_A \otimes \Sigma_B)(V_A^T \otimes V_B^T)$$

yields a singular value decomposition of $A \otimes B$ (after a simple reordering of the diagonal elements of $\Sigma_A \otimes \Sigma_B$ and the corresponding right and left singular vectors).

Thus, we can say that $\|A \otimes B\| = \|A\|\|B\|$. Also, we know that it is an operator norm and thus that it satisfies the scaling property $\|aA\| = |a|\|A\|$, the submultiplicative property $\|AB\| \le \|A\|\|B\|$, and the triangle inequality $\|A + B\| \le \|A\| + \|B\|$. If A is unitary, then $\|A\| = 1$.

Let us define the adjoint operator $\mathrm{ad}_x : y \to [x, y]$.

Lemma 8. Let $X_j = \sum_{i_j=1}^{m_j} A_{i_j}^{(j)}$, for $j = 1, \ldots, p$, where $A_{i_j}^{(j)}$ are elements from the same ring. Then,

$$\mathrm{ad}_{X_p}\mathrm{ad}_{X_{p-1}}\ldots\mathrm{ad}_{X_3}\mathrm{ad}_{X_2}X_1 = \sum_{i_p=1}^{m_p}\sum_{i_{p-1}=1}^{m_{p-1}}\cdots\sum_{i_2=1}^{m_2}\sum_{i_1=1}^{m_1}\mathrm{ad}_{A_{i_p}^{(p)}}\mathrm{ad}_{A_{i_{p-1}}^{(p-1)}}\ldots\mathrm{ad}_{A_{i_3}^{(3)}}\mathrm{ad}_{A_{i_2}^{(2)}}A_{i_1}^{(1)}.$$

Proof. We prove the lemma by induction. First, we consider the following base case:

$$\begin{aligned}\mathrm{ad}_{X_2}X_1 &= \left[\sum_{i_2=1}^{m_2}A_{i_2}^{(2)}, \sum_{i_1=1}^{m_1}A_{i_1}^{(1)}\right] = \left(\sum_{i_2=1}^{m_2}A_{i_2}^{(2)}\right)\left(\sum_{i_1=1}^{m_1}A_{i_1}^{(1)}\right) - \left(\sum_{i_1=1}^{m_1}A_{i_1}^{(1)}\right)\left(\sum_{i_2=1}^{m_2}A_{i_2}^{(2)}\right)\\ &= \sum_{i_2=1}^{m_2}\sum_{i_1=1}^{m_1}\left[A_{i_2}^{(2)}, A_{i_1}^{(1)}\right] = \sum_{i_2=1}^{m_2}\sum_{i_1=1}^{m_1}\mathrm{ad}_{A_{i_2}^{(2)}}A_{i_1}^{(1)}.\end{aligned} \tag{E1}$$

Assume that the result holds for the nested commutators between $X_1, \ldots, X_{p-1}$; i.e.,

$$\begin{aligned}\mathrm{ad}_{X_{p-1}}\ldots\mathrm{ad}_{X_3}\mathrm{ad}_{X_2}X_1 &= \sum_{i_{p-1}=1}^{m_{p-1}}\cdots\sum_{i_2=1}^{m_2}\sum_{i_1=1}^{m_1}\mathrm{ad}_{A_{i_{p-1}}^{(p-1)}}\ldots\mathrm{ad}_{A_{i_3}^{(3)}}\mathrm{ad}_{A_{i_2}^{(2)}}A_{i_1}^{(1)}\\ &= \sum_{i_{p-1}=1}^{m_{p-1}}\cdots\sum_{i_2=1}^{m_2}\sum_{i_1=1}^{m_1}\left[A_{i_{p-1}}^{(p-1)}, \left[\cdots\left[A_{i_2}^{(2)}, A_{i_1}^{(i_1)}\right]\cdots\right]\right].\end{aligned} \tag{E2}$$

Then, using the above equation, we have

$$\begin{aligned}\mathrm{ad}_{X_p}\left(\mathrm{ad}_{X_{p-1}}\dots\mathrm{ad}_{X_3}\mathrm{ad}_{X_2}X_1\right) &= \left[\sum_{i_p=1}^{m_p} A_{i_p}^{(p)}, \sum_{i_{p-1}=1}^{m_{p-1}} \cdots \sum_{i_2=1}^{m_2}\sum_{i_1=1}^{m_1}\left[A_{i_{p-1}}^{(p-1)},\left[\cdots\left[A_{i_2}^{(2)},A_{i_1}^{(i_1)}\right]\cdots\right]\right]\right] \\ &= \sum_{i_p=1}^{m_p}\cdots\sum_{i_2=1}^{m_2}\sum_{i_1=1}^{m_1}\left[A_{i_p}^{(p)},\left[\cdots\left[A_{i_2}^{(2)},A_{i_1}^{(i_1)}\right]\cdots\right]\right] \quad \text{[Eq. (E1)]}\end{aligned}$$

and thus the lemma is proved. ■

Lemma 9.

$$\left[\otimes_{i=1}^{n} A_i, \otimes_{i=1}^{n} B_i\right] = \sum_{k=1}^{n}\left(\bigotimes_{i=1}^{k-1} B_iA_i \otimes [A_k, B_k] \otimes \bigotimes_{i=k+1}^{n} A_iB_i\right).$$

Proof. We prove this by induction.

Base case. Let $n = 2$. Then,

$$\begin{aligned}[A_1 \otimes A_2, B_1 \otimes B_2] &= (A_1 \otimes A_2)(B_1 \otimes B_2) - (B_1 \otimes B_2)(A_1 \otimes A_2) \\ &= (A_1B_1 \otimes A_2B_2) - (B_1A_1 \otimes B_2A_2) \\ &= A_1B_1 \otimes A_2B_2 - B_1A_1 \otimes A_2B_2 + B_1A_1 \otimes A_2B_2 - B_1A_1 \otimes B_2A_2 \\ &= (A_1B_1 - B_1A_1) \otimes A_2B_2 + B_1A_1 \otimes (A_2B_2 - B_2A_2) \\ &= [A_1, B_1] \otimes A_2B_2 + B_1A_1 \otimes [A_2, B_2].\end{aligned}$$

Now assume that the given equality holds for $n = m$; i.e.,

$$\left[\otimes_{i=1}^{m} A_i, \otimes_{i=1}^{m} B_i\right] = \sum_{k=1}^{m}\left(\bigotimes_{i=1}^{k-1} B_iA_i \otimes [A_k, B_k] \otimes \bigotimes_{i=k+1}^{m} A_iB_i\right). \tag{E3}$$

We show that it holds for $n = m + 1$ and hence the lemma is proved:

$$\begin{aligned}&\left[\otimes_{i=1}^{m+1} A_i, \otimes_{i=1}^{m+1} B_i\right] = \otimes_{i=1}^{m+1} A_iB_i - \otimes_{i=1}^{m+1} B_iA_i \\ &= A_1B_1 \otimes \bigotimes_{i=2}^{m+1} A_iB_i - B_1A_1 \otimes \bigotimes_{i=2}^{m+1} A_iB_i + B_1A_1 \otimes \bigotimes_{i=2}^{m+1} A_iB_i - B_1A_1 \otimes \bigotimes_{i=2}^{m+1} B_iA_i \\ &= [A_1, B_1 - B_1A_1] \otimes \bigotimes_{i=2}^{m+1} A_iB_i + B_1A_1 \otimes \left(\otimes_{i=2}^{m+1} A_iB_i - \otimes_{i=2}^{m+1} B_iA_i\right) \\ &= [A_1, B_1] \otimes \bigotimes_{i=2}^{m+1} A_iB_i + B_1A_1 \otimes \left(\left(\sum_{k=2}^{m+1}\bigotimes_{i=2}^{k-1} B_iA_i \otimes [A_k, B_k] \otimes \bigotimes_{i=k+1}^{m+1} A_iB_i\right)\right) \\ &= \sum_{k=1}^{m+1}\left(\bigotimes_{i=1}^{k-1} B_iA_i \otimes [A_k, B_k] \otimes \bigotimes_{i=k+1}^{m+1} A_iB_i\right).\end{aligned}$$

■

Fact 1. For $p + 1$ matrices $A_1, A_2, \dots, A_{p+1}$, we have

$$\mathrm{ad}_{A_{p+1}}\mathrm{ad}_{A_p}\dots\mathrm{ad}_{A_2}A_1 \le 2^p \|A_{p+1}\|\|A_p\|\dots\|A_2\|\|A_1\|.$$

APPENDIX F: LCU DECOMPOSITION OF OPERATORS

Efficient decomposition of operators as a linear combination of unitaries is an important step in many simulation algorithms, such as those in Refs. [4,5,7,8]. For a Hamiltonian H, if $H = \sum_j h_j U_j$ is a decomposition into unitaries U_j, then we denote by $\sum_j |h_j|$ the ℓ_1 norm of the decomposition, which serves as an upper bound on the spectral norm of H. This factor determines the complexity of LCU-based simulation algorithms. The number of unitaries in the decomposition determines the gate and ancilla complexity.

We begin this appendix by describing some general results that pertain to the decomposition of diagonal matrices over the complex field, as a sum of unitaries—identity and signature matrices. A matrix the diagonal elements of which are 0 or 1 is referred to as a diagonal binary matrix and a matrix the diagonal elements of which are 1 and -1 is referred to as a signature matrix (unitary). Existing simulation methods do employ such decompositions but we use a slightly more formal presentation for ease of reference. For integer diagonal matrices, we give a decomposition with exponentially fewer unitaries.

As an example for how the idea of the signature matrix decomposition works, let us first consider the matrix M_{01}, which is a diagonal binary matrix, and, without loss of generality, assume that the basis is chosen such that the zero entries are sorted before the 1 entries:

$$\begin{aligned} M_{01} &= \mathrm{diag}(0,\ldots,0,1,\ldots,1) \\ &= \frac{1}{2}\left(\mathrm{diag}(1,\ldots,1,1,\ldots,1)\right. \\ &\quad \left. - \mathrm{diag}(1,\ldots,1,-1,\ldots,-1)\right). \end{aligned} \tag{F1}$$

This shows that by subtracting an appropriate pattern of positive and negative numbers, any binary diagonal matrix can be formed by a difference between two signature matrices. In general, however, we will wish to deal with diagonal matrices that are nonbinary.

Lemma 10. Let M be a $N \times N$ diagonal matrix, such that there are N' distinct diagonal elements, $m_1 < m_2 < \ldots < m_{N'} = m_{\max}$. (The subscripts do not indicate the position of the element along the diagonal.) Then, M can be written as $M = c_0\mathbb{I} + \sum_{i=1}^{N'-1} c_i D_i$, where the D_i are signature matrices and $\sum_{i=0}^{N'-1}|c_i| = |m_1| + \sum_{i=2}^{N'}|m_i - m_{i-1}|$. Specifically, if every $m_i \geq 0$, then the sum is $m_{\max}$.

Proof. Let B_{m_i} be the diagonal binary matrix, derived from M, such that $B_{m_i}[j,j] = 1$ if $M[j,j] \geq m_i$; else it is 0:

$$\begin{aligned} M &= m_1 B_{m_1} + (m_2 - m_1)B_{m_2 - m_1} + (m_3 - m_2)B_{m_3 - m_2} \\ &\quad + \cdots + (m_{N'} - m_{N'-1})B_{m_{N'} - m_{N'-1}}. \end{aligned}$$

Each of the diagonal binary matrices can be decomposed as a sum of an identity and a signature matrix, as shown before in Eq. (F1). In this way, we decompose M as a sum of $\mathbb{I}$ and $N'-1$ signature matrices:

$$\begin{aligned} |c_0| + \sum_{i=1}^{N'-1}|c_i| &= \left(|m_1| + \frac{1}{2}\sum_{i=2}^{N'}|m_i - m_{i-1}|\right) \\ &\quad + \frac{1}{2}\sum_{i=2}^{N'}|m_i - m_{i-1}| \\ &= |m_1| + \sum_{i=2}^{N'}|m_i - m_{i-1}| \\ &= m_{N'}, \qquad \text{if each } m_i > 0. \qquad \blacksquare \end{aligned}$$

Lemma 11. Let $M_I = \mathrm{diag}(m_1,\ldots,m_N)$ be a $N \times N$ matrix, each entry of which is a non-negative integer, and let $m_{\max} = \max_i m_i$. Then, $M = c_0\mathbb{I} + \sum_{i=1}^{N'} c_i D_i$, where the D_i are signature matrices and $N' \leq \lceil \log_2(m_{\max}+1)\rceil = \zeta$. Also, $\sum_{i=0}^{N'}|c_i| \leq 2^\zeta - 1$.

Proof. The number of qubits required to implement $m_{\max}$ is $\lceil \log_2(m_{\max}+1)\rceil = \zeta$. We represent each diagonal integer in the binary representation. Thus the ith element is as follows:

$$m_i = b_0^{(i)}2^0 + b_1^{(i)}2^1 + b_2^{(i)}2^2 + \cdots + b_{\zeta-1}^{(i)}2^{\zeta-1}.$$

Thus, M_I can be written as follows:

$$\begin{aligned} M_I &= 2^0\mathrm{diag}(b_0^{(1)}, b_0^{(2)}, \ldots, b_0^{(N)}) \\ &\quad + 2^1\mathrm{diag}(b_1^{(1)}, b_1^{(2)}, \ldots, b_1^{(N)}) \\ &\quad + \cdots + 2^{\zeta-1}\mathrm{diag}(b_{\zeta-1}^{(1)}, b_{\zeta-1}^{(2)}, \ldots, b_{\zeta-1}^{(N)}). \end{aligned}$$

We can use Eq. (F1) to decompose each diagonal binary matrix as a sum of $\mathbb{I}$ and one signature matrix. This proves the first decomposition part of the lemma. For the second part, we have the following:

$$\sum_i |c_i| = \frac{1}{2}\sum_{i=0}^{\zeta-1}2^i + \frac{1}{2}\sum_{i=0}^{\zeta-1}2^i = 2^\zeta - 1. \qquad \blacksquare$$

If a diagonal matrix has both positive and negative real values, then we can have the following decompositions. These can be especially useful to reduce the ℓ_1 norm of the coefficients, if the negative entries are quite large. First, we give a decomposition for the case when the entries are not necessarily integers.

Lemma 12. Let M be a $N \times N$ diagonal real matrix, such that there are N' distinct nonzero positive elements and N'' distinct (nonzero) negative elements. Then, M can be written as $M = c_0\mathbb{I} + \sum_{i=1}^{N'+N''} c_i D_i$, where the D_i are signature matrices and $\sum_{i=0}^{N'+N''}|c_i| = m_{\max}$, where $m_{\max}$ is the largest positive diagonal entry.

Proof. We split M as the difference of two matrices, $M = M' - M''$, where $M'[i,i] = M[i,i]$ if $M[i,i] > 0$; else $M'[i,i] = 0$—while $M''[i,i] = |M[i,i]|$ if $M[i,i] < 0$; else $M''[i,i] = 0$. So, both M' and M'' are positive diagonal matrices. Let us order the elements (including 0) of M' and M'', respectively, as follows: $m'_0 < m'_1 < \cdots < m'_{N'}$ and $m''_0 < m''_1 < \cdots < m''_{N''}$. (We note that the subscripts here do not reflect the position of the element along the diagonal.) For both matrices, $m'_0 = m''_0 = 0$. We can use Lemma 10 and decompose the matrices as a sum of identity and signature matrices,

$$M' = \left(m'_0 + \frac{1}{2}\sum_{i=1}^{N'}(m'_i - m'_{i-1})\right)\mathbb{I} + \frac{1}{2}\sum_{i=1}^{N'}(m'_i - m'_{i-1})D'_i,$$

$$M'' = \left(m''_0 + \frac{1}{2}\sum_{i=1}^{N''}(m''_i - m''_{i-1})\right)\mathbb{I} + \frac{1}{2}\sum_{i=1}^{N''}(m''_i - m''_{i-1})D''_i,$$

where D'_i and D''_i are signature matrices. Therefore,

$$M = \left(\frac{1}{2}\sum_{i=1}^{N'}(m'_i - m'_{i-1}) - \frac{1}{2}\sum_{i=1}^{N''}(m''_i - m''_{i-1})\right)\mathbb{I} + \frac{1}{2}\sum_{i=1}^{N'}(m'_i - m'_{i-1})D'_i - \frac{1}{2}\sum_{i=1}^{N''}(m''_i - m''_{i-1})D''_i,$$

since $m'_0 = m''_0 = 0$ and hence the sum of the absolute values of the coefficients is

$$\left(\frac{1}{2}\sum_{i=1}^{N'}(m'_i - m'_{i-1}) - \frac{1}{2}\sum_{i=1}^{N''}(m''_i - m''_{i-1})\right) + \frac{1}{2}\sum_{i=1}^{N'}(m'_i - m'_{i-1}) + \frac{1}{2}\sum_{i=1}^{N''}(m''_i - m''_{i-1}) = \sum_{i=1}^{N'}(m'_i - m'_{i-1}) = m_{N'} = m_{\max}. \tag{F2}$$

■

We can have a similar result when the entries are both positive and negative integers, including 0.

Lemma 13. Let M_I be a $N \times N$ diagonal integer matrix, which has N' positive integers, the maximum value of which is $m'_{\max}$, and N'' negative integers such that $m''_{\max} = \max_i\{|M_I[i,i]| : M_I[i,i] < 0\}$. Then, $M = c_0\mathbb{I} + \sum_{i=1}^{N'+N''} c_i D_i$, where the D_i are signature matrices and $N' \leq \lceil \log_2(m'_{\max} + 1)\rceil = \zeta'$ and $N'' \leq \lceil \log_2(m''_{\max} + 1)\rceil = \zeta''$. Also, $\sum_{i=0}^{N'+N''} |c_i| \leq 2^{\zeta'} - 1$.

Now, we consider some particular matrices that are relevant for the operators that appear in this paper. We give some decompositions as a sum of some fundamental quantum gates.

1. LCU decomposition of A and A^2

First, consider the operator A described as

$$A = \frac{1}{i\Delta}\mathcal{F}\left(\frac{2\pi i}{d}C'\right)\mathcal{F}^\dagger, \tag{F3}$$

where $C' = \text{diag}(0, 1, 2, \ldots, d-1)$.

Lemma 14. Let $U = \mathbb{I}_{(\zeta)} \otimes \ldots \otimes \mathbb{I}_{(\ell+1)} \otimes \mathrm{Z}_{(\ell)} \otimes \mathbb{I}_{(\ell-1)} \otimes \ldots \otimes \mathbb{I}_{(1)}$ is a tensor product of ζ single-qubit unitaries, where Z is applied on qubit ℓ and $\mathbb{I}$ on the rest. Then, U is a diagonal matrix of the following form:

$$\begin{aligned} U_{j,j} &= 1 \quad \text{if } j = 2^\ell k, 2^\ell k + 1, \ldots 2^\ell k + 2^{\ell-1} - 1 \\ &= -1 \quad \text{if } j = 2^\ell k + 2^{\ell-1}, 2^\ell k + 2^{\ell-1} \\ &\qquad + 1, \ldots 2^\ell k + 2^\ell - 1, \end{aligned}$$

where $k = 0, 1, \ldots, 2^{\zeta-\ell} - 1$.

Proof. $\mathbb{I}_{(\ell-1)} \otimes \ldots \otimes \mathbb{I}_{(1)} = \mathbb{I}_{2^{\ell-1}}$ is a $2^{\ell-1} \times 2^{\ell-1}$ identity matrix.

For any matrix M, $\mathrm{Z} \otimes M$ gives a block diagonal matrix with $+M$ in the first or upper block and $-M$ in the second or lower block. Thus, $\mathrm{Z}_{(\ell)} \otimes \left(\mathbb{I}_{(\ell-1)} \otimes \ldots \otimes \mathbb{I}_{(1)}\right) = \mathrm{Z} \otimes \mathbb{I}_{2^{\ell-1}}$ is a diagonal matrix with $+\mathbb{I}_{2^{\ell-1}}$ in the first block and $-\mathbb{I}_{2^{\ell-1}}$ in the second block. This implies that it has $+1$ in the first $2^{\ell-1}$ diagonal entries and -1 in the remaining $2^{\ell-1}$ entries.

$\mathbb{I}_{(\zeta)} \otimes \ldots \otimes \mathbb{I}_{(\ell+1)} = \mathbb{I}_{2^{\zeta-\ell}}$ is a $2^{\zeta-\ell} \times 2^{\zeta-\ell}$ identity matrix.

For any matrix M', $\mathbb{I}_{2^{\zeta-\ell}} \otimes M'$ is a block diagonal matrix with M' embedded along the diagonal. Thus $U = \mathbb{I}_{2^{\zeta-\ell}} \otimes \left(\mathrm{Z} \otimes \mathbb{I}_{2^{\ell-1}}\right)$ is a $2^\zeta \times 2^\zeta$ matrix with $\left(\mathrm{Z} \otimes \mathbb{I}_{2^{\ell-1}}\right)_{2^\ell \times 2^\ell}$ repeating $2^{\zeta-\ell}$ times along the diagonal. This explains the range of the index k in the statement of the lemma. Since in each block the first $2^{\ell-1}$ entries are $+1$ and the remaining ones are -1, we obtain the above-mentioned range of values of the index j. ■

Lemma 15. Let $C' = \text{diag}(0, 1, 2, 3, \ldots, d-1)$. Then, assuming that $d = 2^\zeta$,

$$C' = \frac{2^\zeta - 1}{2}\mathbb{I} - \frac{1}{2}\sum_{i=0}^{\zeta-1} 2^i \mathrm{Z}_{(i+1)},$$

where $\mathrm{Z}_{(i+1)} = \mathbb{I}_{(\zeta)} \otimes \ldots \otimes \mathbb{I}_{(i+2)} \otimes \mathrm{Z}_{(i+1)} \otimes \mathbb{I}_{(i)} \otimes \ldots \otimes \mathbb{I}_{(1)}$.

Proof. Using Lemma 11, we can decompose C' as follows:

$$C' = \sum_{i=0}^{\zeta-1} 2^i \mathrm{diag}\left(b_i^{(0)}, b_i^{(1)}, \ldots, b_i^{(d-1)}\right),$$

where $b_i^{(j)}$ is the ith bit occurring in the binary expansion of j. Using Eq. (F1), we can further decompose each $\mathrm{diag}\left(b_i^{(0)}, b_i^{(1)}, \ldots, b_i^{(d-1)}\right)$ as a sum of an identity and a signature matrix. Now, if we follow the binary decomposition of consecutive integers, then we see that $\mathrm{diag}\left(b_0^{(0)}, b_0^{(1)}, \ldots, b_0^{(d-1)}\right)$ has alternative 0 and 1, which leads to a signature matrix with alternating $+1$ and -1. $\mathrm{diag}\left(b_1^{(0)}, b_1^{(1)}, \ldots, b_1^{(d-1)}\right)$ has two 0s, the next two 1s, and so on. This yields a signature matrix with two $+1$s, then next two -1s, and so on. To generalize, $\mathrm{diag}\left(b_i^{(0)}, b_i^{(1)}, \ldots, b_i^{(d-1)}\right)$ has the first 2^{i+1} entries as 0, while the next 2^{i+1} entries are 1, and so on, and we obtain the corresponding pattern in the signature matrix. Thus, using Lemma 14, we can write

$$\mathrm{diag}\left(b_i^{(0)}, b_i^{(1)}, \ldots, b_i^{(d-1)}\right) = \frac{1}{2}\left(\bigotimes_{j=1}^{\zeta} \mathbb{I}_{(j)} - Z_{(i+1)}\right)$$

and hence the lemma follows. ■

As a corollary, we can have the following LCU decomposition of A.

Corollary 1. Let $d = 2^\zeta$. Then, we can write

$$A = \frac{2\pi}{d\Delta}\left(\frac{2^\zeta - 1}{2}\mathbb{I} - \mathcal{F}\left(\sum_{i=0}^{\zeta-1} 2^{i-1} \mathrm{Z}_{(i+1)}\right)\mathcal{F}^\dagger\right).$$

It can be easily shown that this decomposition not only has the same number of unitaries but also the same ℓ_1 norm, compared to the decomposition obtained by using Lemma 11. The additional advantage is the fact that in this case, we have specified the unitaries in terms of fundamental gates. The following result also follows from the previous corollary.

Corollary 2. Let $d = 2^\zeta$. Then, we can write

$$A^2 = \frac{\pi^2}{d^2\Delta^2}\mathcal{F}\left(\left(c_0^2 + \sum_{i=0}^{\zeta-1} 2^{2i}\right)\mathbb{I} - 2c_0\sum_{i=0}^{\zeta-1} 2^i \mathrm{Z}_{(i+1)} + 2\sum_{i=0}^{\zeta-2}\sum_{j=i+1}^{\zeta-1} 2^{i+j}\mathrm{Z}_{(i+1)}\mathrm{Z}_{(j+1)}\right)\mathcal{F}^\dagger.$$

It can be shown that compared to Lemma 11, this decomposition has the same ℓ_1 norm, i.e.,

$$\begin{aligned}
&\frac{\pi^2}{d^2\Delta^2}\left(c_0^2 + \sum_{i=0}^{\zeta-1} 2^{2i} + 2c_0\sum_{i=0}^{\zeta-1} 2^i + 2\sum_{i=0}^{\zeta-2} 2^i \sum_{j=i+1}^{\zeta-1} 2^j\right) \\
&= \frac{\pi^2}{d^2\Delta^2}\left(c_0^2 + \frac{4^\zeta - 1}{3} + 2c_0(2^\zeta - 1) + 2\sum_{i=0}^{\zeta-2} 2^{i+i+1}\sum_{j=0}^{(\zeta-1)-(i+1)} 2^j\right) \\
&= \frac{\pi^2}{d^2\Delta^2}\left(c_0^2 + \frac{d^2 - 1}{3} + 2c_0(d-1) + 2\sum_{i=0}^{\zeta-3} 2^{i+i+1}(2^{\zeta-(i+1)} - 1) + 2 \times 2^{(\zeta-2)+(\zeta-1)}\right) \\
&= \frac{\pi^2}{d^2\Delta^2}\left(c_0^2 + \frac{d^2 - 1}{3} + 2c_0(d-1) + 2^{\zeta+1}\sum_{i=0}^{\zeta-3} 2^i + 2^{2\zeta-2} - 4\sum_{i=0}^{\zeta-3} 4^i\right) \\
&= \frac{\pi^2}{d^2\Delta^2}\left(c_0^2 + \frac{d^2 - 1}{3} + 2c_0(d-1) + 2^{\zeta+1}(2^{\zeta-2} - 1) + \frac{4^\zeta}{4} - 4\frac{4^{\zeta-2} - 1}{3}\right) \\
&= \frac{\pi^2}{d^2\Delta^2}\left(d^2\left(3 + \frac{1}{3} + \frac{1}{2} + \frac{1}{4} - \frac{1}{12}\right) - 8d + 4\right) = \frac{4\pi^2(d-1)^2}{d^2\Delta^2} \leq \frac{4\pi^2}{\Delta^2},
\end{aligned}$$

but the number of unitaries, i.e.,

$$1 + (\zeta - 1) + ((\zeta - 1) + (\zeta - 2) + \cdots + 1) = \frac{\zeta(\zeta+1)}{2} = \frac{\log_2^2 d + \log_2 d}{2} \tag{F4}$$

is slightly greater. Nonetheless, the advantage is the fact that we have a decomposition in terms of very fundamental quantum gates.

2. LCU decomposition of ∇ and ∇^2

We approximate these differential operators with $(2a+1)$-point central-difference formulas, by which we obtain decompositions as a sum of adders. In general, the approximation error is given by the following lemma.

Lemma 16 ([13,78]).

$$\nabla_\mu^2 \psi(x) = \frac{1}{h^2}\sum_{k=-a}^{a} d_{2a+1,k}\psi(x+kh\hat{e}_\mu) + \mathcal{R}_{2a+1},$$

where $\hat{e}_\mu$ is the unit vector along the μth component of x, $(x+kh\hat{e}_\mu)$ is evaluated modulo the grid length L, $\mathcal{R}_{2a+1} \in O(h^{2a-1})$, and

$$\begin{aligned} d_{2a+1,k\neq 0} = \frac{2(-1)^{a+k+1}(a!)^2}{(a+k)!(a-k)!k^2} \quad d_{2a+1,k=0} \\ = -\sum_{k=-a,k\neq 0}^{a} d_{2a+1,k}. \end{aligned}$$

More specific bounds can be made on the truncation error for these central-difference formulas through the use of Taylor's remainder theorem. Also, the bounds on the 1-norm of the coefficients for the adder decomposition are summarized in the following lemma.

Lemma 17 (Theorem 7 and Lemma 6 in Ref. [13]). Let $\psi(x) \in \mathbb{C}^{2a+1}$ on $x \in \mathbb{R}$ for $a \in \mathbb{Z}_+$. Then, the error in the $(2a+1)$-point centered difference formula for the second derivative of $\psi(x)$ evaluated on a uniform mesh with spacing h is at most

$$|\mathcal{R}_{2a+1}| \le \frac{\pi^{3/2}}{9} e^{2a[1-\ln 2]} h^{2a-1} \max_x \left|\psi^{(2a+1)}(x)\right|.$$

Also, the sum of the norms of the coefficients is bounded from above as follows:

$$\sum_{k=-a,k\neq 0}^{a} \left|d_{2a+1,k}\right| \le \frac{2\pi^2}{3}.$$

Thus ∇^2 is approximated by a sum of $2a+1$ adders and the ℓ_1 norm of the coefficients is at most $4\pi^2/3h^2$.

Next, we need a similar expression for the gradient, so that we can understand how to block encode the result as a function of the number of points used in the decomposition. The first result stems from earlier work by Li [78], which gives a high-order derivative expression using centered differences:

Lemma 18 ([78]).

$$\nabla_\mu \psi(x) = \frac{1}{h}\sum_{k=-a}^{a} d'_{2a+1,k}\psi(x+kh\hat{e}_\mu) + \mathcal{R}'_{2a+1},$$

where $\hat{e}_\mu$ is the unit vector along the μth component of x, $(x_\mu + kh\hat{e}_\mu)$ is evaluated modulo the grid length L, $|\mathcal{R}'_{2a+1}| \in O(h^{2a})$, and

$$d'_{2a+1,k} = \frac{(-1)^{k+1}(a!)^2}{j(a-k)!(a+k)!}, \quad d'_{2a+1,0} = 0.$$

Next, we need to bound the 1-norm of this formula, the bound for which is given in the following lemma.

Lemma 19. The sum of the norms of the coefficients in the $(2a+1)$-point centered finite-difference formula is bounded from above as follows:

$$\begin{aligned} &\sum_{k=-a,k\neq 0}^{a} \left|d'_{2a+1,k}\right| \\ &\quad \le 2\ln a + \gamma, \quad \text{where } \gamma \approx 0.577 \text{ is the Euler-} \\ &\qquad\qquad \text{Mascheroni constant} \\ &\quad \le \ln 2a^2, \qquad \text{when } a \ge \sqrt{e} \approx 1.4. \end{aligned}$$

Proof.

$$\begin{aligned} \sum_{k=-a,k\neq 0}^{a} \left|d'_{2a+1,k}\right| &= \sum_{k=-a,k\neq 0}^{a} \frac{(a!)^2}{|k|(a-k)!(a+k)!} \\ &\le \sum_{k=-a,k\neq 0}^{a} \frac{1}{|k|}, \quad \text{for } |k| \le a \text{ when } a \ge 1 \\ &= 2\sum_{k=1}^{a}\frac{1}{|k|} = 2\ln a + \gamma, \end{aligned}$$

where $\gamma \approx 0.577$ is the Euler-Mascheroni constant. ■

Finally, for completeness, we prove a specific truncation bound on the finite-difference approximation to the gradient.

Lemma 20. Let $\psi(x) \in \mathbb{C}^{2a+1}$ on $x \in \mathbb{R}$ for $a \in \mathbb{Z}_+$. Then, the error in the $(2a+1)$-point centered difference formula for the first derivative of $\psi(x)$ evaluated on a uniform mesh with spacing h is at most

$$\left|\mathcal{R}'_{2a+1}\right| \le \frac{(2\ln a + \gamma)}{6\sqrt{\pi}} e^{2a[1-\ln 2]} h^{2a+1} \max_x \left|\psi^{(2a+1)}(x)\right|.$$

Proof. Using Ref. [78, Corollary 2.1] and the triangle inequality, we have the following:

$$\begin{aligned}\left|\mathcal{R}'_{2a+1}\right| &\le \frac{h^{2a+1}}{(2a+1)!}\max_x\left|\psi^{(2a+1)}(x)\right| \\ &\quad\times\sum_{k=-a,\neq 0}^{a}|d_{2a+1,k}||k|^{2a+1} \\ &\le \frac{h^{2a+1}a^{2a+1}}{(2a+1)!}\max_x\left|\psi^{(2a+1)}(x)\right|\sum_{k=-a,\neq 0}^{a}|d_{2a+1,k}| \\ &< \frac{(2\ln a+\gamma)h^{2a+1}a^{2a+1}}{(2a+1)!}\max_x\left|\psi^{(2a+1)}(x)\right| \\ &\quad\times\text{[using Lemma 19]}. \end{aligned} \tag{F5}$$

Using Stirling's approximation and the fact that $a \ge 1$, we have the following:

$$\frac{a^{2a+1}}{(2a+1)!} \le \frac{\sqrt{a}e^{2a[1-\ln 2]}}{2(2a+1)\sqrt{\pi}} \le \frac{e^{2a[1-\ln 2]}}{6\sqrt{\pi}}.$$

The lemma is proved by substituting the above inequality into Eq. (F5). ■

Thus ∇ can be written as a sum of $2a$ unitaries, which are adders, and the ℓ_1 norm of the coefficients is at most $2\ln a+\gamma \le \ln(2a^2)$.

As a final note, we see here that the accuracy of the discrete derivatives considered increases as we increase the number of points used in the formula provided that the underlying wave function is sufficiently smooth. For our purposes, we will not discuss in detail the specific value of a that is optimal and we will assume that it is a constant. This is because it is, in general, difficult to provide bounds on the values of the higher-order derivatives of the wave function as a function of the evolution time. While, in principle, high-order formulas can be valuable to address accuracy concerns, we need such guarantees in order to understand the optimal order to take for a particular evolution. This is especially relevant since the initial state is not necessarily in C^∞ and thus the asymptotic advantages may disappear for classes of functions that are not sufficiently smooth. For these reasons, we leave detailed discussion of the truncation error to subsequent work and focus on the case in which a is a constant.

3. LCU decomposition of E^2

In the electric link basis, $E^2_{\ell,\mu} = \sum_{\epsilon=-\Lambda}^{\Lambda-1}\epsilon^2\left|\epsilon\right\rangle\left\langle\epsilon\right|_{\ell,\mu}$ is a diagonal positive integer matrix and so we can use Lemma 11 to express it as a linear combination of at most $1+\lceil\log_2(\Lambda^2+1)\rceil \approx 2\log_2\Lambda$ unitaries and the ℓ_1 norm of the coefficients is at most Λ^2. Alternatively, E^2 can be expressed as a linear combination of slightly more number of Z operators but with the same ℓ_1 norm [24]:

$$E^2 = \frac{1}{6}\left(2^{2\zeta-1}+1\right)\mathbb{I}+\sum_{j=0}^{\zeta-1}2^{j-1}Z_j+\sum_{j=0}^{\zeta-2}\sum_{k>j}^{\zeta-1}2^{j+k-1}Z_jZ_k, \tag{F6}$$

where $\zeta = \log_2\Lambda$.

4. LCU decomposition of U

We know that $U = \sum_{\epsilon=-\Lambda}^{\Lambda-1}\left|\epsilon+1\right\rangle\left\langle\epsilon\right| = \exp(i\Delta A) = \mathcal{F}C\mathcal{F}^\dagger$, where C is the Sylvester's "clock" matrix, defined as

$$C = \begin{pmatrix}1 & 0 & 0 & \cdots & 0\\ 0 & \omega & 0 & \cdots & 0\\ 0 & 0 & \omega^2 & \cdots & 0\\ \vdots & \vdots & \vdots & \ddots & \vdots\\ 0 & 0 & 0 & \cdots & \omega^{d-1}\end{pmatrix},$$

where $\omega = e^{2\pi i/d}$ and d is the dimension of C.

Lemma 21. Let $R(2^k) = \begin{bmatrix}1 & 0\\ 0 & \omega^{2^k}\end{bmatrix}$ be a rotation gate. Then,

$$\begin{aligned}&R(2^x)\otimes\cdots\otimes R(2^1)\otimes R(2^0)\\ &\quad= \bigotimes_{k=0}^{x}R(2^k) = \text{diag}(1,\omega,\ldots,\omega^{2^{x+1}-1}).\end{aligned} \tag{F7}$$

Proof. We prove by induction. For the base case, we have

$$\begin{aligned}&R(2^1)\otimes R(2^0)\\ &\quad= \text{diag}(1,\omega^2)\otimes\text{diag}(1,\omega) = \text{diag}(1,\omega,\omega^2,\omega^3).\end{aligned}$$

Let the lemma hold when $k = m-1$, i.e.,

$$\bigotimes_{k=0}^{m-1}R(2^k) = \text{diag}(1,\omega,\ldots,\omega^{2^m-1}).$$

Then,

$$\begin{aligned}&\bigotimes_{k=0}^{m}R(2^k)\\ &\quad= R(2^m)\otimes\left(\bigotimes_{k=0}^{m-1}R(2^k)\right)\\ &\quad= \text{diag}(1,\omega^{2^m})\otimes\text{diag}(1,\omega,\ldots,\omega^{2^m-1})\\ &\quad= \text{diag}(1,\omega,\ldots,\omega^{2^m-1},\omega^{2^m},\omega^{2^m+1},\ldots,\omega^{2^{m+1}-1})\end{aligned}$$

and the lemma follows. ■

Setting $d = 2^{x+1}$, we can have the following decomposition of U and hence the ℓ_1 norm of U is 1.

Corollary 3. Let $R(2^k) = \begin{bmatrix} 1 & 0 \\ 0 & \omega^{2^k} \end{bmatrix}$ be a rotation gate. Then, $U = \mathcal{F}\left(\bigotimes_{k=0}^{\log_2 d-1} R(2^k)\right)\mathcal{F}^{\dagger}$.

5. LCU decomposition of the fragment Hamiltonians

We can decompose the fragment Hamiltonians appearing in this paper [Eq. (20)] as a sum of unitaries, using the LCU decomposition of the above operators and Lemma 10. We briefly describe the decompositions in the points below:

(1) $\mathbf{H_s} = -1/c\sum_{j=1}^{\eta}\sum_{q=1}^{N}\sum_{\mu\neq\nu\neq\xi=1}^{3}\sigma_{j,\mu}\otimes\mathbb{I}\otimes\left(\nabla_\nu A_{q,\xi} - \nabla_\xi A_{q,\nu}\right)$. Using the LCU decompositions of ∇ (Lemma 18) and A (Corollary 1), we can write it as a sum of $2\times 3\eta\times N(2a+1)(\lceil\log_2 d\rceil + 1) \approx 12\eta Na\log_2 d$ unitaries and using the triangle inequality (Appendix E), we obtain the ℓ_1 norm as $\leq (1/c)3\eta N\times 2\times\ln(2a^2)/h\times 2\pi/\Delta = 12\pi\eta N\ln(2a^2)/ch\Delta$.

(2) $\mathbf{H_{V_{ee}}} = 1/\Delta\sum_{k<j}^{\eta}\sum_{\mathbf{q},\mathbf{r}}^{N}\left(\mathbb{I}\otimes 1/\|\mathbf{q}-\mathbf{r}\|_2\,|\mathbf{q}\rangle\langle\mathbf{q}|_k\,|\mathbf{r}\rangle\langle\mathbf{r}|_j\otimes\mathbb{I}\right)$. Here, $\sum_{\mathbf{q},\mathbf{r}}^{N}|\mathbf{q}\rangle\langle\mathbf{q}|_k\otimes|\mathbf{r}\rangle\langle\mathbf{r}|_j$ is a diagonal operator. Using Lemma 10, we can express $\sum_{\mathbf{q},\mathbf{r}} 1/\|\mathbf{q}-\mathbf{r}\|_2\,|\mathbf{q}\rangle\langle\mathbf{q}|_i\otimes|\mathbf{r}\rangle\langle\mathbf{r}|_j$ as a sum of $\mathbb{I}$ and $N-1$ signature matrices and the ℓ_1 norm of the decomposition is $(1/\|\mathbf{q}-\mathbf{r}\|_2)_{\max} = 1/\Delta$. Hence, $H_{V_{ee}}$ can be decomposed as a sum of at most $\eta(\eta-1)N/2$ unitaries with ℓ_1 norm at most $\eta(\eta-1)/2\Delta^2$. Since $\Delta = \Omega^{1/3}/N^{1/3}$, the dependence on N is sort of implicit in the norm.

(3) $\mathbf{H_{V_{ne}}} = -1/\Delta\sum_{j}^{\eta}\sum_{\kappa}^{K}\sum_{\mathbf{q}}^{N}\left(\mathbb{I}\otimes Z_\kappa/\|\mathbf{q}-\mathbf{R}_\kappa\|_2\,|\mathbf{q}\rangle\langle\mathbf{q}|_j\otimes\mathbb{I}\right)$. Here, $\sum_{\mathbf{q}}^{N}|\mathbf{q}\rangle\langle\mathbf{q}|$ is a diagonal operator. The number of distinct values of $Z_\kappa/\|\mathbf{q}-\mathbf{R}_\kappa\|_2$, for a particular value of κ, is at most N. So, using Lemma 10, we can decompose $\sum_q Z_\kappa/\|\mathbf{q}-\mathbf{R}_\kappa\|_2\,|\mathbf{q}\rangle\langle\mathbf{q}|$ as a sum of $\mathbb{I}$ and at most $N-1$ signature matrices and the ℓ_1 norm is at most $Z_\kappa/d_{\min}$, where $d_{\min} = (\|\mathbf{q}-\mathbf{R}_\kappa\|_2)_{\min} = \Delta$. Hence $H_{V_{ne}}$ can be decomposed as a sum of at most ηKN unitaries and the ℓ_1 norm is at most $\eta Z_{\text{sum}}/\Delta^2$, where $Z_{\text{sum}} = \sum_{\kappa=1}^{K}|Z_\kappa|$. Here too, the dependence of the norm on N is implied due to Δ.

(4) $\mathbf{H_{f1}} = \sum_q^N\sum_\mu^3\mathbb{I}\otimes\mathbb{I}\otimes\frac{1}{2}E_{q,\mu}^2$. Since $E_{q,\mu}^2$ is a diagonal positive integer matrix, we can use Lemma 11. Thus H_{f1} can be decomposed as a sum of at most $3N\left(1+\lceil\log_2\left(\Lambda^2+1\right)\rceil\right)\approx 6N\log_2\Lambda$ unitaries with ℓ_1 norm at most $3N\Lambda^2/2$.

(5) $\mathbf{H_{f2}} = -\sum_q^N\sum_{\mu\neq\nu}^3\mathbb{I}\otimes\mathbb{I}\otimes\left(W_{q,\mu,\nu}^2 + \text{H.c.}\right)$. Using Corollary 3 and the definition of W^2 [Eq. (9)], we can decompose H_{f2} as a sum of $6N$ unitaries, with ℓ_1 norm at most $6N$.

(6) $\mathbf{H_{1\pi}} = -\frac{1}{2}\sum_j^\eta\sum_q^N\sum_\mu^3\mathbb{I}\otimes\nabla_{j,\mu}^2\otimes\mathbb{I}$. Using Lemma 16, we can express it as a sum of at most $6a\eta N$ unitaries and the ℓ_1 norm is at most $6\eta N(4\pi^2/3h^2) = 8\pi^2\eta N/h^2$.

(7) $\mathbf{H_{2\pi}} = 1/c\sum_j^\eta\sum_q^N\sum_\mu^3\mathbb{I}\otimes(i\nabla_{j,\mu})\otimes A_{q,\mu}$. Using Lemma 18 and Corollary 1, we have a decomposition with a sum of at most $6a\eta N\log_2 d$ unitaries and using Lemma 19, the ℓ_1 norm is at most $12\pi\eta N\ln(2a^2)/ch\Delta$.

(8) $\mathbf{H_{3\pi}} = 1/2c^2\sum_j^\eta\sum_q^N\sum_\mu^3\mathbb{I}\otimes\mathbb{I}\otimes A_{q,\mu}^2$. We use Lemma 11 to decompose $\operatorname{diag}\left(0^2, 1^2, 2^2, \ldots, (d-1)^2\right)$ and hence A^2, as a sum of at most $\lceil\log_2(d-1)^2+1\rceil + 1 \lessapprox 2\log_2 d$ unitaries. Thus $H_{3\pi}$ can be expressed as a sum of at most $6\eta N\log_2 d$ unitaries and the ℓ_1 norm is at most $3\eta N(4\pi^2/c^2\Delta^2) = 12\pi^2\eta N/c^2\Delta^2$.

In Table II, we summarize the number of unitaries in the LCU decomposition of various operators and Hamiltonians and also mention an upper bound on the ℓ_1 norm.

APPENDIX G: CIRCUIT DECOMPOSITIONS FOR SIMULATION CIRCUITS

The following four subsections describe the algorithms to simulate the exponential of the four Hamiltonian terms that comprise our Hamiltonian, depicted as leaves in Fig. 2, thus proving Lemma 2–6. As mentioned before, we describe the circuits in terms of Clifford+T and (controlled)-rotation gates.

1. Algorithm to simulate $e^{-iH_{12}\tau_1} = e^{i\tau_1\sum_{q=1}^{N}\sum_{\mu\neq\nu=1}^{3}\mathbb{I}\otimes\mathbb{I}\otimes W_{q,\mu,\nu}^2}$

In this section, we prove the complexity of simulating $e^{-iH_{12}\tau_1}$ using qubitization, thus proving Lemma 2. We know that $H_{12} = H_{f2}$ [Eq. (22)], which corresponds to the plaquette terms in the dynamics of the system. In Corollary 3, we show that the raising operator $U_{q,\mu}$ (defined in Eq. (8)) is as follows:

$$U_{q,\mu} = \mathcal{F}_{q,\mu}\left(\bigotimes_{k=1}^{\log_2 d-1} R_z(\theta_k)\right)_{q,\mu}\mathcal{F}_{q,\mu}^{\dagger}, \tag{G1}$$

where $\theta_k = \frac{2\pi}{d}2^k$ and $\mathcal{F}$ is the Fourier transform.

This shows that an individual $U_{q,\mu}$ can be implemented using $\log_2(d)$ single-qubit rotations. The plaquette operator $W_{q,\mu,\nu}$ can be implemented using four such terms and thus $W_{q,\mu,\nu}^2$ [Eq. (9)] can be implemented by a layer of at most $4\log_2 d$ parallel rotations, conjugated by Fourier transformation. The ancilla-preparation subroutine does the following:

$$\text{PREP}_{f2}\,|0\rangle^{*} = \left(\frac{1}{\sqrt{N}}\sum_{q=1}^{N}|q\rangle\right) \otimes \left(\frac{1}{\sqrt{6}}\sum_{\mu\neq\nu=1}^{3}\sum_{k=0}^{1}|\mu\rangle\,|\nu\rangle\,|k\rangle\right). \tag{G2}$$

First, we have the $\log_2 N$-qubit electric link index register that stores the N electric link indices in equal superposition. Next, we have the $(4+1)$-qubit spin-index register. The first four qubits store the value of μ,ν. The last qubit indicates whether we apply the H.c. If $\mu=\nu$ or $\mu,\nu>3$, then we discard. Throughout this paper, by "discarding" we mean unfollowing a computation path. This is indicated by an ancilla qubit, which when set to $|1\rangle$, we only apply $\mathbb{I}$. All the registers are in equal superposition and so we require $5+\log_2 N$ H gates. Comparing the constraints on μ and ν takes $O(1)$ extra gates and ancillas.

The unitary-selection subroutine does the following:

$$\begin{aligned}
\text{SELECT}_{f2} : |q\rangle\,|\mu,\nu,0\rangle &\left(\bigotimes_{q=1}^{N}\bigotimes_{\mu'=1}^{3}|f_e=0\rangle\right)|\phi\rangle \\
\mapsto |q\rangle\,|\mu,\nu,0\rangle &\left(|1\rangle_{q,\mu}\,|1\rangle_{q+1_\mu,\nu}\,|1\rangle_{q+1_\nu,\mu}\,|1\rangle_{q,\nu}\right)\mathcal{F}\left(\bigotimes_{k=1}^{\log_2 d-1}R_z(\theta_k)\right)_{q,\mu}\left(\bigotimes_{k=1}^{\log_2 d-1}R_z(\theta_k)\right)_{q+1_\mu,\nu} \\
\times &\left(\bigotimes_{k=1}^{\log_2 d-1}R_z(-\theta_k)\right)_{q+1_\nu,\mu}\left(\bigotimes_{k=1}^{\log_2 d-1}R_z(-\theta_k)\right)_{q,\nu}\mathcal{F}^{\dagger}\,|\phi\rangle\,.
\end{aligned} \tag{G3}$$

Throughout this paper, for an operator U and subspace indexed by some letter q, we write $(U)_q$ to imply identity acts on the remaining subspaces. The above selection operator can also be expressed as

$$\begin{aligned}
\text{SELECT}_{f2} &= \sum_{q=1}^{N}\sum_{\mu\neq\nu=1}^{3}\sum_{k=0}^{1}|q,\mu,\nu,0\rangle\,\langle q,\mu,\nu,0|\otimes U_{q,\mu}U_{q+1_\mu,\nu}U_{q+1_\nu,\mu}U_{q,\nu} \\
&+\sum_{q=1}^{N}\sum_{\mu\neq\nu=1}^{3}\sum_{k=0}^{1}|q,\mu,\nu,1\rangle\,\langle q,\mu,\nu,1|\otimes U^{\dagger}_{q,\nu}U^{\dagger}_{q+1_\nu,\mu}U^{\dagger}_{q+1_\mu,\nu}U^{\dagger}_{q,\mu},
\end{aligned}$$

by which we can conveniently prove that

$$\langle 0|\,\text{PREP}^{\dagger}_{f2}\cdot\text{SELECT}_{f2}\cdot\text{PREP}_{f2}\,|0\rangle = \frac{H_{f2}}{6N},$$

providing a $(6N,.,0)$ block encoding if H_{f2} and we also observe that $\|H_{f2}\|\leq 6N$, from Table II. In the following sections, we have preferred to follow the format of Eq. (G3), for convenience in explaining the transformations of the states of the registers, including some ancilla qubits. This also helps in explaining the number of controls in some multicontrolled gates.

In each of the $3N$ subspaces, we allocate one ancilla f_e, initialized to $|0\rangle$ for selection. We use N $C^{\log_2 N}X$ gates, controlled on the link-index register to select a link subspace. We use $3N$ C^5X gates to select spin subspaces. The four controls are on the spin register and the last one is controlled on the target qubits of the $C^{\log_2 N}X$ gates. In short, $|f_e\rangle$ is flipped to $|1\rangle$ if both the link-register state $|q\rangle$ and the spin-register state $|\mu\rangle$ match. The remaining operations are all controlled on the state of f_e. We use the same set of gates at the end of the operations for uncomputing. We use the optimization technique of Theorem 2 to synthesize the $NC^{\log_2 N}X$ gates. If we split the ancillas into M_{f2} sets, such that the ith set contains $\log_2 N/r_i$ qubits, then the total number of pairs of multicontrolled-X gates that we require is

$$\sum_{i=1}^{M_{f2}}N^{\frac{1}{r_i}}C^{\frac{\log_2 N}{r_i}}X+NC^{M_{f2}}X+3NC^5X. \tag{G4}$$

In each of the $3N$ subspaces, we apply rotation gates controlled on $|f_e=1\rangle$ and the third qubit in the spin register. If the latter is $|0\rangle$, then the angles are as shown in Eq. (G3); else we apply the H.c., i.e., the negative of these angles. Thus, in each subspace, we have two multicontrolled-rotation gates. These rotation gates are conjugated by $\log_2 d$-qubits QFT. If we use the approximate quantum Fourier transform (AQFT) [79], then we incur a T-gate cost of about $2 \times 3N \left(8(\log_2 d)(\log_2 \log_2 d - 2) + 1.2 \log_2^2(\log_2 d)\right)$ and an H-gate cost of about $2 \times 3N \log_2 d$.

Thus, for one block encoding of $\frac{H_{f\,2}}{6N}$, the number of controlled-rotation gates required is

$$\mathcal{G}_1^r = 6N \tag{G5}$$

and the number of T gates required is

$$\begin{aligned} \mathcal{G}_1^t &\leq 48N(\log_2 d)(\log_2 \log_2 d) + 7.2N \log_2^2(\log_2 d) \\ &\quad + 4\sum_{i=1}^{M_{f\,2}} N^{\frac{1}{r_i}} \frac{\log_2 N}{r_i} + 4NM_{f\,2} + 48N, \end{aligned} \tag{G6}$$

while the number of CNOT gates required is

$$\mathcal{G}_1^c \leq 4\sum_{i=1}^{M_{f\,2}} N^{\frac{1}{r_i}} \frac{\log_2 N}{r_i} + 4NM_{f\,2} + 51N. \tag{G7}$$

Counting the H gates, the total number of gates required for the block encoding of $H_{12}/6N$ is

$$\begin{aligned} \mathcal{G}_1' &\leq 6N \log_2 d + \log_2 N + 5 + 105N \\ &\quad + 8\sum_{i=1}^{M_{f\,2}} N^{\frac{1}{r_i}} \frac{\log_2 N}{r_i} + 8NM_{f\,2} \\ &\in O\left(N \log_2 d\right) \quad \text{when } \frac{1}{r_i} \leq \frac{1}{2}, \end{aligned} \tag{G8}$$

assuming the $M_{f\,2}$ is a constant. Using Ref. [8, Corollary 60], we need

$$O\left(N\tau_1 + \frac{\log(1/\delta_{12})}{\log\log(1/\delta_{12})}\right) \tag{G9}$$

calls to the SELECT$_{f\,2}$ and PREP$_{f\,2}$ oracles that define the block encoding of $H_{f\,2}/6N$ in order to implement a δ_1-precise block encoding of $e^{-iH_{f\,2}\tau_1}$. Thus the number of gates required for simulating $e^{-iH_{f\,2}\tau_1}$ is as follows:

$$\mathcal{G}_1 \in O\left(N^2\tau_1 \log d + \frac{\log(1/\delta_{12})}{\log\log(1/\delta_{12})} N \log d\right). \tag{G10}$$

2. Algorithm to simulate $e^{-iH_{21}\tau_2} = e^{-i\tau_2 \sum_{q=1}^{N} \sum_{\mu=1}^{3} \mathbb{I}\otimes\mathbb{I}\otimes\frac{1}{2}E_{q,\mu}^2}$

We know that $H_{21} = H_{f\,1}$ [Eq. (22)] and since $[E_{\ell,\mu}^2, E_{q,\nu}^2] = 0$, if $\ell \neq q$, then $e^{-iH_{f\,1}\tau_2} = \prod_{q=1}^{N} \prod_{\mu=1}^{3} \mathbb{I} \otimes \mathbb{I} \otimes e^{-i(1/2)E_{q,\mu}^2\tau_2}$. If $\zeta = 1 + \log_2 \Lambda$, then E^2 can be written as a sum of Z operators, as shown below, and we simulate $e^{-iH_{f\,1}\tau_2}$ by Trotterization, as done in Ref. [24]:

$$E^2 = \frac{1}{6}\left(2^{2\zeta-1} + 1\right)\mathbb{I} + \sum_{j=0}^{\zeta-1} 2^{j-1}\mathrm{Z}_j + \sum_{j=0}^{\zeta-2}\sum_{k>j}^{\zeta-1} 2^{j+k-1}\mathrm{Z}_j\mathrm{Z}_k. \tag{G11}$$

Lemma 22 (Lemma 2 in Ref. [24]). There exists a circuit that implements $e^{-iE^2\tau_2}$ on ζ qubits exactly, up to an (efficiently computable) global phase, using $(\zeta + 2)(\zeta - 1)/2$ CNOT operations and $\zeta(\zeta + 1)/2$ single-qubit rotations. Here, $\zeta = 1 + \log_2 \Lambda$.

Since E^2 is expressed as a sum of Pauli operators, we can use the algorithm in Ref. [61] to optimize the rotation gates at the cost of a small increase in the number of Toffoli gates, which has T-count 7 [80] or 4 [81], if using classical measurements. Then, the number of (controlled) rotations is equal to the number of nonzero distinct eigenvalues (ignoring the sign) of E^2, which is Λ. This can give fewer rotation gates up to $\zeta = 4$. Since Toffolis are exactly implementable, this can even lead to fewer T gates, especially for the low-synthesis-error regime. The number of CNOT gates can be further optimized using algorithms such as those in Refs. [82,83], with or without using connectivity constraints.

Since the product terms of $e^{-iH_{f\,1}\tau_2}$ mutually commute, there is no error introduced in the simulation of this Hamiltonian and the total number of rotation gates for one Trotter step is

$$\mathcal{G}_2^r \leq 3N\frac{(1 + \log_2 \Lambda)(2 + \log_2 \Lambda)}{2}, \tag{G12}$$

while the number of CNOT gates is

$$\mathcal{G}_2^c \leq 3N\frac{\log_2 \Lambda(3 + \log_2 \Lambda)}{2}. \tag{G13}$$

Thus the number of gates required to implement $e^{-iH_{f\,1}\tau_2}$ is

$$\begin{aligned} \mathcal{G}_2 = \mathcal{G}_2^r + \mathcal{G}_2^c &\leq 3N\left(\log_2^2 \Lambda + 3\log_2 \Lambda + 1\right) \\ &\in O\left(N \log_2^2 \Lambda\right). \end{aligned} \tag{G14}$$

Alternatively, we can use qubitization to simulate $e^{-iH_{21}\tau_2}$. Algorithm II, described in Sec. II D, applies qubitization on the entire Hamiltonian $\hat{H}_{\mathrm{PF}}$ and for this we need to block encode H_{21} and that is the main motivation for explaining this here.

The ancilla-preparation subroutine is defined as follows:

$$\mathrm{PREP}_{f\,1}\,|0\rangle^{*} = \left(\frac{1}{\sqrt{N}}\sum_{q=1}^{N}|q\rangle\right)\otimes\left(\frac{1}{\sqrt{3}}\sum_{\mu=1}^{3}|\mu\rangle\right)$$
$$\otimes\left(\sum_{k=1}^{\frac{\log^2(2\Lambda)+\log(2\Lambda)+2}{2}}\sqrt{\frac{w_k}{\sum_k w_k}}\,|k\rangle\right). \quad \text{(G15)}$$

Here, the w_k are the weights of the unitaries in the LCU decomposition of E^2, as given in Eq. (G11). In the first $\log_2 N$-qubit electric link index register, we store the N electric link indices in equal superposition, using $\log_2 N$ H gates. In the next two-qubit spin-index register, we store the values of μ, using two H gates. Since E^2 is a sum of $(\log_2^2(2\Lambda)+\log_2(2\Lambda)+2)/2 = (\log_2^2\Lambda + 3\log_2\Lambda + 4)/2$ unitaries [Eq. (G11)], the last register of $\log_2\left(\log_2^2\Lambda + 3\log_2\Lambda + 4\right) - 1$ qubits stores the indices of the unitaries in a superposition, weighted according to Eq. (G11). To obtain proper weighting of the basis states, we can use any arbitrary state-preparation algorithm (see, e.g., Refs. [74,75,84]), so we require at most $\log_2\left(\log_2^2\Lambda + 3\log_2\Lambda + 4\right)$ H gates, $\log_2^2\Lambda + 3\log_2\Lambda + 3\log_2\left(\log_2^2\Lambda + 3\log_2\Lambda + 4\right)$ CNOT gates, and $\log_2^2\Lambda + 3\log_2\Lambda + 2$ rotation gates.

The unitary-selection subroutine does the following:

$$\mathrm{SELECT}_{f\,1} : |q\rangle\,|\mu\rangle\,|k\rangle\left(\bigotimes_{q=1}^{N}\bigotimes_{\mu'=1}^{3}|f_e = 0\rangle_{q,\mu'}\right)|\phi\rangle$$
$$\mapsto |q\rangle\,|\mu\rangle\,|k\rangle\,(|1\rangle)_{q,\mu}\left(E_k^2\right)_{q,\mu}|\phi\rangle \quad \text{(G16)}$$

and it follows in a straightforward manner that

$$\langle 0|\,\mathrm{PREP}^{\dagger}_{f\,1}\cdot\mathrm{SELECT}_{f\,1}\cdot\mathrm{PREP}_{f\,1}\,|0\rangle = \frac{H_{f\,1}}{3N\Lambda^2/2};$$

here too we keep in mind that $\|H_{f\,1}\| \le 3N\Lambda^2/2$, from Table II. In each of the $3N$ subspaces, we allocate an ancilla f_e, initialized to $|0\rangle$ for selection. Using N $C^{\log_2 N}X$ gates controlled on the link index register, a link subspace is selected. We use $3N$ C^3X gates to select the spin subspaces. The two controls are on the spin register and the last one is controlled on the target qubits of the $C^{\log_2 N}X$ gates. In short, $|f_e\rangle$ is flipped to $|1\rangle$ if both the link-register state $|q\rangle$ and the spin-register state $|\mu\rangle$ match. The remaining operations are all controlled on the state of f_e. The same set of gates is used at the end of the operations for uncomputing. We use the optimization technique of Theorem 2 to synthesize the $NC^{\log_2 N}X$ gates. If we split the ancillas into $M_{f\,1}$ sets, such that the ith set has $\log_2 N/r_i$ qubits, then the total number of multicontrolled-X gates that we require is

$$\sum_{i=1}^{M_{f\,1}} N^{\frac{1}{r_i}}C^{\frac{\log_2 N}{r_i}}X + NC^{M_{f\,1}}X + 3NC^3X. \quad \text{(G17)}$$

In each of the $3N$ subspaces, we use $(\log_2^2\Lambda + 3\log_2\Lambda + 4)/2$ $C^{\log_2(\log^2\Lambda+3\log\Lambda+4)/2}X$ gates to select and apply the unitaries in the decomposition of E^2, i.e., $\log_2^2(2\Lambda)$ controlled-Z (CZ) gates. Using the optimization technique of Theorem 2, the number of multicontrolled-X gates that we require is

$$\sum_{i=1}^{M'_{f\,1}}\left(\frac{\log^2\Lambda + 3\log\Lambda + 4}{2}\right)^{\frac{1}{r_i}} C^{\frac{\log(\log^2\Lambda+3\log\Lambda+4)-1}{r_i}}X$$
$$+ \frac{\log^2\Lambda + 3\log\Lambda + 4}{2}C^{M'_{f\,1}}X, \quad \text{(G18)}$$

where $M'_{f\,1}$ is a constant. Thus, for one block encoding of $H_{f\,1}$, the number of rotation gates required is

$$\mathcal{G}_2^{r'} \le \log_2^2\Lambda + 3\log_2\Lambda + 2; \quad \text{(G19)}$$

the number of T gates required is

$$\mathcal{G}_2^{t'} \le 4\sum_{i=1}^{M_{f\,1}} N^{\frac{1}{r_i}}\frac{\log_2 N}{r_i} + 4NM_{f\,1}$$
$$+ 12N\sum_{i=1}^{M'_{f\,1}}\left(\frac{\log_2^2\Lambda + 3\log_2\Lambda + 4}{2}\right)^{\frac{1}{r_i}}$$
$$\times \log\left(\log_2^2\Lambda + 3\log_2\Lambda + 4\right)$$
$$+ 6NM'_{f\,1}\left(\log_2^2\Lambda + 3\log_2\Lambda + 4\right); \quad \text{(G20)}$$

the number of CNOT gates required is asymptotically the same as for the T gates; and so counting the H and CZ gates, the total number of gates required for $(3N\Lambda^2/2, ., 0)$ block encoding of H_{21} is

$$\mathcal{G}'_2 \in O\left(N\log_2^2\Lambda\right), \quad \text{(G21)}$$

assuming that $M_{f\,1}$ and $M'_{f\,1}$ are constants. We have deliberately skipped the middle argument while specifying the block-encoding constant of H_{21}. This argument basically denotes the number of extra ancillas that we require in the PREP$_{f\,1}$ subroutine and we do not need this for our gate complexity. So, for simplicity and convenience, we have dropped it and we will do so henceforth. Sometimes, we will be even more crisp and simply say "block encoding of $H_{21}/3N\Lambda^2/2$." So we require

$$O\left(N\Lambda^2\tau_2 + \frac{\log(1/\delta_{21})}{\log\log(1/\delta_{21})}\right)$$

calls to the $\textsc{prep}_{f1}$ and $\textsc{select}_{f1}$ oracles in order to implement a δ_{21}-precise block encoding of $e^{-iH_{21}\tau_2}$. Thus the number of gates required for simulating $e^{-iH_{21}\tau_2}$ is

$$\mathcal{G}_{21} \in O\left(N^2\Lambda^2\log^2\Lambda\tau_2 + \frac{\log(1/\delta_{21})}{\log\log(1/\delta_{21})}N\log^2\Lambda\right).$$

3. Algorithm to simulate $e^{-iH_{31}\tau_3}$

We block encode $H_{31} = H_s + H_{3\pi}$ in a recursive manner, using Theorem 1 repeatedly:

$$\begin{aligned}
\text{Let } H_s^{j,q} &= -\sum_{\mu\neq\nu\neq\xi=1}^{3}\left(\sigma_{j,\mu}\otimes\mathbb{I}\right)\otimes\left(\nabla_\nu A_{q,\xi} - \nabla_\xi A_{q,\nu}\right) \\
&= \sum_{\mu\neq\nu\neq\xi=1}^{3}\left(\sigma_{j,\mu}\otimes\mathbb{I}\right)\otimes\left(\nabla_\xi A_{q,\nu} - \nabla_\nu A_{q,\xi}\right) \\
\text{and } H_{3\pi}^{j,q} &= \sum_{\mu=1}^{3}\mathbb{I}\otimes\mathbb{I}\otimes A_{q,\mu}^2, \\
\text{such that}\quad H_{31}^{j,q} &= \frac{1}{c}H_s^{j,q} + \frac{1}{2c^2}H_{3\pi}^{j,q}, \qquad H_{31}^{j} = \sum_{q=1}^{N}H_{31}^{j,q}, \qquad H_{31} = \sum_{j=1}^{\eta}H_{31}^{j}.
\end{aligned} \tag{G22}$$

a. Block encoding of $H_s^{j,q}$

The ancilla-preparation subroutine, denoted by $\textsc{prep}_s^{j,q}$ does the following:

$$\begin{aligned}
\textsc{prep}_s^{j,q}\,|0\rangle^* = &\left(\frac{1}{\sqrt{6}}\sum_{\mu\neq\nu\neq\xi}^{3}\sum_{b=0}^{1}|\mu\rangle\,|\nu\rangle\,|\xi\rangle\,|b\rangle\right) \\
&\otimes\left(\sum_{k=-a}^{a}\sqrt{\frac{|d'_{2a+1,k}|}{\sum_k|d'_{2a+1,k}|}}\,|k+a\rangle\right) \\
&\otimes\left(\sum_{k'=1}^{\log_2 d}\sqrt{\frac{w'_{k'}}{\sum_{k'}w'_{k'}}}\,|k'\rangle\right).
\end{aligned} \tag{G23}$$

The first $(2\times 3+1) = 7$-qubit spin-index register stores directions or spins in equal superposition and we need seven H gates for this. If μ, ν, and ξ are not unequal or any of them is greater than 3, then we discard the computational path. The last qubit of this register selects between $\nabla_\nu A_{q,\xi}$ and $\nabla_\xi A_{q,\nu}$. The second and third registers, with $\log_2(2a)$ and $\log_2\log_2 d$ qubits, respectively, indicate which adder to apply or on which qubit the Z gate should be applied. These are unitaries obtained in the LCU decomposition of ∇ (Lemma 18) and A (Corollary 1) in Appendix F. To obtain proper weighting of the basis states, we require at most $2a+\log_2 d-4$ rotation gates, $2a+\log_2 d+3\log_2(2a\log_2 d)-14$ CNOT gates, and $\log_2(2a\log_2 d)$ H gates [75].

We denote the next subroutine by $\textsc{select}_s^{j,q}$, which is described as follows:

$$\begin{aligned}
&\textsc{select}_s^{j,q}: |\mu,\nu,\xi,0\rangle\,|k''\rangle\,|k'\rangle\,|\phi\rangle \\
&\quad\mapsto |\mu,\nu,\xi,0\rangle\,|k''\rangle\,|k'\rangle\left(\sigma_\mu\otimes\mathbb{I}\right)_j(\nabla_{k''})_{q,\nu}\,(A_{k'})_{q,\xi}\,|\phi\rangle\,.
\end{aligned} \tag{G24}$$

Controlled on $|\mu\rangle$, we apply σ_μ on the spin subspace of the jth particle. Controlled on $|\nu,\xi\rangle$, we select spin subspaces of the qth link register. This step require $O(1)$ gates. Controlled on $|k''\rangle$ and $|k'\rangle$, we apply the k''th and k'th unitaries in the LCU decompositions of ∇ and A, respectively. If the third qubit in the spin register is $|1\rangle$, then we apply ∇_ξ and A_ν. All the unitaries in the decomposition of ∇ and A act on $\log_2 d$ qubits and they are controlled on $\log_2(2a)$ and $\log_2\log_2 d$ qubits, respectively. A is a sum of $\log_2 d$ Z gates; thus to select and implement these unitaries, we require $\log_2 d$ compute-uncompute pairs of $C^{\log_2\log_2 d}X$ gates and $\log_2 d$ CZ gates. Similarly, we can use $2a$ pairs of $C^{\log_2(2a)}X$ gates and $2a$ single-controlled adders to select and implement the unitaries in the LCU decomposition of ∇. Using Theorem 2, we find that the number of pairs of multicontrolled-X gates that we require is

$$\begin{aligned}
&\sum_{i=1}^{M_{s1}}(\log_2 d)^{\frac{1}{r_i}}C^{\frac{\log_2\log_2 d}{r_i}}X + \log_2 dC^{M_{s1}}X \\
&\quad+\sum_{i=1}^{M_{s2}}(2a)^{\frac{1}{r_i}}C^{\frac{\log_2(2a)}{r_i}}X + (2a)C^{M_{s2}}X,
\end{aligned} \tag{G25}$$

where we have split the $\log_2 \log_2 d$ control qubits for A into M_{s1} sets and the $\log_2(2a)$ control qubits for ∇ into M_{s2} sets.

It follows that

$$\langle 0|\,\mathrm{PREP}_s^{j,q\dagger}\cdot\mathrm{SELECT}_s^{j,q}\cdot\mathrm{PREP}_s^{j,q}\,|0\rangle=\frac{H_s^{j,q}}{12\pi\,\ln 2a^2/h\Delta},$$

and thus we have a $(12\pi\,\ln 2a^2/h\Delta,.,0)$ block encoding of $H_s^{j,q}$.

b. Block encoding of $H_{3\pi}^{j,q}$

The first ancilla-preparation subroutine is described as follows:

$$\mathrm{PREP}_{3\pi}^{j,q}\,|0\rangle^{*}=\left(\frac{1}{\sqrt{3}}\sum_{\mu'=1}^{3}|\mu'\rangle\right)\otimes\left(\sum_{k=1}^{\frac{\log^2 d+\log d}{2}}\sqrt{\frac{w_k'}{\sum_k w_k'}}\,|k\rangle\right).\tag{G26}$$

The first two-qubit register is the spin-index register. Since A^2 is a sum of $(\log_2^2 d+\log_2 d)/2$ unitaries (Table II), we prepare a $\log_2\left[(\log_2^2 d+\log_2 d)/2\right]$-qubit register in a superposition weighted according to the LCU decomposition of A^2 (Corollary 2 in Sec. F) and this can be done with $\log_2(\log_2^2 d+\log_2 d)/2$ H gates, $\log_2^2 d+\log_2 d+3\log_2\left[(\log_2^2 d+\log_2 d)/2\right]-7$ CNOT gates, and $\log_2^2 d+\log_2 d-2$ rotation gates.

The next subroutine is described as follows:

$$\mathrm{SELECT}_{3\pi}^{j,q}:|\mu'\rangle\,|k\rangle\,|\phi\rangle\mapsto|k\rangle\left(A_k^2\right)_{q,\mu'}|\phi\rangle\,.\tag{G27}$$

To implement A^2, controlled on the $|k\rangle$ register, we require $(\log_2^2 d+\log_2 d)/2$ pairs of $C^{\log_2[(\log^2 d+\log d)/2]}X$ and $\log_2 d+2[(\log_2 d-1)\log_2 d/2]=\log_2^2 d$ CZ gates. For the latter, we have taken into account single Z gates and ZZ operators, appearing in the LCU decomposition of A^2 (Corollary 2). Using Theorem 2, we find that the number of pairs of multicontrolled-X gates that we require is

$$\sum_{i=1}^{M_{3\pi}}\left(\frac{\log_2^2 d+\log_2 d}{2}\right)^{\frac{1}{r_i}}C^{\frac{\log_2\frac{\log_2^2 d+\log_2 d}{2}}{r_i}}X+\frac{\log_2^2 d+\log_2 d}{2}C^{M_{3\pi}}X,\tag{G28}$$

where we have split the $\log_2(\log_2^2 d+\log_2 d)/2$ control qubits into $M_{3\pi}$ sets.

It follows that

$$\langle 0|\,\mathrm{PREP}_{3\pi}^{j,q\dagger}\cdot\mathrm{SELECT}_{3\pi}^{j,q}\cdot\mathrm{PREP}_{3\pi}^{j,q}\,|0\rangle=\frac{H_{3\pi}^{j,q}}{24\pi^2/\Delta^2}$$

and thus we have a $(24\pi^2/\Delta^2,.,0)$ block encoding of $H_{3\pi}^{j,q}$.

c. Block encoding of H_{31}

We use Theorem 1 repeatedly. First, we block encode $H_{31}^{j,q}=(1/c)H_s^{j,q}+(1/2c^2)H_{3\pi}^{j,q}$, with $O(1)$ extra gate cost. Next, we consider $H_{31}^{j}=\sum_{q=1}^{N}H_{31}^{j,q}$, where each of the summand Hamiltonians acts on a separate link register. So we can prepare $\log_2 N$ ancilla qubits in an equal superposition of all the link indices using $\log_2 N$ H gates. Similarly, for $H_{31}=\sum_{j=1}^{\eta}H_{31}^{j}$, we prepare $\log_2\eta$ qubits in an equal superposition of all the η indices with $\log_2\eta$ H gates. Thus the overall ancilla-preparation subroutine is

$$\begin{aligned}\mathrm{PREP}_{31}\,|0\rangle^{*}=&\left(\frac{1}{\sqrt{\eta}}\sum_{j=1}^{\eta}|j\rangle\right)\otimes\left(\frac{1}{\sqrt{N}}\sum_{q=1}^{N}|q\rangle\right)\\&\otimes\left(\sqrt{\frac{\lambda_s}{c\mathcal{A}}}\,|0\rangle+\sqrt{\frac{\lambda_{3\pi}}{2c^2\mathcal{A}}}\,|1\rangle\right)\\&\otimes\mathrm{PREP}_s^{j,q}\otimes\mathrm{PREP}_{3\pi}^{j,q},\end{aligned}\tag{G29}$$

where $\lambda_s=\|H_s^{j,q}\|=12\pi\,\ln 2a^2/h\Delta$, $\lambda_{3\pi}=\|H_{3\pi}^{j,q}\|=24\pi^2/\Delta^2$, and $\mathcal{A}=(\lambda_s/c)+(\lambda_{3\pi}/2c^2)$. The overall unitary-selection subroutine is as follows:

$$\begin{aligned}&\mathrm{SELECT}_{31}:|j,q,0\rangle\,|\mu,\nu,\xi,b,k'',k'\rangle\,|\mu',k\rangle\,|\phi\rangle\\&\quad\mapsto|j,q,0\rangle\,|\mu',k\rangle\,\mathrm{SELECT}_s^{j,q}\left(|\mu,\nu,\xi,b,k'',k'\rangle\,|\phi\rangle\right),\\&\mathrm{SELECT}_{31}:|j,q,1\rangle\,|\mu,\nu,\xi,b,k'',k'\rangle\,|\mu',k\rangle\,|\phi\rangle\\&\quad\mapsto|j,q,1\rangle\,|\mu,\nu,\xi,b,k'',k'\rangle\,\mathrm{SELECT}_{3\pi}^{j,q}\left(|\mu',k\rangle\,|\phi\rangle\right).\end{aligned}$$

It is straightforward to check that

$$\langle 0|\,\mathrm{PREP}_{31}^{\dagger}\cdot\mathrm{SELECT}_{31}\cdot\mathrm{PREP}_{31}\,|0\rangle=\frac{H_{31}}{\eta N\mathcal{A}},$$

where $\eta N\mathcal{A}=(12\pi\eta N\ln 2a^2/ch\Delta)+(12\pi^2\eta N/c^2\Delta^2)$, which is also the sum of the norms of the Hamiltonians H_s and $H_{3\pi}$ in Table II. Thus we have a $(\eta N\mathcal{A},.,0)$ block encoding of H_{31}.

Using η pairs of $C^{\log_2\eta}X$ gates, we select a particle register by flipping a qubit initialized to $|0\rangle$. Also, using N pairs of $C^{\log_2 N}X$ gates, we select a link register by flipping another qubit. Thus, using Theorem 2, we find that the number of pairs of multicontrolled-X gates that we require is

$$\sum_{i=1}^{M_{31}}N^{\frac{1}{r_i}}C^{\frac{\log_2 N}{r_i}}X+NC^{M_{31}}X+\sum_{i=1}^{M_{31}'}\eta^{\frac{1}{r_i}}C^{\frac{\log_2\eta}{r_i}}X+\eta C^{M_{31}'}X,\tag{G30}$$

where we have split the $\log_2 N$ and $\log_2\eta$ control qubits into M_{31} and M_{31}' sets, respectively. In this case, the unitaries in the decomposition of ∇, A, A^2 have three controls and they are applied on each of the $3N$ link subspaces. σ, with three controls, are applied on each of the η-particle subspaces. Overall, we require $3N \times 2a = 6aN$ three-qubit-controlled $\log_2 d$-qubit adders, which can be decomposed as $6aN$ one-qubit-controlled adders and $12aN$ Toffoli pairs. Using the construction in Ref. [68], we require $6aN \times 4(\log_2 d - 1)$ controlled-T gates and $6aN \times (5\log_2 d - 4)$ controlled-CNOT gates to implement the controlled adders. There are other constructions of adders (see, e.g., Refs. [85–87]) and usually there are trade-offs between these constructions. We have taken the estimates from Ref. [68], because of the better bound on the T-gate cost. We also require $3N \times (\log_2 d + \log_2^2 d)$ Z gates (for A, A^2), each controlled on three qubits. Each of these can be decomposed as a CZ and two Toffoli pairs. Also, we require 3η Paulis, each controlled on three qubits.

Hence, for block encoding of $H_{31}/\eta N\mathcal{A}$, the number of controlled rotations required is

$$\mathcal{G}_{31}^r \leq 2a + 2\log_2 d + \log_2^2 d, \tag{G31}$$

the number of T gates required is

$$\begin{aligned}
\mathcal{G}_{31}^t \leq\ & 4\sum_{i=1}^{M_{31}} N^{\frac{1}{r_i}} \frac{\log_2 N}{r_i} + 4NM_{31} + 4\sum_{i=1}^{M'_{31}} \eta^{\frac{1}{r_i}} \frac{\log_2 \eta}{r_i} + 4\eta M_{31} \\
& + 12N\sum_{i=1}^{M_{s1}} (\log_2 d)^{\frac{1}{r_i}} \frac{\log_2 \log_2 d}{r_i} + 12N\log_2 dM_{s1} + 12N\sum_{i=1}^{M_{s2}} (2a)^{\frac{1}{r_i}} \frac{\log_2(2a)}{r_i} + 24aNM_{s2} \\
& + 12N\sum_{i=1}^{M_{3\pi}} \left(\frac{\log_2^2 d + \log_2 d}{2}\right)^{\frac{1}{r_i}} \frac{\log_2 \frac{\log_2^2 d + \log_2 d}{2}}{r_i} + 6N\left(\log_2^2 d + \log_2 d\right) M_{3\pi} \\
& + 24aN\log_2 d - 24aN + 24aN + 12N(\log_2 d + \log_2^2 d) + 6aN(5\log_2 d - 4),
\end{aligned} \tag{G32}$$

while the number of CNOT gates required is some constant times $\mathcal{G}_{31}^t$. Counting the rotation, H, CZ, and other gates, the total number of gates required for the block encoding of $H_{31}/\eta N\mathcal{A}$ is

$$\mathcal{G}'_{31} \in O\left(\eta + N(a + \log_2 d)\log_2 d\right), \tag{G33}$$

assuming that M_{s1}, M_{s2}, $M_{3\pi}$, M_{31}, and M'_{31} are constants and that each $1/r_i \leq \frac{1}{2}$. From Table II,

$$\begin{aligned}
\|H_{31}\| &\leq \frac{12\pi^2\eta N}{c^2\Delta^2} + \frac{12\pi\eta N\ln(2a^2)}{ch\Delta} \\
&= \frac{12\pi\eta N}{c\Delta^2}\left(\frac{\pi}{c} + \frac{\Delta\ln(2a^2)}{h}\right) \\
&\leq \frac{K_{31}\eta N\ln(2a^2)}{\Delta^2} \quad [K_{31} = \text{constant}],
\end{aligned} \tag{G34}$$

where we have assumed that $h \leq K_h\Delta$, for some constant K_h. So we need

$$R_{31} \in O\left(\frac{\eta N\ln(2a^2)}{\Delta^2}\tau_3 + \frac{\log(1/\delta_{31})}{\log\log(1/\delta_{31})}\right) \tag{G35}$$

calls to the block encoding of $H_{31}/\eta N\mathcal{A}$ in order to implement a δ_{31}-precise block encoding of $e^{-iH_{31}\tau_3}$ [8]. Thus the number of gates required for simulating $e^{-iH_{31}\tau_3}$ is

$$\begin{aligned}
\mathcal{G}_{31} &\in O(R_{31}\cdot\mathcal{G}'_{31}) \\
&\in O\Bigg(\frac{\eta^2N\ln(2a^2)}{\Delta^2}\tau_3 + \frac{\eta N^2\ln(2a^2)\log d}{\Delta^2}(a + \log d)\tau_3 \\
&\quad + \frac{\log(1/\delta_{31})}{\log\log(1/\delta_{31})}\left(\eta + N(a + \log d)\log d\right)\Bigg).
\end{aligned} \tag{G36}$$

4. Algorithm to simulate $e^{-iH_{32}\tau_3}$

We know that $H_{32} = H_V + H_{1\pi} + H_{2\pi}$ and here also we use Theorem 1 to block encode in a recursive manner. We define the following:

$$H_{1\pi}^{j,q,\mu} = -\mathbb{I}\otimes\nabla_{j,\mu}^2\otimes\mathbb{I}, \quad H_{2\pi}^{j,q,\mu} = \mathbb{I}\otimes\left(i\nabla_{j,\mu}\right)\otimes A_{q,\mu},$$

$$H_{12\pi}^{j,q,\mu} = \frac{1}{2}H_{1\pi}^{j,q,\mu} + \frac{1}{c}H_{2\pi}^{j,q,\mu}, \quad H_{12\pi} = \sum_{j=1}^{\eta}\sum_{q=1}^{N}\sum_{\mu=1}^{3} H_{12\pi}^{j,q,\mu}.$$

a. Block encoding of $H_{12\pi}$

As in the case of H_{31}, we first block encode $H_{1\pi}^{j,q,\mu}$ and $H_{2\pi}^{j,q,\mu}$ separately, using the ancilla-preparation subroutines $\text{PREP}_{1\pi}^{j,q,\mu}$ and $\text{PREP}_{2\pi}^{j,q,\mu}$, respectively, followed by the unitary-selection subroutines $\text{SELECT}_{1\pi}^{j,q,\mu}$ and $\text{SELECT}_{2\pi}^{j,q,\mu}$, respectively. Then, we block encode $H_{12\pi}^{j,q,\mu}$ and $H_{12\pi}$, as discussed in Theorem 1. Whenever the same Hamiltonian is applied on disjoint spaces, we apply the optimization described in Remark 1. Thus, our overall ancilla-preparation subroutine is as follows:

$$\begin{aligned}\text{PREP}_{12\pi}\,|0\rangle^{*} &= \left(\frac{1}{\sqrt{\eta}}\sum_{j=1}^{\eta}|j\rangle\right)\otimes\left(\frac{1}{\sqrt{N}}\sum_{q=1}^{N}|q\rangle\right)\\ &\otimes\left(\frac{1}{\sqrt{3}}\sum_{\mu=1}^{3}|\mu\rangle\right)\\ &\otimes\left(\sqrt{\frac{\lambda_1}{2\mathcal{A}'}}\,|0\rangle+\sqrt{\frac{\lambda_2}{c\mathcal{A}'}}\,|1\rangle\right)\\ &\otimes\text{PREP}_{1\pi}^{j,q,\mu}\otimes\text{PREP}_{2\pi}^{j,q,\mu},\end{aligned}\tag{G37}$$

where $\lambda_1=\|2H_{1\pi}\|$, $\lambda_2=\|cH_{2\pi}\|$, $\mathcal{A}'=(\lambda_1/2)+(\lambda_2/c)=(8\pi^2\eta N/h^2)+(12\pi\eta N\ln 2a^2/ch\Delta)$, and

$$\text{PREP}_{1\pi}^{j,q,\mu}\,|0\rangle^{*}=\left(\sum_{k=-a}^{a}\sqrt{\frac{|d_{2a+1,k}|}{\sum_k|d_{2a+1,k}|}}\,|k+a\rangle\right),\tag{G38}$$

$$\begin{aligned}\text{PREP}_{2\pi}^{j,q,\mu}\,|0\rangle^{*} &= \left(\sum_{k_1=-a}^{a}\sqrt{\frac{|d''_{2a+1,k_1}|}{\sum_{k_1}|d''_{2a+1,k_1}|}}\,|k_1+a\rangle\right)\\ &\otimes\left(\sum_{k_2=1}^{\log_2 d}\sqrt{\frac{w_{k_2}}{\sum_{k_2}w_{k_2}}}\,|k_2\rangle\right).\end{aligned}\tag{G39}$$

We use $\log_2\eta$, $\log_2 N$, and two H gates to prepare an equal superposition of η-particle indices, N link indices, and three spins in the first, second, and third register, respectively. In the fourth register, we require two rotations. $\text{PREP}_{1\pi}^{j,q,\mu}$ acts on the approximately $\log_2(2a)$-qubit fifth register, where we store the indices of the adders in the decomposition of ∇^2 (Lemma 16) with appropriate weights. This can be done using $\log_2(2a)$ H gates, $4a+3\log_2(2a)-7$ CNOT gates, and $4a-2$ rotation gates. $\text{PREP}_{2\pi}^{j,q,\mu}$ acts on the last two registers. The second last one has $\log_2(2a)$ qubits and stores the indices of the adders in the LCU decomposition of ∇ (Lemma 18). We observe that we work with $i\nabla$ because it is Hermitian and this factor is adjusted in the weights. The last register has $\log_2\log_2 d$ qubits and stores the indices of the Z gates occurring in the LCU decomposition of A (Corollary 1). To prepare these superpositions, we require $\log_2(2a)+\log_2\log_2 d=\log_2(2a\log_2 d)$ H gates, $(4a+3\log_2(2a)-7)+(2\log_2 d+3\log_2\log_2 d-7)=4a+2\log_2 d+3\log_2(2a\log_2 d)-14$ CNOT gates, and $(4a-2)+(2\log_2 d-2)=4a+2\log_2 d-4$ rotation gates.

The overall unitary-selection subroutine is as follows:

$$\text{SELECT}_{1\pi}^{j,q,\mu}:|k'\rangle\,|\phi\rangle\mapsto|k'\rangle\left(\mathbb{I}\otimes\nabla_{k'}^{2}\right)_{j,\mu}|\phi\rangle,\tag{G40}$$

$$\text{SELECT}_{2\pi}^{j,q,\mu}:|k'_1\rangle\,|k'_2\rangle\,|\phi\rangle\mapsto|k'_1\rangle\,|k'_2\rangle\left(\nabla_{k'_1}\right)_{j,\mu}\left(A_{k'_2}\right)_{q,\mu}|\phi\rangle,\tag{G41}$$

$$\begin{aligned}\text{SELECT}_{12\pi} &: |j,q,\mu,0\rangle\,|k'\rangle\,|k'_1,k'_2\rangle\,|\phi\rangle\\ &\mapsto|j,q,\mu,0\rangle\,|k'_1,k'_2\rangle\,\text{SELECT}_{1\pi}^{j,q,\mu}\left(|k'\rangle\,|\phi\rangle\right),\\ \text{SELECT}_{12\pi} &: |j,q,\mu,1\rangle\,|k'\rangle\,|k'_1,k'_2\rangle\,|\phi\rangle\\ &\mapsto|j,q,\mu,1\rangle\,|k'\rangle\,\text{SELECT}_{2\pi}^{j,q,\mu}\left(|k'_1,k'_2\rangle\,|\phi\rangle\right).\end{aligned}$$

Using η pairs of $C^{\log_2\eta}X$ gates and three pairs of C^2X gates, we select a particle-spin register by flipping a qubit initialized to $|0\rangle$. Using N pairs of $C^{\log_2 N}X$ gates, we select a link subspace by flipping another qubit. Due to $H_{1\pi}$, in each of the 3η registers, we apply a controlled-∇^2 operator [Eq. (G40)], which is a sum of approximately $2a$ adders, each acting on $\log_2 N^{1/3}=\frac{1}{3}\log_2 N$ qubits, controlled on $\log_2(2a)$ qubits. Thus we require approximately $3\eta\times 2a$ pairs of $C^{\log_2(2a)}X$ gates and $3\eta\times 2a$ controlled adders. Due to $H_{2\pi}$, we apply controlled-∇ and controlled-A operators [Eq. (G41)] in each of the 3η and $3N$ particle and link registers, respectively. ∇ is a sum of $2a$ adders, each acting on $\frac{1}{3}\log_2 N$ qubits, controlled on $\log_2(2a)$ qubits. A is a sum of $\log_2 d$ Z gates, each controlled on $\log_2 d\log_2 d$ qubits. So, here we require $3\eta\times 2a$ pairs of $C^{\log_2(2a)}X$ gates, $3\eta\times 2a$ controlled adders, $3N\times\log_2 d$ pairs of $C^{\log_2\log_2 d}X$ gates, and $3N\times\log_2 d$ CZ gates. We can implement the controlled adders using $12\eta a\times 4(\frac{1}{3}\log_2 N-1)$ controlled-T gates and $12\eta a\times(\frac{5}{3}\log_2 N-4)$ controlled-CNOT gates.

Using Theorem 2, we find that the number of pairs of multicontrolled-X gates that we require is

$$\begin{aligned}&\sum_{i=1}^{M_1}N^{\frac{1}{r_i}}C^{\frac{\log_2 N}{r_i}}X+NC^{M_1}X+\sum_{i=1}^{M_2}\eta^{\frac{1}{r_i}}C^{\frac{\log_2\eta}{r_i}}X\\ &\quad+\eta C^{M_2}X+3C^2X\\ &\quad+3\eta\left(\sum_{i=1}^{M_3}(2a)^{\frac{1}{r_i}}C^{\frac{\log_2(2a)}{r_i}}X+2aC^{M_3}X\right)\\ &\quad+3N\left(\sum_{i=1}^{M_4}(\log_2 d)^{\frac{1}{r_i}}C^{\frac{\log_2\log_2 d}{r_i}}X+\log_2 dC^{M_4}X\right).\end{aligned}$$

It can be verified in a straightforward manner that

$$\langle 0|\,\mathrm{PREP}^{\dagger}_{12\pi}\cdot\mathrm{SELECT}_{12\pi}\cdot\mathrm{PREP}_{12\pi}\,|0\rangle = \frac{H_{12\pi}}{\mathcal{A}'},$$

where $\mathcal{A}' = (8\pi^2\eta N/h^2) + (12\pi\eta N\ln 2a^2/ch\Delta)$, which is also the sum of the norms of $H_{1\pi}$ and $H_{2\pi}$ (Table II).

So, for block encoding of $H_{12\pi}/\mathcal{A}'$, the number of rotation gates required is

$$\mathcal{G}^r_{12\pi} \le 8a + 2\log_2 d \tag{G42}$$

and the number of T gates required is

$$\begin{aligned}\mathcal{G}^t_{12\pi} \le\ & 4\sum_{i=1}^{M_1} N^{\frac{1}{r_i}}\frac{\log_2 N}{r_i} + 4NM_1\\ & + 4\sum_{i=1}^{M_2}\eta^{\frac{1}{r_i}}\frac{\log_2\eta}{r_i} + 4\eta M_2\\ & + 12\eta\left(\sum_{i=1}^{M_3}(2a)^{\frac{1}{r_i}}\frac{\log_2(2a)}{r_i} + 2aM_3\right)\\ & + 12N\left(\sum_{i=1}^{M_4}(\log_2 d)^{\frac{1}{r_i}}\frac{\log_2\log_2 d}{r_i} + \log_2 dM_4\right)\\ & + 16\eta a\log_2 N \end{aligned}\tag{G43}$$

while the number of CNOT gates is a constant times $\mathcal{G}^c_{12\pi}$ and hence the total number of gates is

$$\mathcal{G}'_{12\pi} \in O\left(\eta a\log_2 N + N\log_2 d\right), \tag{G44}$$

where we have assumed that each $1/r_i \le \frac{1}{2}$ and that M_1, M_2, M_3, and M_4 are constants.

b. Block encoding of H_V

We know that $H_V = H_{V_{ee}} + H_{V_{ne}}$ and we block encode it, following the approach taken in Refs. [18,20], with some modifications and incorporating the optimizations in Theorem 2. The ancilla-preparation subroutine is as follows:

$$\begin{aligned}&\mathrm{PREP}_V\,|1\rangle\,|0\rangle^{*}\\ &\propto |0\rangle\sum_{i<j}^{\eta}\sum_{v_x,v_y,v_z=-N^{1/3}}^{N^{1/3}}\frac{1}{\|\mathbf{v}\|_2}\,|i\rangle\,|j\rangle\,|v_x,v_y,v_z\rangle\\ &\quad-|1\rangle\sum_{i=1}^{\eta}\sum_{\kappa=1}^{K}\sum_{v_x,v_y,v_z=-N^{1/3}}^{N^{1/3}}\frac{\sqrt{Z_\kappa}}{\|\mathbf{v}\|_2}\,|i\rangle\,|\kappa\rangle\,|v_x,v_y,v_z\rangle\,.\end{aligned}\tag{G45}$$

We apply an H gate on the first ancilla, initialized to $|1\rangle$. The resulting state $\frac{1}{\sqrt{2}}(|0\rangle - |1\rangle)$ is used to select between the two Hamiltonians, $|0\rangle$ for $H_{V_{ee}}$ and $|1s\rangle$ for $H_{V_{ne}}$. Also, the -1 phase of $H_{V_{ne}}$ is taken care of at this stage. Next, we have a $\log_2\eta$-qubit register, where we store the particle indices in equal superposition using $\log_2\eta$ H gates. The next register is also of $\log_2\eta$ qubits (assuming that $K\le\eta$). If the first particle-index register is $|0\rangle$, then we prepare the second register in equal superposition over the particle indices and this requires $\log_2\eta$ H gates. We impose the constraint $i\ge j$ by flagging a qubit, in which case we discard the computational path. If the first qubit is $|1\rangle$, then we prepare the second register in a superposition over $|\kappa\rangle$ (positions of neutrons), weighted by nuclear $\sqrt{Z_\kappa}$, the nuclear charge. This is given by a classical database with complexity $O(K)$. We can use the QROM and subsampling strategies, discussed in Ref. [19]. We assume that $K\le\eta$. For a material, in practice, there will be a limited number of nuclear charges with nuclei in a regular array, so this complexity will instead be $O(\log_2 K)$. We follow the state-preparation procedure, described in Ref. [18], to prepare $\sum_{v_x,v_y,v_z=-N^{1/3}}^{N^{1/3}}(1/\|v\|_2)\,|\mathbf{v}\rangle$. This is described in Appendix I. The overall complexity obtained is $O\left(\log_2 N\log_2(N/\delta') + \log_2\eta\right)$, where δ' is an upper bound on the tolerable error for the block encoding of H_V. If a full classical database for the nuclei is required, then the complexity will have an additional factor of $O\left(K\log 1/\delta''\right)$, where δ'' is the relative precision with which the positions of the nuclei are specified.

The unitary-selection subroutine is described as follows:

$$\begin{aligned}&\mathrm{SELECT}_V : |0\rangle\,|i\rangle\,|j\rangle\,|\mathbf{v}\rangle\,|\mathbf{q}_1,\ldots,\mathbf{q}_i,\ldots,\mathbf{q}_j,\ldots,\mathbf{q}_\eta\rangle\,|0\rangle\\ &\mapsto |0\rangle\,|i\rangle\,|j\rangle\,|\mathbf{v}\rangle\,|\mathbf{q}_1,\ldots,\mathbf{q}_i,\ldots,\mathbf{q}_j,\ldots,\mathbf{q}_\eta\rangle\,|\mathbf{q}_i-\mathbf{q}_j\rangle\,,\\ &\mathrm{SELECT}_V : |1\rangle\,|i\rangle\,|\kappa\rangle\,|\mathbf{v}\rangle\,|\mathbf{q}_1,\ldots,\mathbf{q}_i,\ldots,\mathbf{q}_\eta\rangle\,|0\rangle\\ &\mapsto |1\rangle\,|i\rangle\,|\kappa\rangle\,\mathbf{v}\,|\mathbf{q}_1,\ldots,\mathbf{q}_i,\ldots,\mathbf{q}_\eta\rangle\,|\mathbf{R}_\kappa-\mathbf{q}_i\rangle\end{aligned}\tag{G46}$$

If the first qubit is $|0\rangle$, we discard if $\mathbf{q}_i-\mathbf{q}_j\ne\mathbf{v}$, i.e., we flag this state as failure and perform identity along this computational path. Since for each pair of $\mathbf{q}_i$ and $\mathbf{q}_j$, only one value of $\mathbf{v}$ survives, the probability distribution is unaffected. We can use η pairs of $C^{\log_2\eta}X$ gates to select the particle registers. It takes $O(\log_2 N)$ gates for comparing and calculating the difference in the position coordinates.

If the first register is $|1\rangle$, then we do the following. We use a classical database to access $\mathbf{R}_\kappa$ and this has complexity $O(K)$. With η pairs of $C^{\log_2\eta}X$ gates, we select the particle, controlled on the particle-index register. We take the difference $\mathbf{R}_\kappa-\mathbf{q}_i$ and discard the computational path if it is not equal to $\mathbf{v}$. This step has complexity $O(\log_2 N)$.

Thus we obtain a block encoding of H_V/λ_V, where $\lambda_V = \|H_V\| = (\eta(\eta-1)/2\Delta^2) + (\eta Z_{\mathrm{sum}}/\Delta^2)$, and incorporating the optimizations of Theorem 2, the total number of gates required is

$$\mathcal{G}'_V \in O\left(\eta + \log_2 N \log_2 \frac{N}{\delta'} + K \log_2 \frac{1}{\delta''}\right). \tag{G47}$$

c. Block encoding of H_{32}

Since H_V has a probabilistic ancilla-preparation subroutine, we can block encode $H_{32} = H_V + H_{12\pi}$ using the procedure described in Ref. [20], by repeating the PREP$_V$ subroutine a constant number of times. This does not change the asymptotic gate complexity. Thus the total number of gates required to encode H_{32}/λ_{32}, where $\lambda_{32} = \|H_V\| + \|H_{12\pi}\| = (\eta(\eta-1)/2\Delta^2) + (\eta Z_{\text{sum}}/\Delta^2) + (8\pi^2\eta N/h^2) + (12\pi\eta N \ln 2a^2/ch\Delta)$, is

$$\mathcal{G}'_{32} \in O\left(\eta a \log_2 N + N \log_2 d + \log_2 N \log_2 \frac{N}{\delta'} + K \log_2 \frac{1}{\delta''}\right). \tag{G48}$$

Now, we can bound the sum of the ℓ_1 norm of H_V, $H_{1\pi}$, and $H_{2\pi}$, (and hence λ_{32}) as follows:

$$\begin{aligned}
&\frac{12\pi\eta N \ln(2a^2)}{ch\Delta} + \frac{8\pi^2\eta N}{h^2} + \frac{\eta(\eta-1)}{2\Delta^2} + \frac{\eta Z_{\text{sum}}}{\Delta^2} \\
&\quad \leq \frac{\eta N}{\Delta^2}\left(\frac{12\pi \ln(2a^2)}{c} \times \frac{\Delta}{h} + \frac{8\pi\Delta^2}{h^2} + \left(\frac{\eta + 2Z_{\text{sum}}}{2N}\right)\right) \\
&\quad \lessapprox K_{32}\frac{\eta N}{\Delta^2}\left(1 + \frac{\eta_s}{N}\right),
\end{aligned}$$

where K_{32} is a constant, $\eta_s = \eta + 2Z_{\text{sum}}$, and $Z_{\text{sum}} = \sum_{\kappa=1}^{K} |Z_\kappa|$. Thus, to obtain a δ_{32}-precise implementation of $e^{-i(H_V + H_{1\pi} + H_{2\pi})\tau_3}$, we need to repeat the block encoding of the Hamiltonian

$$R_{32} \in O\left(\frac{\eta N}{\Delta^2}\left(1 + \frac{\eta_s}{N}\right)\tau_3 + \frac{\log(1/\delta_{32})}{\log\log(1/\delta_{32})}\right) \tag{G49}$$

times and hence the gate complexity is

$$\begin{aligned}
\mathcal{G}_{32} &\in O(R_{32} \cdot \mathcal{G}'_{32}) \\
&\in O\left(\frac{\eta N}{\Delta^2}\left(1 + \frac{\eta_s}{N}\right)\tau_3\left(\eta a \log N + N \log d + \log N \log \frac{N}{\delta'} + K \log \frac{1}{\delta'}\right)\right. \\
&\qquad \left. + \frac{\log(1/\delta_{32})}{\log\log(1/\delta_{32})}\left(\eta a \log N + N \log d + \log N \log \frac{N}{\delta'} + K \log \frac{1}{\delta'}\right)\right).
\end{aligned} \tag{G50}$$

APPENDIX H: TROTTER ERROR AND COMMUTATORS

Let $H = \sum_{\gamma=1}^{\Gamma} H_\gamma$ be a time-independent operator and let the evolution generated by H be $e^{-it\sum_{\gamma=1}^{\Gamma} H_\gamma}$. Such evolutions can be approximated by a product of exponentials, using product formulas such as the first-order Lie-Trotter formula:

$$\mathscr{S}_1(t) = e^{tH_\Gamma} \ldots e^{tH_1} \tag{H1}$$

and higher-order Suzuki formulas [57] defined recursively via

$$\begin{aligned}
\mathscr{S}_2(t) &= e^{\frac{t}{2}H_1} \ldots e^{\frac{t}{2}H_\Gamma} e^{\frac{t}{2}H_\Gamma} \ldots e^{\frac{t}{2}H_1}, \\
\mathscr{S}_{2k}(t) &= \mathscr{S}^2_{2k-2}(u_k t)\mathscr{S}_{2k-2}((1-4u_k)t)\mathscr{S}^2_{2k-2}(u_k t),
\end{aligned} \tag{H2}$$

where $u_k = 1/4 - 4^{1/(2k-1)}$. Quite a few bounds on the Trotter error have been derived before [17,88,89] but we use the one in Ref. [58], which shows the dependence on nested commutators. Specifically, the authors show that for a pth-order Trotter-Suzuki formula, $\mathscr{S}_p(t) = e^{-itH} + \mathscr{A}(t)$, where

$$\|\mathscr{A}(t)\| \in O\left(\widetilde{\alpha}_{\text{comm}} t^{p+1}\right), \tag{H3}$$

if the H_γ are Hermitian. Also, in the above,

$$\widetilde{\alpha}_{\text{comm}} = \sum_{\gamma_1,\gamma_2,\ldots,\gamma_{p+1}=1}^{\Gamma} \|[H_{\gamma_{p+1}}, \ldots [H_{\gamma_2}, H_{\gamma_1}]]\|. \tag{H4}$$

Lemma 23. Consider the following sum of nested commutators, obtained from distinct Hamiltonians from the set $\{H_1, \ldots, H_k\}$. Let $H'_1, H'_2, \ldots, H'_{p'}$ be $p'+1$ Hamiltonians that may or may not belong to the set:

$$H_{\text{nest}} = \sum_{\gamma_1,\ldots,\gamma_{p-p'}=1}^{k} \Big[H_{\gamma_{p-p'}}, [H_{\gamma_{p-p'-1}}, [\ldots [H_{\gamma_1}, [H'_{p'+1}, [\ldots [H'_3, [H'_2, H'_1]] \ldots]]] \ldots]\Big].$$

Then,

$$\|H_{\text{nest}}\| \leq 2^{p-(p'+1)} \|[H'_{p'+1}, [\ldots [H'_3, [H'_2, H'_1]] \ldots]]\| \times \left(\sum_{i=1}^{k} \|H_i\|\right)^{p-p'}.$$

Proof. Consider one group of summands as follows. Among $H_{\gamma_1},\ldots,H_{\gamma_{p-p'}}$, the number of occurrences of H_1 is $0 \leq i_1 \leq p-p'$, the number of occurrences of H_2 is $0 \leq i_2 \leq p-p'-i_1$, the number of occurrences of H_3 is $0 \leq i_3 \leq p-p'-i_1-i_2$, and so on, i.e., the number of occurrences of H_k is $0 \leq i_k \leq p-p'-i_1-i_2-\cdots-i_{k-1}$. Using Fact 1, we can upper bound the norm of the sum of this group of summands as follows:

$$\|[H'_{p'+1},[\ldots[H'_3,[H'_2,H'_1]]\ldots]]\|2^{p-(p'+1)}\binom{p-p'}{i_1}\|H_1\|^{i_1}\binom{p-p'-i_1}{i_2}\|H_2\|^{i_2}$$
$$\ldots\binom{p-p'-i_1-\cdots-i_{k-2}}{i_{k-1}}\|H_{k-1}\|^{i_{k-1}}\|H_k\|^{p-p'-\cdots-i_{k-1}}.$$

Thus the total sum can be upper bounded as follows.

$$\begin{aligned}\|H_{\text{nest}}\| &\leq 2^{p-(p'+1)}\|[H'_{p'+1},[\ldots[H'_3,[H'_2,H'_1]]\ldots]]\|\\ &\times\sum_{i_1=0}^{p-p'}\sum_{i_2=0}^{p-p'-i_1}\cdots\sum_{i_{k-1}=0}^{p-p'-\cdots-i_{k-2}}\binom{p-p'}{i_1}\cdots\binom{p-p'-\cdots-i_{k-2}}{i_{k-1}}\|H_1\|^{i_1}\ldots\|H_k\|^{p-p'-\cdots-i_{k-1}}\\ &= 2^{p-(p'+1)}\|[H'_{p'+1},[\ldots[H'_3,[H'_2,H'_1]]\ldots]]\|\left(\sum_{i=1}^{k}\|H_i\|\right)^{p-p'}.\end{aligned}$$

■

Thus we immediately prove Lemma 7, which we are restating here for completeness.

Lemma 24. Let $H=\sum_{\gamma=1}^{\Gamma}H_\gamma$ and $\widetilde{\alpha}_{\text{comm}}=\sum_{\gamma_1,\gamma_2,\ldots,\gamma_{p+1}=1}^{\Gamma}\|[H_{\gamma_{p+1}},\ldots[H_{\gamma_2},H_{\gamma_1}]]\|$. Then, for any integer $1\leq p'\leq p$,

$$\widetilde{\alpha}_{\text{comm}}\leq 2^{p-(p'+1)}\sum_{\gamma_{i_1},\gamma_{i_2},\ldots,\gamma_{i_{p'+1}}}\|[H_{\gamma_{p'+1}},[\ldots[H_{\gamma_3},[H_{\gamma_2},H_{\gamma_1}]]\ldots]]\|\left(\sum_{\gamma=1}^{\Gamma}\|H_\gamma\|\right)^{p-p'}.$$

Ideally, we would want to compute tight bounds for the nested commutators, preferably by exploiting some structure or properties of the Hamiltonians. The use of norms does not always give tight bounds. But suppose that we can compute such tight bounds up to level p' of nesting, while we want a bound up to level p. Then, these results can be very useful because we can look at them as though we have combined the tighter analysis up to level p' with a less tight analysis for the rest of the levels of nesting. In fact, we observe that in Lemma 24, we actually group the terms with the same inner commutators up to level p' and then apply Lemma 23 to bound the sum of each such group, absolutely independent of the other groups. So, we can vary p' for each group and vary the groupings appropriately in order to apply Lemma 23. This can make the bound tighter for many applications. In this sense, we have some flexibility.

We have explained before how we compute the ℓ_1 norm. Now, we explain how we calculate the innermost pairwise commutators. For all the pairs, the bounds have been derived by expanding the commutators using Lemmas 8 and 9 and then using the triangle inequality (Appendix E). For $[H_\pi,H_{V_{ee}}]$ and $[H_\pi,H_{V_{ne}}]$, we use the following additional lemma. So first, we explain these two cases.

Similarly to the particle configuration considered in this paper, let S be a 3D cubic lattice each side of which is of length L. Each side has $N^{1/3}$ points and thus the interpoint spacing is $\Delta=L/N^{1/3}$. So we can say that the cube is subdivided into N unit-cells, each of length Δ. For any two points $q=(q_x,q_y,q_z)$ and $r=(r_x,r_y.r_z)$ in the lattice, let the distance between them be denoted by $d_{qr}=\|q-r\|_2=\sqrt{(q_x-r_x)^2+(q_y-r_y)^2+(q_z-r_z)^2}$.

Lemma 25. Assume that S consists of at least $N=1$ unit cells and has side length $\Delta>0$. Then,

$$\sum_{q\neq r}\frac{1}{d_{qr}}\leq\frac{2\times N^{5/3}}{\Delta}.$$

Proof. Consider the points on a two-dimensional (2D) lattice, i.e., when $q_z-r_z=0$. We assume that all points within the lattice have positive coordinates and that one corner is $(0,0,.)$. Let us fix q to be this corner. We ignore the third coordinate, because it is not relevant in the 2D plane.

We divide the points of the lattice into different sets and then compute the sum of the inverse of the distances of q from the points within each set. First, consider the points within the square with length Δ, cornered at q. We include these points in set $\mathcal{S}_1$. Apart from q, there are 2×1 points at distance $\Delta\sqrt{1^2+0^2}$ from q there is and one point at distance $\Delta\sqrt{1^2+1^2}$ from q. The sum of the inverses of these distances is

$$2\frac{1}{\Delta\sqrt{1^2+0^2}}+\frac{1}{\Delta\sqrt{1^2+1^2}}.$$

Next, we build the set $\mathcal{S}_2$, that includes all points within a square of sides 2Δ, cornered at q, but not those in $\mathcal{S}_0$. There are 2×2 points at distances $\Delta\sqrt{2^2+0^2}, \Delta\sqrt{2^2+1^2}$ and it is straightforward to see that for each distance, there are two points, one translated in the X and the other in the Y direction. There is one point at the corner, which is at distance $\Delta\sqrt{2^2+2^2}$. The sum of the inverses of these distances is

$$\frac{1}{\Delta}\left[2\left(\frac{1}{\sqrt{2^2+0^2}}+\frac{1}{\sqrt{2^2+1^2}}\right)+\frac{1}{\sqrt{2^2+2^2}}\right].$$

Similarly, we consider the set $\mathcal{S}_3 = \{$points within a square of side 3Δ, cornered at $q\} \setminus \left(\mathcal{S}_2 \bigcup \mathcal{S}_1\right)$. There are 2×3 points, at distances $\Delta\sqrt{3^2+0^2}, \Delta\sqrt{3^2+1^2}, \Delta\sqrt{3^2+2^2}$ from q; and one corner point at distance $\Delta\sqrt{3^2+3^2}$. The sum of the inverse is

$$\frac{1}{\Delta}\left[2\left(\frac{1}{\sqrt{3^2+0^2}}+\frac{1}{\sqrt{3^2+1^2}}+\frac{1}{\sqrt{3^2+2^2}}\right)+\frac{1}{\sqrt{3^2+3^2}}\right].$$

We go on in this way until we build the last set:

$$\mathcal{S}_{N^{1/3}} = \big\{\text{points within a square of side } N^{1/3}\Delta, \text{ cornered at } q\big\} \setminus \left(\bigcup_{i=1}^{N^{1/3}-1} \mathcal{S}_i\right).$$

There are $2 \times N^{1/3}$ points, at distances

$$\Delta\sqrt{N^{2/3}+0^2}, \Delta\sqrt{N^{2/3}+1^2}, \Delta\sqrt{N^{2/3}+2^2}, \ldots, \Delta\sqrt{N^{2/3}+(N^{1/3}-1)^2}$$

from q; and one corner point at distance $\Delta\sqrt{N^{2/3}+N^{2/3}}$. The sum of the inverse of these distances is

$$\frac{1}{\Delta}\left[2\left(\frac{1}{\sqrt{N^{2/3}+0^2}}\cdots+\frac{1}{\sqrt{N^{2/3}+(N^{1/3}-1)^2}}\right)+\frac{1}{\sqrt{N^{2/3}+N^{2/3}}}\right].$$

We claim that

$$f(k) = 2\sum_{i=0}^{k-1}\left(\frac{1}{\sqrt{k^2+i^2}}\right)+\frac{1}{\sqrt{k^2+k^2}} \leq 2 \qquad \text{(H5)}$$

when $k > 4$. This is because $f(k)$ is continuous and differentiable in $[1, N']$, where N' is finite. Also,

$$f'(k) = -2\sum_{i=0}^{k-1} k(k^2+i^2)^{-3/2} - \frac{1}{\sqrt{2}k^2} < 0$$

in this finite interval and hence the function $f(k)$ is monotonically decreasing. Since $f(k) \leq 2$ when $k \geq 4$, our claim follows.

Thus, for one particular 2D plane, the sum of the inverse of the distances is at most $2 \times N^{1/3}/\Delta$.

Now, a 3D cubic lattice can be generated by translations of this 2D square lattice along the z direction. Now, as we translate along the Z direction, $q_z - r_z > 0$, so the distances from $q = (0,0,0)$ increase and hence the sum of the inverse of these distances can again be bounded by $2 \times N^{1/3}/\Delta$. Since a cube is generated by $N^{1/3}$ such translations,

$$\sum_r \frac{1}{d_{0r}} \leq \frac{2 \times N^{2/3}}{\Delta}.$$

Hence $\sum_{q\neq r}\sum_r 1/d_{qr} \leq N(2 \times N^{2/3}/\Delta)$ and the lemma follows. ■

Given this result, we can turn our attention to bounding the commutators of all remaining terms in the Hamiltonian. We proceed in the following to enumerate each possible commutator that can emerge in the error bound. These bounds will be used in our Trotter-error-bound estimates.

I. $\|[\mathbf{H}_\pi, \mathbf{H}_{\mathbf{V}_{\mathbf{ee}}}]\|$ and $\|[\mathbf{H}_\pi, \mathbf{H}_{\mathbf{V}_{\mathbf{ne}}}]\|$

We know that

$$H_\pi = \frac{1}{2}\sum_{j=1}^{\eta}\sum_{\mu=1}^{3}\sum_{q=1}^{N}\left(-\mathbb{I}\otimes\nabla_{j,\mu}^2\otimes\mathbb{I}+i\frac{2}{c}\mathbb{I}\otimes\nabla_{j,\mu}\otimes A_{q,\mu}+\frac{1}{c^2}\mathbb{I}\otimes\mathbb{I}\otimes A_{q,\mu}^2\right),$$

$$H_{V_{ee}} = \frac{1}{\Delta}\sum_{j'<k=1}^{\eta}\sum_{x_1,x_2=1}^{N}\mathbb{I}\otimes\frac{1}{\|x_1-x_2\|_2}(|x_1\rangle\langle x_1|_{j'}\otimes|x_2\rangle\langle x_2|_k)\otimes\mathbb{I},$$

$$H_{V_{ne}} = -\frac{1}{\Delta}\sum_{j'=1}^{\eta}\sum_{\kappa=1}^{K}\sum_{x=1}^{N}\mathbb{I}\otimes\frac{Z_\kappa}{\|x-R_\kappa\|_2}|x\rangle\langle x|_j\otimes\mathbb{I}.$$

Let $\|x_1-x_2\|_2 = d_{x_1x_2}$ and $\|x-R_\kappa\|_2 = d_{x\kappa}$. Using Lemmas 8 and 9 and the fact that $[A^2,\mathbb{I}]=0$, we obtain

$$\begin{aligned}[H_\pi, H_{V_{ee}}] = &-\frac{1}{2\Delta}\sum_{\substack{j=j'\text{ or }k\\ \mu,q,x_1,x_2}}\mathbb{I}\otimes\frac{1}{d_{x1x2}}[\nabla_{j,\mu}^2,|x_1\rangle\langle x_1|_{j'}|x_2\rangle\langle x_2|_k]\otimes\mathbb{I}\\ &+\frac{i2}{c\Delta}\sum_{\substack{j=j'\text{ or }k\\ \mu,q,x_1,x_2}}\mathbb{I}\otimes\frac{1}{d_{x1x2}}[\nabla_{j,\mu},|x_1\rangle\langle x_1|_{j'}|x_2\rangle\langle x_2|_k]\otimes A_{q,\mu}.\end{aligned}$$

From Lemma 25, we know that $\sum_{x1x2} 1/d_{x_1x_2} \le 2N^{5/3}/\Delta$. The spectral norm of the commutator is bounded as follows:

$$\begin{aligned}\|[H_\pi, H_{V_{ee}}]\| &\le 2\left(\frac{1}{2\Delta}\frac{2\times 3\eta(\eta-1)N}{2}\|\nabla_j^2\|\sum_{x_1,x_2}\frac{1}{d_{x1x2}}+\frac{2}{c\Delta}\frac{2\times 3\eta(\eta-1)N}{2}\|\nabla_j\|\|A_\mu\|\sum_{x_1,x_2}\frac{1}{d_{x1x2}}\right)\\ &\le \frac{3\eta(\eta-1)N}{\Delta}\frac{4\pi^2}{3h^2}\frac{N^{5/3}}{\Delta}+\frac{12\eta(\eta-1)N}{c\Delta}\frac{\ln(2a^2)}{h}\frac{2\pi}{\Delta}\frac{N^{5/3}}{\Delta}\\ &\le \frac{4\pi\eta(\eta-1)N^{8/3}}{h^2\Delta^2}\left(\pi+\frac{6h\ln(2a^2)}{c\Delta}\right).\end{aligned}$$

With similar arguments, we can prove that

$$\|[H_\pi, H_{V_{ne}}]\| \le \frac{4\pi\eta N^{5/3}KZ_{\max}}{h^2\Delta^2}\left(\pi+\frac{6h\ln(2a^2)}{c\Delta}\right), \tag{H6}$$

where $(Z_\kappa)_{\max} = Z_{\max}$. In this case, we have $\sum_\kappa Z_\kappa\sum_x 1/d_{x\kappa} \le Z_{\max}\sum_{\kappa,x}1/d_{x\kappa}$. Similarly to Lemma 25, we can prove that $\sum_x 1/d_{\kappa r} \le N^{2/3}/\Delta$, for some fixed κ. Hence $\sum_{\kappa x}1/d_{x\kappa} \le KN^{2/3}/\Delta$. Here, we make another observation, which has been important in the groupings that we make. If $H_\pi = H_{1\pi}+H_{2\pi}+H_{3\pi}$ as defined in Eq. (21), then $[H_{3\pi}, H_{V_{ee}}] = [H_{3\pi}, H_{V_{ne}}] = 0$.

II. $\|[\mathbf{H}_\mathbf{s}, \mathbf{H}_\pi]\|$

We know that

$$H_s = -\frac{1}{c}\sum_{j=1}^{\eta}\sum_{q=1}^{N}\sum_{\mu\neq\nu\neq\xi=1}^{3}\sigma_{j,\mu}\otimes\mathbb{I}\otimes\left(\nabla_\nu A_{q,\xi}-\nabla_\xi A_{q,\nu}\right).$$

Using Lemmas 8 and 9 and the facts that $[(\nabla_\nu A_{q,\xi} - \nabla_\xi A_{q,\nu}), A_{q',\mu'}] = [(\nabla_\nu A_{q,\xi} - \nabla_\xi A_{q,\nu}), A^2_{q',\mu'}] =$ if $q \neq q'$ and $\mu' \neq \nu, \xi$, we have

$$[H_s, H_\pi] = i\frac{1}{c^2} \sum_{\substack{j,j',q\\ \mu\neq\nu\neq\xi\\ \mu'=\nu \text{ or } \xi}} \sigma_{j,\mu} \otimes \nabla_{j',\mu'} \otimes [(\nabla_\nu A_{q,\xi} - \nabla_\xi A_{q,\nu}), A_{q,\mu'}]$$

$$+ \frac{1}{2c^3} \sum_{\substack{j,j',q\\ \mu\neq\nu\neq\xi\\ \mu'=\nu \text{ or } \xi}} \sigma_{j,\mu} \otimes \mathbb{I} \otimes [(\nabla_\nu A_{q,\xi} - \nabla_\xi A_{q,\nu}), A^2_{q,\mu'}]$$

and hence

$$\begin{aligned}
\|[H_s, H_\pi]\| &\leq 2\left(\frac{1}{c^2} 6N\eta^2 \|\nabla_{j',\mu'}\| \|(\nabla_\nu A_{q,\xi} - \nabla_\xi A_{q,\nu})\| \|A_{q,\mu'}\| + \frac{1}{2c^3} 6N\eta^2 \|(\nabla_\nu A_{q,\xi} - \nabla_\xi A_{q,\nu})\| \|A^2_{q,\mu'}\|\right) \\
&\leq \frac{6\eta^2 N}{c^2}\left(2\frac{2\ln a + \gamma}{h}\frac{4\pi(2\ln a + \gamma)}{h\Delta}\frac{2\pi}{\Delta} + \frac{1}{c}\frac{4\pi(2\ln a + \gamma)}{h\Delta}\frac{4\pi^2}{\Delta^2}\right) \\
&= \frac{96\pi^2\eta^2 N(2\ln a + \gamma)}{hc^2\Delta^2}\left(\frac{2\ln a + \gamma}{h} + \frac{\pi}{c\Delta}\right) \\
&\leq \frac{96\pi^2\eta^2 N \ln(2a^2)}{hc^2\Delta^2}\left(\frac{\ln(2a^2)}{h} + \frac{\pi}{c\Delta}\right).
\end{aligned} \tag{H7}$$

III. $\|[\mathbf{H_s}, \mathbf{H_{V_{ee}}}]\|$ and $\|[\mathbf{H_s}, \mathbf{H_{V_{ne}}}]\|$

Expanding, using Lemmas 8 and 9, we find that both of these commutators are 0.

IV. $\|[\mathbf{H_f}, \mathbf{H_{V_{ee}}}]\|$ and $\|[\mathbf{H_f}, \mathbf{H_{V_{ne}}}]\|$

We know that

$$H_{f\,1} = \frac{1}{2}\sum_{q'=1}^{N}\sum_{\mu'=1}^{3} \mathbb{I} \otimes \mathbb{I} \otimes E^2_{q',\mu'},$$

$$H_{f\,2} = -\sum_{q'=1}^{N}\sum_{\mu'\neq\nu'=1}^{3} \mathbb{I} \otimes \mathbb{I} \otimes W^2_{q',\mu',\nu'}.$$

Using Lemmas 8 and 9, we find that both of these commutators are 0.

V. $\|[\mathbf{H_{f1}}, \mathbf{H_{f2}}]\|$

For a tighter bound on the commutator, we consider the following definitions of $E^2_{q,\mu}$ and $U_{q,\mu}$, as given in Sec. II A:

$$E^2_{q,\mu} = \sum_{\epsilon=-\Lambda}^{\Lambda-1} \epsilon^2 \left|\epsilon\right\rangle \left\langle\epsilon\right|_{q,\mu}, \tag{H8}$$

$$U_{q,\mu} = \sum_{\epsilon=-\Lambda}^{\Lambda-1} \left|\epsilon+1\right\rangle \left\langle\epsilon\right|_{q,\mu}. \tag{H9}$$

The commutator between these two operators is

$$\begin{aligned}
\|[E^2_{q,\mu}, U_{q,\mu}]\| &= \|E^2_{q,\mu}U_{q,\mu} - U_{q,\mu}E^2_{q,\mu}\| \\
&= \| \sum_{\epsilon=-\Lambda}^{\Lambda-1} (\epsilon+1)^2 \left|\epsilon+1\right\rangle \left\langle\epsilon\right| - \sum_{\epsilon=-\Lambda}^{\Lambda-1} \epsilon^2 \left|\epsilon+1\right\rangle \left\langle\epsilon\right| \| \\
&= \| \sum_{\epsilon=-\Lambda}^{\Lambda-1} (2\epsilon+1) \left|\epsilon+1\right\rangle \left\langle\epsilon\right| \| = 2\Lambda - 1.
\end{aligned} \tag{H10}$$

Now, from its definition, the plaquette operator $W^2_{q',\mu',\nu'}$ is the product of four such U operators that act on the sides of a plaquette. So $E^2_{q,\mu}$ has a nonzero commutator with $W^2_{q',\mu',\nu'}$ if and only if the link (q,μ) is any one of the four links of this plaquette. Thus,

$$\|[H_{f\,1}, H_{f\,2}]\| \le 3N \times 2(2\Lambda - 1) \le 12N\Lambda. \tag{H11}$$

VI. $\|[\mathbf{H_f}, \mathbf{H_\pi}]\|$

Using similar arguments as before to obtain the indices for nonzero commutators, we have

$$\begin{aligned}
[H_f, H_\pi] = &-\frac{i}{2c}\sum_{j,\mu,q} \mathbb{I}\otimes\nabla_{j,\mu}\otimes[E^2_{q,\mu}, A_{q,\mu}] + \frac{1}{2c^2}\sum_{j,\mu,q}\mathbb{I}\otimes\mathbb{I}\otimes[E^2_{q,\mu}, A^2_{q,\mu}] \\
&- i\frac{2}{c}\sum_{\substack{j,\mu\neq\nu,q\\ \mathbf{q}'=q \text{ or } q+1\\ \mu'=\mu \text{ or } \nu}} \mathbb{I}\otimes\nabla_{j,\mu'}\otimes[W^2_{q,\mu,\nu}, A_{q',\mu'}] - \frac{1}{c^2}\sum_{\substack{j,\mu\neq\nu,q\\ \mathbf{q}'=q \text{ or } q+1\\ \mu'=\mu \text{ or } \nu}} \mathbb{I}\otimes\mathbb{I}\otimes[W^2_{q,\mu,\nu}, A^2_{q',\mu'}]
\end{aligned}$$

and so

$$\begin{aligned}
\|[H_f, H_\pi]\| &\le 2\left(\frac{3\eta N}{2c}\|\nabla_{j\mu}\|\|E^2_{q\mu}\|\|A_{q,\mu}\| + \frac{3\eta N}{2c^2}\|E^2_{q\mu}\|\|A^2_{q,\mu}\| + \frac{24\eta N}{c}\|\nabla_{j\mu'}\|\|W^2_{q,\mu,\nu}\|\|A_{q',\mu'}\| \right.\\
&\qquad\left. + \frac{12\eta N}{c^2}\|W^2_{q,\mu,\nu}\|\|A^2_{q',\mu'}\|\right) \\
&\le \frac{3\eta N}{c}\left(\frac{2\ln a+\gamma}{h}\Lambda^2\frac{2\pi}{\Delta} + \frac{1}{c}\Lambda^2\frac{4\pi^2}{\Delta^2} + 16\frac{2\ln a+\gamma}{h}2\frac{2\pi}{\Delta} + \frac{8}{c}2\times\frac{4\pi^2}{\Delta^2}\right) \\
&= \frac{6\pi\eta N\Lambda^2}{c\Delta}\left(\frac{2\ln a+\gamma}{h} + \frac{2\pi}{c\Delta}\right) + \frac{198\pi\eta N}{c\Delta}\left(\frac{2\ln a+\gamma}{h} + \frac{\pi}{c\Delta}\right) \\
&\le \frac{6\pi\eta N}{c\Delta}\left(\left(\frac{\ln(2a^2)}{h} + \frac{2\pi}{c\Delta}\right)(\Lambda^2+33) - \frac{33\pi}{c\Delta}\right).
\end{aligned} \tag{H12}$$

VII. $\|[\mathbf{H_s}, \mathbf{H_{f1}}]\|$ and $\|[\mathbf{H_s}, \mathbf{H_{f2}}]\|$

We know that

$$\begin{aligned}
H_s &= -\frac{1}{c}\sum_{j=1}^{\eta}\sum_{q=1}^{N}\sum_{\mu\neq\nu\neq\xi=1}^{3}\sigma_{j,\mu}\otimes\mathbb{I}\otimes\left(\nabla_\nu A_{q,\xi} - \nabla_\xi A_{q,\nu}\right), \\
H_{f\,1} &= \frac{1}{2}\sum_{q'=1}^{N}\sum_{\mu'=1}^{3}\mathbb{I}\otimes\mathbb{I}\otimes E^2_{q',\mu'}, \\
H_{f\,2} &= -\sum_{q'=1}^{N}\sum_{\mu'\neq\nu'=1}^{3}\mathbb{I}\otimes\mathbb{I}\otimes W^2_{q',\mu',\nu'}.
\end{aligned}$$

$[(\nabla_\nu A_{q,\xi} - \nabla_\xi A_{q,\nu}), E^2_{q',\mu'}] = 0$ if $q \neq q'$ and $\mu' \neq \xi, \nu$. Also, $[(\nabla_\nu A_{q,\xi} - \nabla_\xi A_{q,\nu}), W_{q',\mu',\nu'}] \neq 0$ if the link (q,ξ) or (q,ν) is equal to any of the links (q',μ'), $(q'+1_{\mu'},\nu')$, $(q'+1_{\nu'},\mu')$, or (q',ν'). This can happen if ν' (or μ') is either ν or ξ and the other one varies; and if $\nu' = \nu$ (say), then $(q,\nu) = (q',\nu')$ or $(q,\nu) = (q'+1_{\mu'},\nu')$. In the following equations, we refer to the latter condition as $q = q'$ or $q'+1$, for brevity. Using Lemmas 8 and 9, we have the following:

$$[H_s, H_{f\,1}] = -\frac{1}{2c} \sum_{\substack{q,j \\ \mu\neq\nu\neq\xi \\ \mu'=\nu \text{ or } \xi}} \sigma_{j,\mu} \otimes \mathbb{I} \otimes [(\nabla_\nu A_{q,\xi} - \nabla_\xi A_{q,\nu}), E^2_{q,\mu'}],$$

$$\left[H_s, H_{f\,2}\right] = \frac{1}{c} \sum_{\substack{q,j \\ \mu\neq\nu\neq\xi,\mu' \\ \ell=q,q+1}} \sigma_{j,\mu} \otimes \mathbb{I} \otimes [(\nabla_\nu A_{q,\xi} - \nabla_\xi A_{q,\nu}), W^2_{q,\mu'\nu}].$$

We have used the following facts. Using the bounds in Table II, we have

$$\|[H_s, H_{f\,1}]\| \leq 2\frac{1}{2c} 6\eta N \|\nabla_\nu A_{q,\xi} - \nabla_\xi A_{q,\nu})\| \|E^2_{q\mu'}\| \leq \frac{24\pi\eta N \Lambda^2 \ln(2a^2)}{ch\Delta},$$
$$\|[H_s, H_{f\,2}]\| \leq 2\frac{1}{c} 18\eta N \|\nabla_\nu A_{q,\xi} - \nabla_\xi A_{q,\nu})\| \|W^2_{q',\mu',\nu'}\| \leq \frac{288\pi\eta N \ln(2a^2)}{ch\Delta}.$$

In Table III, we summarize the bounds on all the necessary pairwise commutators that we have derived.

APPENDIX I: STATE-PREPARATION ALGORITHM

In this appendix, we describe an algorithm to prepare a state proportional to the following:

$$\sum_{\vec{v}\in G} \frac{1}{\sqrt{\|\vec{v}\|}} |\vec{v}\rangle, \quad \text{where } G = [-N^{1/3}, N^{1/3}]^3 \setminus \{0,0,0\}. \tag{I1}$$

We follow the algorithm in Refs. [18,20], with appropriate changes to take care of the difference in weights. The approach is to use a hierarachy of nested boxes in G indexed by μ, each box being larger than the previous one by a factor of 2. For each box μ, we prepare a set of $\vec{v}$ values in that cube. We use eight registers $|\mu\rangle\,|v_x\rangle\,|v_y\rangle\,|v_z\rangle\,|m\rangle\,|0\rangle$ to hold this state. These subsystems are used as follows:

(a) $|\mu\rangle$ indexes the box used.
(b) $|v_x, v_y, v_z\rangle$ are the three components of $\vec{v}$ given as signed integers.
(c) $|m\rangle$ is an ancilla in an equal superposition, used to give the correct amplitude via an inequality test.
(d) $|0\rangle$ flags that the state preparation is successful.

There are four aspects due to which we have a failure probability:

(1) The preparation of μ can fail.
(2) The signed integers can be negative zero, which is not allowed.
(3) There is a failure probability associated with the test of whether $\vec{v}$ is inside a certain box.
(4) An inequality test made during the preparation also introduces a probability of failing.

Let $n_p = 1 + \log_2\left(N^{1/3}+1\right)$ be the number of qubits required to represent v_x, v_y, and v_z, i.e., each will give numbers from $-(2^{n_p-1}-1)$ to $2^{n_p-1}-1$. The state-preparation procedure can be summarized in the following steps.

1. Step I

We prepare a superposition state

$$\sqrt{\frac{3}{4^{n+1}-16}} \sum_{\mu=2}^{n_p} 2^\mu\,|\mu\rangle, \tag{I2}$$

which ensures that we obtain the correct weighting for each cube. We use a unary encoding for $|\mu\rangle$. We use a ladder of n_p controlled-H gates. More details can be found in Ref. [20]. Each H gate can be implemented with two H gate, two T gates, and one CNOT gate.

2. Step II

Controlled by μ, we apply an H gate on μ of the qubits representing v_x, v_y, and v_z to represent the values from $-(2^{\mu-1}-1)$ to $2^{\mu-1}-1$. We require at most $3n_p$

controlled-H gates. We will flag a minus zero as a failure. This can be done by checking each of $|v_x\rangle, |v_y\rangle$, and $|v_z\rangle$, to determine whether the sign bit is 1 and the remaining bits are 0. This requires three pairs of compute-uncompute $C^{n_p}X$ gates. Decomposing these, we require $2(4n_p - 8)$ T gates, $2(4n_p - 7)$ CNOT gates and $n_p - 1$ ancillas.

The total number of combinations before flagging the failure is $2^{3\mu}$ and so the squared amplitude is the inverse of this. At this stage, the state is

$$\sqrt{\frac{3}{4^{n+1}-16}}\sum_{\mu=2}^{n}\sum_{v_x,v_y,v_z=-(2^{\mu-1}-1)}^{2^{\mu-1}-1} 2^{-\mu/2}\,|\mu\rangle\,|v_x,v_y,v_z\rangle\,. \tag{I3}$$

3. Step III

We test whether $|v_x|, |v_y|, |v_z| < 2^{\mu-2}$. If they are, then the point is inside the box for the next lower value of μ and we flag failure on the last ancilla qubit. For $\mu = 2$, this implies that we test whether $\vec{v} = \vec{0}$, which we exclude. This requires testing whether all the three qubits for v_x, v_y, and v_z are 0. Since the qubits tested are dependent on μ, the complexity is $O(n_p)$.

Let B_μ (for box μ) be the set of $\vec{v}$ such that the absolute values of v_x, v_y, and v_z are less than $2^{\mu-1}$, but let it not be the case that they are all less than $2^{\mu-2}$, i.e.,

$$\begin{aligned}B_\mu = \Big\{\vec{v} : (0 \le |v_x| < 2^{\mu-1}) \bigwedge (0 \le |v_y| < 2^{\mu-1})\\ \bigwedge (0 \le |v_z| < 2^{\mu-1}) \bigwedge \big((|v_x| \ge 2^{\mu-2})\\ \vee (|v_y| \ge 2^{\mu-2}) \vee (|v_z| < 2^{\mu-2})\big)\Big\}.\end{aligned}$$

At this stage, the state, excluding the failures, is

$$\sqrt{\frac{3}{4^{n+1}-16}}\sum_{\mu=2}^{n}\sum_{\vec{v}\in B_\mu}\frac{1}{2^{\mu/2}}\,|\mu\rangle\,|v_x,v_y,v_z\rangle\,. \tag{I4}$$

4. Step IV

We prepare an ancilla register in an equal superposition of $|m\rangle$ for $m = 0$ to $M - 1$, where M is a power of 2 and is chosen to be large enough to provide a sufficiently accurate approximation of the overall state preparation. This superposition can be done entirely with H gates. Then, we test the inequality

$$\frac{2^{\mu-2}}{\|\vec{v}\|} > \frac{m}{M}.$$

The left-hand side can be as large as 1 in this region, because we can have just one of v_x, v_y, and v_z as large as $2^{\mu-2}$ and the other two equal to 0. That is, we are at the center of a face of the inner cube. To avoid costly divisions, we test the following equivalent inequality:

$$\left(2^{\mu-2}\times M\right)^2 > m^2\left(v_x^2 + v_y^2 + v_z^2\right).$$

The number of values of m satisfying the above inequality is $Q = \lceil M2^{\mu-2}/\|\vec{v}\|\rceil$. At this stage, the resulting state, ignoring the part that fails, is

$$\sqrt{\frac{3}{M(4^{n+1}-16)}}\sum_{\mu=2}^{n}\sum_{\vec{v}\in B_\mu}\sum_{m=0}^{Q-1}\frac{1}{2^{\mu/2}}\,|\mu\rangle\,|v_x,v_y,v_z\rangle\,|m\rangle\,. \tag{I5}$$

The square of the amplitude for each $\vec{v}$ will then be

$$\frac{3\lceil M2^{\mu-2}/\|\vec{v}\|\rceil}{M(4^{n+1}-16)2^{\mu}} \approx \frac{3}{4(4^{n+1}-16)}\frac{1}{\|\vec{v}\|} \tag{I6}$$

and hence the amplitude for each $\vec{v}$ will be proportional to $1/\sqrt{\|\vec{v}\|}$.

Now, we consider the error in the state preparation due to the finite value of M. The relevant quantity is the sum of the errors in the squared amplitudes, as that gives the error in the weightings of the operations applied to the target state. That error is upper bounded by

$$\begin{aligned}\frac{3}{M(4^{n+1}-16)}\sum_{\mu=2}^{n}\sum_{\vec{v}\in B_\mu}\frac{1}{2^{\mu}} &< \frac{3}{M(4^{n+1}-16)}\sum_{\mu=2}^{n}2^{2\mu}\\ &= \frac{1}{M}.\end{aligned} \tag{I7}$$

If $n_M = \lceil \log_2 M\rceil$, then we require $O(n_p^2 + n_p + n_M n_p + n_M)$ gates for this step [20]. If we take $n_M = \log(1/\delta')$, for some $\delta' > 0$, then the gate complexity for this state-preparation procedure is in $O\left(\log N + \log 1/\delta' + \log^2 N + \log N \log 1/\delta'\right) \in O\left(\log N \log N/\delta'\right)$.

[1] R. P. Feynman, Simulating physics with computers, Int. J. Theor. Phys. **21**, 467 (1982).

[2] D. W. Berry, G. Ahokas, R. Cleve, and B. C. Sanders, Efficient quantum algorithms for simulating sparse Hamiltonians, Commun. Math. Phys. **270**, 359 (2007).

[3] A. M. Childs and N. Wiebe, Hamiltonian simulation using linear combinations of unitary operations, Quantum Inf. Comput. **12**, 901 (2012).

[4] D. W. Berry, A. M. Childs, R. Cleve, R. Kothari, and R. D. Somma, Simulating Hamiltonian dynamics with a truncated Taylor series, Phys. Rev. Lett. **114**, 090502 (2015).

[5] G. H. Low and I. L. Chuang, Optimal Hamiltonian simulation by quantum signal processing, Phys. Rev. Lett. **118**, 010501 (2017).

[6] S. Hadfield and A. Papageorgiou, Divide and conquer approach to quantum Hamiltonian simulation, New J. Phys. **20**, 043003 (2018).

[7] G. H. Low and I. L. Chuang, Hamiltonian simulation by qubitization, Quantum **3**, 163 (2019).

[8] A. Gilyén, Y. Su, G. H. Low, and N. Wiebe, in *Proceedings of the 51st Annual ACM SIGACT Symposium on Theory of Computing* (2019), p. 193.

[9] X. Yuan, J. Sun, J. Liu, Q. Zhao, and Y. Zhou, Quantum simulation with hybrid tensor networks, Phys. Rev. Lett. **127**, 040501 (2021).

[10] A. J. Daley, I. Bloch, C. Kokail, S. Flannigan, N. Pearson, M. Troyer, and P. Zoller, Practical quantum advantage in quantum simulation, Nature **607**, 667 (2022).

[11] A. Rajput, A. Roggero, and N. Wiebe, Hybridized methods for quantum simulation in the interaction picture, Quantum **6**, 780 (2022).

[12] J. Casanova, A. Mezzacapo, L. Lamata, and E. Solano, Quantum simulation of interacting fermion lattice models in trapped ions, Phys. Rev. Lett. **108**, 190502 (2012).

[13] I. D. Kivlichan, N. Wiebe, R. Babbush, and A. Aspuru-Guzik, Bounding the costs of quantum simulation of many-body physics in real space, J. Phys. A: Math. Theor. **50**, 305301 (2017).

[14] W. Hofstetter and T. Qin, Quantum simulation of strongly correlated condensed matter systems, J. Phys. B: At., Mol. Opt. Phys. **51**, 082001 (2018).

[15] C. Kokail, C. Maier, R. van Bijnen, T. Brydges, M. K. Joshi, P. Jurcevic, C. A. Muschik, P. Silvi, R. Blatt, and C. F. Roos, *et al.*, Self-verifying variational quantum simulation of lattice models, Nature **569**, 355 (2019).

[16] R. Barends, L. Lamata, J. Kelly, L. García-Álvarez, A. G. Fowler, A. Megrant, E. Jeffrey, T. C. White, D. Sank, and J. Y. Mutus *et al.* Digital quantum simulation of fermionic models with a superconducting circuit, Nat. Commun. **6**, 7654 (2015).

[17] D. Wecker, M. B. Hastings, N. Wiebe, B. K. Clark, C. Nayak, and M. Troyer, Solving strongly correlated electron models on a quantum computer, Phys. Rev. A **92**, 062318 (2015).

[18] R. Babbush, D. W. Berry, J. R. McClean, and H. Neven, Quantum simulation of chemistry with sublinear scaling in basis size, npj Quantum Inf. **5**, 1 (2019).

[19] R. Babbush, C. Gidney, D. W. Berry, N. Wiebe, J. McClean, A. Paler, A. Fowler, and H. Neven, Encoding electronic spectra in quantum circuits with linear T complexity, Phys. Rev. X **8**, 041015 (2018).

[20] Y. Su, D. W. Berry, N. Wiebe, N. Rubin, and R. Babbush, Fault-tolerant quantum simulations of chemistry in first quantization, PRX Quantum **2**, 040332 (2021).

[21] D. Marcos, P. Rabl, E. Rico, and P. Zoller, Superconducting circuits for quantum simulation of dynamical gauge fields, Phys. Rev. Lett. **111**, 110504 (2013).

[22] E. Zohar, J. Ignacio Cirac, and B. Reznik, Quantum simulations of lattice gauge theories using ultracold atoms in optical lattices, Rep. Progr. Phys. **79**, 014401 (2015).

[23] J. Liu and Y. Xin, Quantum simulation of quantum field theories as quantum chemistry, J. High Energy Phys. **2020**, 1 (2020).

[24] A. F. Shaw, P. Lougovski, J. R. Stryker, and N. Wiebe, Quantum algorithms for simulating the lattice Schwinger model, Quantum **4**, 306 (2020).

[25] B. Nachman, D. Provasoli, W. A. De Jong, and C. W. Bauer, Quantum algorithm for high energy physics simulations, Phys. Rev. Lett. **126**, 062001 (2021).

[26] Y. Tong, V. V. Albert, J. R. McClean, J. Preskill, and Y. Su, Provably accurate simulation of gauge theories and bosonic systems, Quantum **6**, 816 (2022).

[27] W. C. Myrvold, J. Christian, and L. Hardy, in *Quantum Reality, Relativistic Causality, and Closing the Epistemic Circle: Essays in Honour of Abner Shimony* (Springer, 2009), p. 379.

[28] L. García-Álvarez, I. L. Egusquiza, L. Lamata, A. Del Campo, J. Sonner, and E. Solano, Digital quantum simulation of minimal AdS/CFT, Phys. Rev. Lett. **119**, 040501 (2017).

[29] T. Faulkner, T. Hartman, M. Headrick, M. Rangamani, and B. Swingle, Snowmass white paper: Quantum information in quantum field theory and quantum gravity, Preprint ArXiv:2203.07117 (2022).

[30] I. Shapoval, V. P. Su, W. de Jong, M. Urbanek, and B. Swingle, Towards quantum gravity in the lab on quantum processors, Preprint ArXiv:2205.14081 (2022).

[31] R. van der Meer, Z. Huang, M. Correa Anguita, D. Qu, P. Hooijschuur, H. Liu, M. Han, J. J. Renema, and L. Cohen, Experimental simulation of loop quantum gravity on a photonic chip, npj Quantum Inf. **9**, 32 (2023).

[32] R. Dovesi, B. Civalleri, C. Roetti, V. R. Saunders, and R. Orlando, Ab initio quantum simulation in solid state chemistry, Rev. Comput. Chem. **21**, 1 (2005).

[33] I. M. Georgescu, S. Ashhab, and F. Nori, Quantum simulation, Rev. Mod. Phys. **86**, 153 (2014).

[34] X. Yuan, S. Endo, Q. Zhao, Y. Li, and S. C. Benjamin, Theory of variational quantum simulation, Quantum **3**, 191 (2019).

[35] B. Bauer, S. Bravyi, M. Motta, and G. K.-L. Chan, Quantum algorithms for quantum chemistry and quantum materials science, Chem. Rev. **120**, 12685 (2020).

[36] K. Head-Marsden, J. Flick, C. J. Ciccarino, and P. Narang, Quantum information and algorithms for correlated quantum matter, Chem. Rev. **121**, 3061 (2020).

[37] X. Wu, X. Liang, Y. Tian, F. Yang, C. Chen, Y.-C. Liu, M. Khoon Tey, and L. You, A concise review of Rydberg atom based quantum computation and quantum simulation, Chin. Phys. B **30**, 020305 (2021).

[38] N. Klco, A. Roggero, and M. J. Savage, Standard model physics and the digital quantum revolution: Thoughts about the interface, Rep. Progr. Phys. **85**, 064301 (2022).

[39] I. Kassal, S. P. Jordan, P. J. Love, M. Mohseni, and A. Aspuru-Guzi, Polynomial-time quantum algorithm for the simulation of chemical dynamics, Proc. Natl. Acad. Sci. **105**, 18681 (2008).

[40] H. Mabuchi and A. C. Doherty, Cavity quantum electrodynamics: Coherence in context, Science **298**, 1372 (2002).

[41] O. Benson, Assembly of hybrid photonic architectures from nanophotonic constituents, Nature **480**, 193 (2011).

[42] H. Ritsch, P. Domokos, F. Brennecke, and T. Esslinger, Cold atoms in cavity-generated dynamical optical potentials, Rev. Mod. Phys. **85**, 553 (2013).

[43] J. Flick, M. Ruggenthaler, H. Appel, and A. Rubio, Atoms and molecules in cavities, from weak to strong coupling in quantum-electrodynamics (QED) chemistry, Proc. Natl. Acad. Sci. **114**, 3026 (2017).

[44] K. Ramasesha, S. R. Leone, and D. M. Neumark, Real-time probing of electron dynamics using attosecond time-resolved spectroscopy, Annu. Rev. Phys. Chem. **67**, 41 (2016).

[45] M. Schultze, M. Fieß, N. Karpowicz, J. Gagnon, M. Korbman, M. Hofstetter, S. Neppl, A. L. Cavalieri, Y. Komninos, and Th. Mercouris, *et al.*, Delay in photoemission, Science **328**, 1658 (2010).

[46] A. S. Kheifets and I. A. Ivanov, Delay in atomic photoionization, Phys. Rev. Lett. **105**, 233002 (2010).

[47] J. C. Baggesen and L. B. Madsen, Polarization effects in attosecond photoelectron spectroscopy, Phys. Rev. Lett. **104**, 043602 (2010).

[48] L. R. Moore, M. A. Lysaght, J. S. Parker, H. W. Van Der Hart, and K. T. Taylor, Time delay between photoemission from the $2p$ and $2s$ subshells of neon, Phys. Rev. A **84**, 061404 (2011).

[49] S. Nagele, R. Pazourek, J. Feist, K. Doblhoff-Dier, C. Lemell, K. Tőkési, and J. Burgdörfer, Time-resolved photoemission by attosecond streaking: Extraction of time information, J. Phys. B: At., Mol. Opt. Phys. **44**, 081001 (2011).

[50] R. Pazourek, J. Feist, S. Nagele, and J. Burgdörfer, Attosecond streaking of correlated two-electron transitions in helium, Phys. Rev. Lett. **108**, 163001 (2012).

[51] J. Feist, O. Zatsarinny, S. Nagele, R. Pazourek, J. Burgdörfer, X. Guan, K. Bartschat, and B. I. Schneider, Time delays for attosecond streaking in photoionization of neon, Phys. Rev. A **89**, 033417 (2014).

[52] J. J. Omiste and L. B. Madsen, Attosecond photoionization dynamics in neon, Phys. Rev. A **97**, 013422 (2018).

[53] J. Vinbladh, J. Marcus Dahlström, and E. Lindroth, Many-body calculations of two-photon, two-color matrix elements for attosecond delays, Phys. Rev. A **100**, 043424 (2019).

[54] J. J. Omiste and L. B. Madsen, Photoionization of aligned excited states in neon by attosecond laser pulses, J. Phys. B: At., Mol. Opt. Phys. **54**, 054001 (2021).

[55] R. Pazourek, S. Nagele, and J. Burgdörfer, Attosecond chronoscopy of photoemission, Rev. Mod. Phys. **87**, 765 (2015).

[56] H. Spohn, *Dynamics of Charged Particles and Their Radiation Field* (Cambridge University Press, 2004).

[57] M. Suzuki, General theory of fractal path integrals with applications to many-body theories and statistical physics, J. Math. Phys. **32**, 400 (1991).

[58] A. M. Childs, Y. Su, M. C. Tran, N. Wiebe, and S. Zhu, Theory of Trotter error with commutator scaling, Phys. Rev. X **11**, 011020 (2021).

[59] J. Haah, M. B. Hastings, R. Kothari, and G. H. Low, Quantum algorithm for simulating real time evolution of lattice Hamiltonians, SIAM J. Comput. **52**, FOCS18–250 (2021).

[60] G. Hao Low, Y. Su, Y. Tong, and M. C. Tran, Complexity of implementing Trotter steps, PRX Quantum **4**, 020323 (2023).

[61] P. Mukhopadhyay, N. Wiebe, and H. T. Zhang, Synthesizing efficient circuits for Hamiltonian simulation, npj Quantum Inf. **9**, 31 (2023).

[62] T. Tomesh, N. Allen, and Z. Saleem, Quantum-classical tradeoffs and multi-controlled quantum gate decompositions in variational algorithms, Preprint ArXiv:2210.04378 (2022).

[63] M. Möttönen, J. J. Vartiainen, V. Bergholm, and M. M. Salomaa, Transformation of quantum states using uniformly controlled rotations, Quantum Inf. Comput. **5**, 467 (2005).

[64] M. Schuld and F. Petruccione, *Machine Learning with Quantum Computers* (Springer, 2021).

[65] V. Giovannetti, S. Lloyd, and L. Maccone, Architectures for a quantum random access memory, Phys. Rev. A **78**, 052310 (2008).

[66] T. H. Cormen, C. E. Leiserson, R. L. Rivest, and C. Stein, *Introduction to Algorithms* (The MIT Press, 2022).

[67] Y. He, M.-X. Luo, E. Zhang, H.-K. Wang, and X.-F. Wang, Decompositions of n-qubit Toffoli gates with linear circuit complexity, Int. J. Theor. Phys. **56**, 2350 (2017).

[68] C. Gidney, Halving the cost of quantum addition, Quantum **2**, 74 (2018).

[69] M. A. Nielsen and I. L. Chuang, *Quantum Computation and Quantum Information* (Cambridge University Press, 2010).

[70] V. Kliuchnikov, D. Maslov, and M. Mosca, Practical approximation of single-qubit unitaries by single-qubit quantum Clifford and T circuits, IEEE Trans. Comput. **65**, 161 (2015).

[71] A. Bocharov, M. Roetteler, and K. M. Svore, Efficient synthesis of universal repeat-until-success quantum circuits, Phys. Rev. Lett. **114**, 080502 (2015).

[72] N. J. Ross and P. Selinger, Optimal ancilla-free Clifford+T approximation of z-rotations, Quantum Inf. Comput. **16**, 901 (2016).

[73] V. Gheorghiu, M. Mosca, and P. Mukhopadhyay, T-count and T-depth of any multi-qubit unitary, npj Quantum Inf. **8**, 1 (2022).

[74] I. F. Araujo, D. K. Park, F. Petruccione, and A. J. da Silva, A divide-and-conquer algorithm for quantum state preparation, Sci. Rep. **11**, 1 (2021).

[75] P. Niemann, R. Datta, and R. Wille, in *2016 IEEE 46th International Symposium on Multiple-Valued Logic (ISMVL)* (IEEE, 2016), p. 247.

[76] M. Plesch and Č. Brukner, Quantum-state preparation with universal gate decompositions, Phys. Rev. A **83**, 032302 (2011).

[77] A. J. Laub, *Matrix Analysis for Scientists and Engineers* (Siam, 2005), Vol. 91.

[78] J. Li, General explicit difference formulas for numerical differentiation, J. Comput. Appl. Math. **183**, 29 (2005).

[79] Y. Nam, Y. Su, and D. Maslov, Approximate quantum Fourier transform with $O(n\log(n))$ T gates, npj Quantum Inf. **6**, 1 (2020).

[80] M. Mosca and P. Mukhopadhyay, A polynomial time and space heuristic algorithm for T-count, Quantum Sci. Technol. **7**, 015003 (2021).

[81] C. Jones, Low-overhead constructions for the fault-tolerant Toffoli gate, Phys. Rev. A **87**, 022328 (2013).

[82] V. Gheorghiu, J. Huang, S. M. Li, M. Mosca, and P. Mukhopadhyay, Reducing the CNOT count for Clifford+T circuits on NISQ architectures, IEEE Trans. Comput.-Aided Des. Integrated Circ. Syst. **42**, 1873 (2023).

[83] M. Amy, P. Azimzadeh, and M. Mosca, On the controlled-NOT complexity of controlled-NOT–phase circuits, Quantum Sci. Technol. **4**, 015002 (2018).

[84] K. N. Patel, I. L. Markov, and J. P. Hayes, Optimal synthesis of linear reversible circuits, Quantum Inf. Comput. **8**, 282 (2008).

[85] T. G. Draper, Addition on a quantum computer, Preprint ArXiv:quant-ph/0008033 (2000).

[86] L. Ruiz-Perez and J. C. Garcia-Escartin, Quantum arithmetic with the quantum Fourier transform, Quantum Inf. Process. **16**, 1 (2017).

[87] S. A. Cuccaro, T. G. Draper, S. A. Kutin, and D. Petrie Moulton, A new quantum ripple-carry addition circuit, Preprint ArXiv:quant-ph/0410184 (2004).

[88] J. Huyghebaert and H. De Raedt, Product formula methods for time-dependent Schrodinger problems, J. Phys. A: Math. General **23**, 5777 (1990).

[89] N. Wiebe, D. Berry, P. Høyer, and B. C. Sanders, Higher order decompositions of ordered operator exponentials, J. Phys. A: Math. Theor. **43**, 065203 (2010).